

Towards a better understanding of neuron-NG2 glia signaling

Comparative studies in the hippocampus and cerebellum

Dissertation

zur

Erlangung des Doktorgrades (Dr. rer. nat.)

der

Mathematisch-Naturwissenschaftlichen Fakultät

der

Rheinischen Friedrich-Wilhelms-Universität Bonn

vorgelegt von

Dario Tascio

aus

Viterbo

Bonn, June 2023

Angefertigt mit Genehmigung der Mathematisch-Naturwissenschaftlichen Fakultät
der Rheinischen Friedrich-Wilhelms-Universität Bonn

1. Gutachter:

Prof. Dr. Christian Steinhäuser

Institut für Zelluläre Neurowissenschaften

Universität Bonn

2. Gutachter:

Prof. Dr. Gerhard von der Emde

Institut für Zoologie

Universität Bonn

Tag der Promotion: 19.01.2024

Erscheinungsjahr: 2024

Acknowledgements

First, I am truly grateful to my first supervisor Prof. Dr. Christian Steinhäuser for his exceptional guidance, comments and constant support which have played a crucial role in shaping the direction of this work. I would like to express my gratitude to Prof. Dr. Gerhard von der Emde, Prof. Dr. Walter Witke and Prof. Dr. Karl Schilling for accepting my request to be part of the examination committee and for their time and efforts in reviewing and evaluating my thesis.

I am deeply thankful to PD Dr. Gerald Seifert for his daily advices, hints and suggestions, which have been fundamental for overcoming challenges and ensuring the smooth progress of my research. Moreover, his technical expertise and help with mRNA analyses, genotyping, mouse handling, tamoxifen injections and behavioural tests have been indispensable. I am also indebted to PD Dr. Ronald Jabs for his countless, invaluable, outside the box suggestions and support on any kind of theoretical and technical issue. His talent in statistics, programming and physics has greatly enhanced the quality of my work, all in exchange for just a few gummy bears.

Special recognition goes to Aline Timmermann, who has been a great colleague and mentor, teaching me patch-clamp with outstanding patience and precision; to Michael Rabenstein for sharing life-saving knowledge and tips about cerebellar physiology; to Petr, Stefan, Daniel and Kirsten for always being ready to share their experiences and provide irreplaceable insights for this project. I want to say thank you to Jessica which was a great PhD pal: our shared experiences, discussions and indulgence in Mexican candies have made these years much more enjoyable. Thanks also to Nehal, with whom I shared many hours in the lab, she was a unique accomplice in the long days at the HET and outside. I would also like to acknowledge Michela Palmisano and Dr. Andras Bilkei-Gorzu for their help in the behavioural tests and all the students and colleagues that always created a nice environment to work in: Alberto, Björn, Camille, Catia, Daniel, Dmitry, Kamyab, Linda, Lukas, Mandana, Marieke, Noortje, Oussama, Paula, Peter, Stefan H. and Zhou. I also want to acknowledge Prof. Dr. Christian Henneberger for providing valuable advice during our weekly seminars, Thomas Erdmann and Dr. Silke Künzel for their great technical and administrative support.

My most profound appreciation goes to my family and friends for being always supportive and encouraging. Finally, my sincerest gratitude is for my girlfriend Mara for her love, kindness, patience and to have always motivated me, making this time in Bonn unique and unrepeatable.

Table of contents

1 Introduction	8
1.1 The cerebellum	8
1.1.1 Cerebellar anatomy	8
1.1.2 Cerebellar circuitry	9
1.1.3 Cerebellar stripes	11
1.1.4 Cerebellar glia	12
1.2 The hippocampus	13
1.2.1 Hippocampal glia	15
1.3 NG2 glia	15
1.4 Neurotransmitter receptors and ion channels	19
1.4.1 AMPA receptors	19
1.4.2 GABA receptors	20
1.4.3 Inwardly rectifying potassium (Kir) 4.1 channels	22
1.5 Synaptic transmission and plasticity	23
1.5.1 Short-term plasticity	23
1.5.2 Long-term plasticity	25
1.5.3 Long-term plasticity in the cerebellum	26
1.6 Neurotrophins	27
1.6.1 BDNF	27
2 Aim of the Study	29
3 Materials	31
3.1 Substances	31
3.2 Devices	33
3.3 Software	34
3.4 Solutions	35
3.4.1 Intracellular solutions	35

3.4.2 Extracellular solutions.....	36
4 Methods.....	37
4.1 Animals.....	37
4.1.1 NG2-YFP knock-in mouse line.....	37
4.1.2 NG2-CreERT2 x Rosa26-EYFP.....	37
4.1.3 NG2-CreERT2 x GluAfl/fl x Rosa26-EYFP.....	37
4.1.4 NG2-CreERT2 x Kir4.1fl/fl x Rosa26-EYFP.....	38
4.2 Inducible CreERT2-loxP recombination system.....	38
4.3 Electrophysiology.....	38
4.3.1 Acute brain slice preparation.....	38
4.3.2 Patch-clamp setup.....	39
4.3.3 Patch-clamping protocol.....	40
4.3.4 Liquid junction potential.....	41
4.3.5 Passive membrane properties.....	41
4.3.6 Bath application of kainate.....	43
4.3.7 Evoked post-synaptic current (ePSC) recordings.....	44
4.3.7.1 Glutamatergic ePSCs in the cerebellum.....	45
4.3.7.2 Glutamatergic ePSCs in the hippocampus.....	45
4.3.7.3 GABAergic ePSCs in the hippocampus.....	45
4.3.7.4 Analysis of ePSCs.....	45
4.3.8 Miniature PSCs.....	46
4.3.9 Field potential recordings.....	46
4.3.10 Measurement of neuronal intrinsic firing properties.....	48
4.4 Behavioural tests.....	50
4.4.1 Novel object location recognition (NOLR) test.....	50
4.4.2 Partner recognition test (PRT).....	51
4.4.3 Y-maze test.....	52
4.4.4 Beam-walking test.....	53

4.5 Molecular analyses.....	54
4.5.1 FAC sorting	54
4.5.2 Semiquantitative RT-qPCR	54
4.5.3 Single-cell RT-PCR.....	55
4.6 Statistics.....	57
5 Results.....	58
5.1 Developmental and regional differences of AMPAR expression in NG2 glia.	58
5.1.1 CP-AMPARs in developing hippocampal NG2 glia.....	58
5.1.2 CP-AMPARs in cerebellar NG2 glia.....	60
5.1.3 Multivesicular release from CFs contributes to a larger glutamate transient	63
5.1.4 Short-term plasticity at CF-NG2 synapses.....	65
5.2 Impact of NG2 glia AMPARs on neuronal signalling and behaviour	67
5.2.1 Inducible deletion of AMPARs in NG2 glia entails loss of receptor currents in the cerebellum.	67
5.2.2 Long-term plasticity is impaired in the cerebellum of GluAko mice.....	68
5.2.2.1 LTP can be rescued by a TrkB agonist.....	71
5.2.3 Purkinje neurons show altered AP firing in GluAko mice.....	73
5.2.4 Behavioural tests	76
5.2.4.1 NOLR test.....	76
5.2.4.2 Partner recognition test	77
5.2.4.3 Y-maze test	79
5.2.4.4 Beam-walking test	79
5.2.5 NG2 glia CP-AMPARs regulate neuronal signalling in hippocampus and cerebellum	81
5.3 Deletion of Kir 4.1 channels in NG2 glia	83
5.3.1 Miniature PSCs decay is prolonged in Kir 4.1 ko mice.....	83
5.3.2 Reduced PTP and LTP in Kir 4.1 ko mice can be rescued by 7,8-DHF	85
5.4 Developmental regulation of GABA _A receptors in NG2 glia	87
5.4.1 Increased kinetics of ePSCs and developmental switch to a spillover mechanism	87

6 Discussion	89
6.1 CP-AMPARs in developing hippocampal NG2 glia.....	89
6.2 High synaptic efficiency of CF-NG2 synapses is mediated by CP-AMPARs and multivesicular release.....	90
6.3 Short-term plasticity at CF-NG2 synapses	92
6.4 AMPAR deletion in NG2 glia impairs neuronal plasticity and PC firing.....	93
6.5 GluAko mice exhibit a reduction in locomotor activity	95
6.6 CP-AMPARs mediate LTP in hippocampus and cerebellum	96
6.7 Kir 4.1 mice dysfunctions in hippocampus and cerebellum.....	96
6.8 GABA _A R signalling switches to a spillover-mediated transmission in adult NG2 glia.....	97
7 Perspectives.....	98
8 Summary	99
9 References	101
10 Appendix.....	133
10.1 Abbreviations.....	133
10.2 List of figures.....	136
10.3 List of tables.....	137
Declaration	138

1 Introduction

Glial cells, constituting around 50% of the cell population in the human brain (Azevedo *et al.*, 2009), were first described in the mid of the nineteenth century by Rudolf Virchow, who termed them “nerve-cement” (see Kettenmann and Verkhratsky, 2008) considering them a “substance which holds nerves together”. This view persisted for almost two centuries, during which many histologists started to describe different glial cell types. While glial knowledge was slowly increasing during the 20th century, these cells were always believed to have only a passive and supportive role in the central nervous system (CNS), mainly functioning as insulators to improve neurons electrical signals. On the other hand, neurons were soon found to be directly associated with brain functions and pathologies, so most of the effort of neuroscientists was put to describe this cell type and develop new pharmacological strategies to target it and treat brain-related disorders. Nevertheless, as knowledge on glial cells started to increase abruptly in the last decades, it became clear that they have not only a supporting role for neurons but they also shape neuronal circuits by regulating synapse stability and neurotransmission (Ullian, Christopherson and Barres, 2004; Stevens *et al.*, 2007; Perea and Araque, 2010; Sancho, Contreras and Allen, 2021; Auguste *et al.*, 2022) and their malfunction can bring to the onset of neurological and psychiatric disorders (Di Benedetto and Rupprecht, 2013; Binder and Steinhäuser, 2021). Nowadays, it is essential to consider glial cells just as important as neurons to face the many challenges related to the understanding of the mammalian brain. In this study, I will focus on one of the more enigmatic glial cell types, NG2 glia, concentrating on its singular ability to form functional synapses with neurons in two brain regions: the cerebellum and the hippocampus (Jabs *et al.*, 2005; Lin *et al.*, 2005).

1.1 The cerebellum

The cerebellum (from latin “small brain”) is a phylogenetically conserved structure of the vertebrate brain, involved in sensory-motor and cognitive functions (Buckner, 2013). Defects in the excitability of cerebellar neurons have been linked to ataxic disorders (Shields *et al.*, 2012) but cerebellar dysfunctions can go beyond motor deficits leading to affective, cognitive and behavioural abnormalities.

1.1.1 Cerebellar anatomy

The cerebellum is part of the hindbrain, located in the posterior cranial fossa and isolated from the cerebral hemispheres by the cerebellar tentorium, an extension of the dura mater (Roostaei *et al.*, 2014). The external structure of the cerebellum is unique, comprising several parallel

grooves called folia, finely separated by fissures which hide most of the tissue in the inner part (Fig. 1.1A). This largely folded structure is the grey matter of the cerebellar cortex, which surrounds a tree-shaped internal layer of white matter called arbor vitae. The arbor vitae surround three pairs of deep cerebellar nuclei (DCNs), which constitute the sole output of the cerebellum. On a sagittal plane, the cerebellar cortex can be further subdivided into a central vermis which separates the two lateral hemispheres (Fig. 1.1 A). The vermis is composed by 10 lobules (I-X), each serving a specific function (Fig. 1.1 B). A functional subdivision further separates the cerebellum into three parts: a vestibulocerebellum, which is connected to the axial musculature to maintain balance; a spinocerebellum, which integrates sensory inputs to control motor coordination; and a cerebrocerebellum, connected to the cerebral cortex and involved in movement planning and cognitive functions (Fig. 1.1 D). A series of fibres, called peduncles, carrying both afferent and efferent connections, link the cerebellum with the rest of the nervous system.

1.1.2 Cerebellar circuitry

While cerebellar morphology can vary greatly across species, the basic internal structure of the cerebellar cortex is surprisingly conserved in all vertebrates (Hashimoto and Hibi, 2012) and composed of a repetitive and stereotyped neural machinery, which is maintained in all the cerebellar lobules (Fig. 1.2). It contains around 60% of the total number neurons in the mouse brain and 80% in the human brain (Herculano-Houzel, 2010). We can easily identify three main layers: the granular layer (GL), the Purkinje cell layer and the molecular layer (ML). Excitatory fibers reach the cerebellar cortex through two main pathways: the first is the mossy fiber (MFs) pathway, coming from various brain structures like the spinal cord, the pontine nuclei and the reticular formation; and the second is the climbing fiber (CFs) pathway, originating in the inferior olivary complex of the brain stem. The GL is the most internal and densely packed layer, containing mainly small glutamatergic neurons, named granule cells, and inhibitory interneurons. The few dendrites of a granule cell enlarge to form the so-called dendritic claws, which make synapses with enlargements of the MFs.

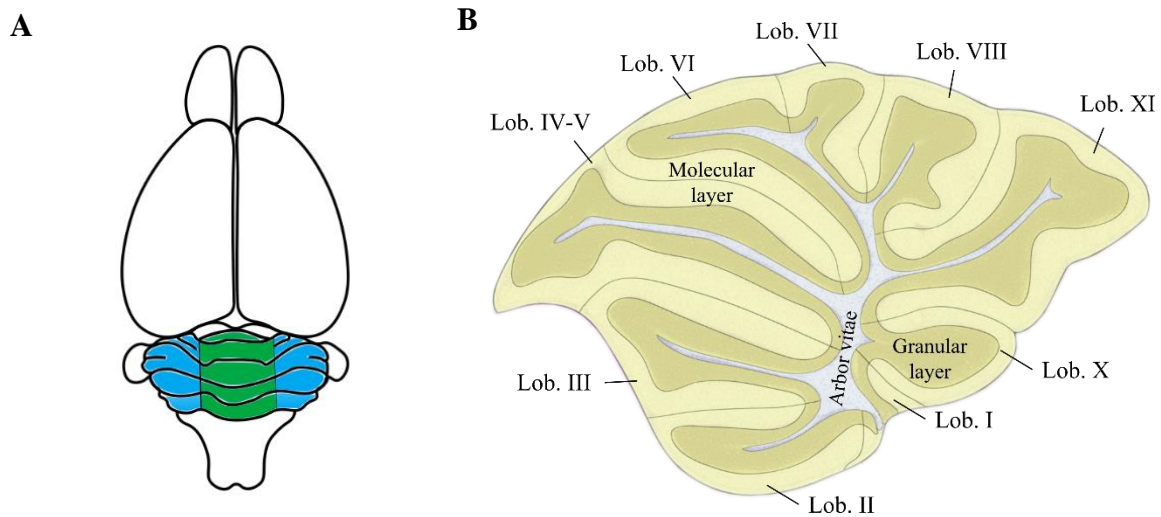


Fig. 1.1. Cerebellar localization and anatomy **A)** Dorsal view of the mouse brain. The cerebellum occupies the posterior part, at the border of the brainstem. The lateral cerebellar hemispheres, corresponding to the cerebrocerebellum, are highlighted in blue. The cerebrocerebellum is connected to the cerebral cortex through the superior peduncle for motor planning and cognitive control. Cerebellar vermis and paravermal regions are highlighted in green and constitute the spinocerebellum, receiving afferent connections from the spinal cord. **B)** Sagittal view of the cerebellar vermis. The cerebellar cortex is divided into lobules, each comprising three layers: light yellow: molecular layer; dark yellow: granular layer; white: white matter. Adapted from Allen Brain Atlas, <https://atlas.brain-map.org/>.

These contacts, together with the synaptic innervation by interneurons and ensheathment from glial cells, form the so-called cerebellar glomerulus. The thin and amyelinic axon of granule cells reaches the outer part of the cerebellar cortex, the molecular layer. Here, these fibers diverge perpendicularly in opposite directions and form glutamatergic parallel fibers (PFs). Multiple PFs innervate the large dendritic tree of Purkinje cells (PCs), each making only a few synapses. Purkinje cells (PCs) are the sole output from the cerebellar cortex to the deep cerebellar nuclei. Their large cell bodies are arranged on a single layer. Single CFs can innervate up to 10 PCs but, importantly, a single PC receives hundreds of synaptic contacts from only one CF. This strong synaptic input from CFs induces a large depolarization called “complex spike” (Eccles, Llinás and Sasaki, 1966) which consists of a fast Na^+ spike followed by a burst of smaller spikelets. ML interneurons, namely stellate cells and basket cells, innervate PCs or glutamatergic fibers providing feed-forward and lateral inhibition and modulate the temporal dynamics of action potential (AP) firing from PCs (Häusser and Clark, 1997). The strong inhibitory output of PCs will contact neurons in the DCNs, influencing the activity of their downstream target structures (Dum and Strick, 2003; Chen *et al.*, 2014).

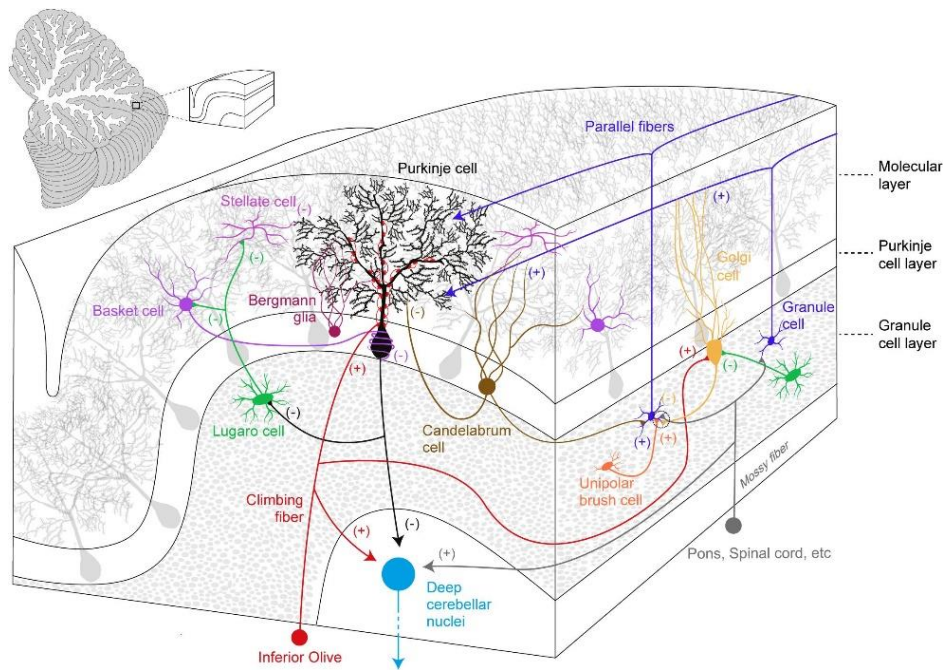


Fig. 1.2. Simplified overview of the cerebellar cortical organization and its circuitry. Excitatory (+) and inhibitory (–) components are represented within the cerebellar cortex and deep cerebellar nuclei. Purkinje neurons integrate multiple excitatory and inhibitory signals and send their output to deep cerebellar nuclei. (Binda, Pernaci and Saxena, 2020).

1.1.3 Cerebellar stripes

Molecular analyses of PCs have shown that the cerebellar cortex can be further subdivided into a series of rostro-caudally oriented bands, also called sagittal stripes. Many markers have been used to make such subdivisions, the most widely used being Zebrin II (Brochu, Maler and Hawkes, 1990), which has been later identified as a marker for the enzyme aldolase C (Ahn *et al.*, 1994). This way, the cerebellum can be divided into hundreds of functional modules which are very conserved across mammals (Sillitoe *et al.*, 2005). Zebrin II negative (Z-) and zebrin II positive (Z+) PCs have a quite different molecular profile, which gives them different electrophysiological characteristics (Cerminara *et al.*, 2015, Fig. 1.3). Notably, the firing frequency of PCs is higher in Z- bands probably because of a higher expression of the transient receptor potential cation channel type C3 (TRPC3, Zhou *et al.*, 2014). Moreover, LTP is larger in Z- zones thanks to a phosphatase-dependent block of small conductance Ca^{2+} -activated K^{+} channels (SK channels), which in turn control PCs intrinsic firing (Viet *et al.*, 2022). These data add complexity to the cerebellar cortex and it is thus important to take cerebellar sagittal stripes into account when performing electrophysiological recordings from PCs.

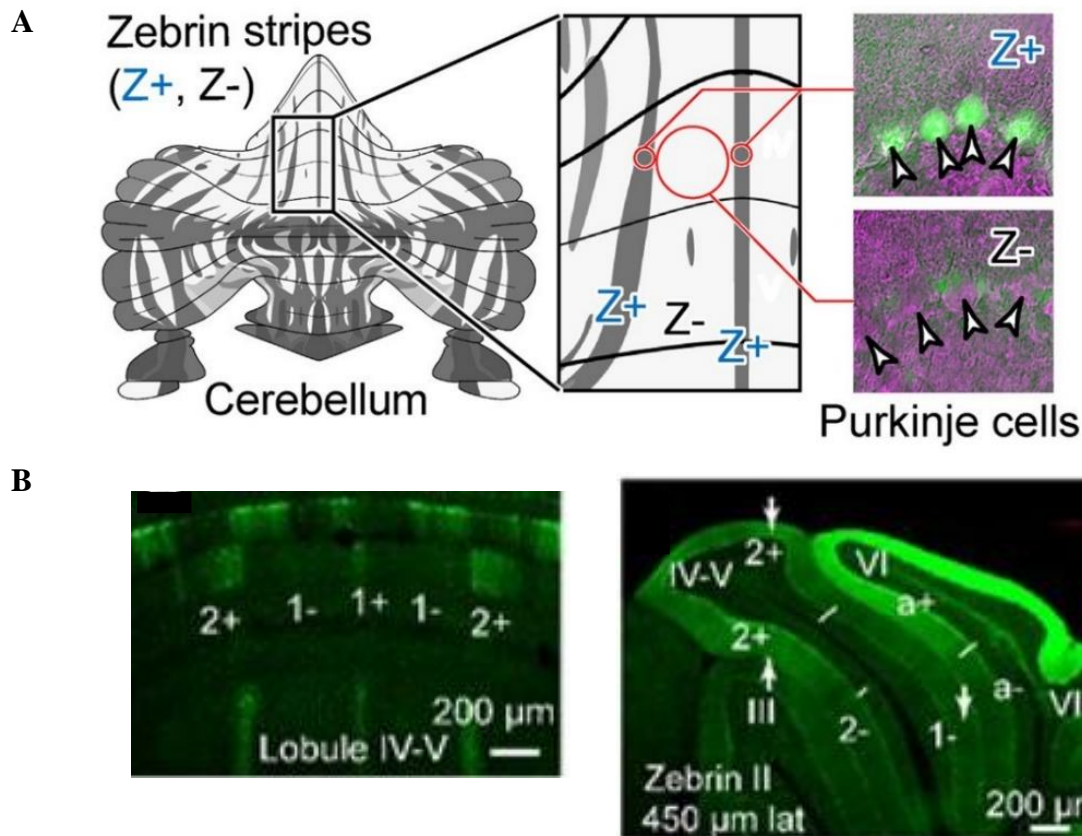


Fig. 1.3. Sagittal cerebellar stripes. **A)** Dorsal view of the cerebellar cortex. The striped pattern appears upon staining with aldolase C. On the right, Z⁺ and Z⁻ PCs in slice preparations. (Viet *et al.*, 2022). **B)** Left: coronal sections of vermal lobules IV-V and VI in a mouse model in which PCs are stained for aldolase C (Aldoc V mouse line); right: sagittal section of 450 μm showing zebryn zones in lobules IV-V and VI and neighboring lobules in the Aldoc V mouse. Short white lines indicate approximate boundaries of zebryn zones (Nguyen-Minh *et al.*, 2020).

1.1.4 Cerebellar glia

While neurons in the cerebellum constitute the largest cell population and glia-to-neuron ratios are extremely lower compared to other brain regions, e.g., the cerebral cortex (Herculano-Houzel, Mota and Lent, 2006; von Bartheld, Bahney and Herculano-Houzel, 2016; Keller, Erö and Markram, 2018), the cerebellar cortex still contains a diverse repertoire of glial cells (see Buffo and Rossi, 2013). In the cerebellar white matter, oligodendrocytes are important for both the development of the cerebellar tissue and the maintenance of cerebellar connections during adulthood (Mathis, Collin and Borrelli, 2003; Rossi, Gianola and Corvetti, 2006, 2007), while fibrous astrocytes participate in glutamate homeostasis and control myelination (Lee, Kim and Kim, 2022). Specialized astrocytes in the ML are commonly named Bergmann glia (BG). BG exerts prominent roles in the cerebellum during development, aiding cerebellar foliation (Hoser

et al., 2007), migration of granule cells and ML interneurons (Kullmann *et al.*, 2012; Ango *et al.*, 2008; Guijarro *et al.*, 2006) and maturation of PCs (Dahmane and Ruiz-i-Altaba, 1999; Lordkipanidze and Dunaevsky, 2005). In the mature cerebellum, BG fibers surround PCs, interneurons and blood vessels making contacts with thousands of synapses (Reichenbach, Derouiche and Kirchhoff, 2010). These processes tightly enwrap synapses between PCs and both CFs and PFs forming “microdomains” (Špaček, 1985; Grosche, Kettenmann and Reichenbach, 2002; Yamada and Watanabe, 2002). Here, the rapid removal of excess glutamate from the synaptic cleft (Barbour *et al.*, 1994) is dynamically regulated by BGs, which are able to sense changes in neural activity (Bellamy and Ogden, 2006). BGs can control synaptic transmission also through modulating extracellular concentrations of K^+ which interfere with PCs membrane potential (Wang *et al.*, 2012), or through release of glutamate (Sasaki *et al.*, 2012). Remarkably, ablation of α -amino-3-hydroxy-5-methyl-4-isoxazolepropionic acid (AMPA) receptors expressed by BGs, leads to behavioural deficits in fine motor coordination in mice (Saab *et al.*, 2012). While BG properties are being extensively studied, the cerebellar cortex contains also NG2 glia and microglia. The former, which will be widely described in the next chapters, forms functional synapses with CFs and PFs (Lin *et al.*, 2005). The latter has a role in developmental and pathological processes in the cerebellum, even if more studies are necessary to unveil further roles (Marín-Teva *et al.*, 2004; Cardoso *et al.*, 2015). In summary, also in the cerebellum, glial cells play an essential role in guiding and managing neuronal computations.

1.2 The hippocampus

The hippocampus, located in the medial temporal lobe, is part of the limbic system and the hippocampal formation. It has a role in memory processing, emotions, learning and spatial navigation. Together with the hippocampus proper, the hippocampal formation also includes the dentate gyrus (DG), the subicular complex and the entorhinal cortex (Schultz and Engelhardt, 2014). The hippocampus can be divided into three main regions, named Cornu Ammoni (CA) fields due to their form: CA1, CA2 and CA3 (Fig. 1.4A). These fields differ in their connectivity and dendritic configurations (Lorente De Nó, 1934), but their laminar structure is similar. Here, the principle neuronal layer is constituted by pyramidal cells.

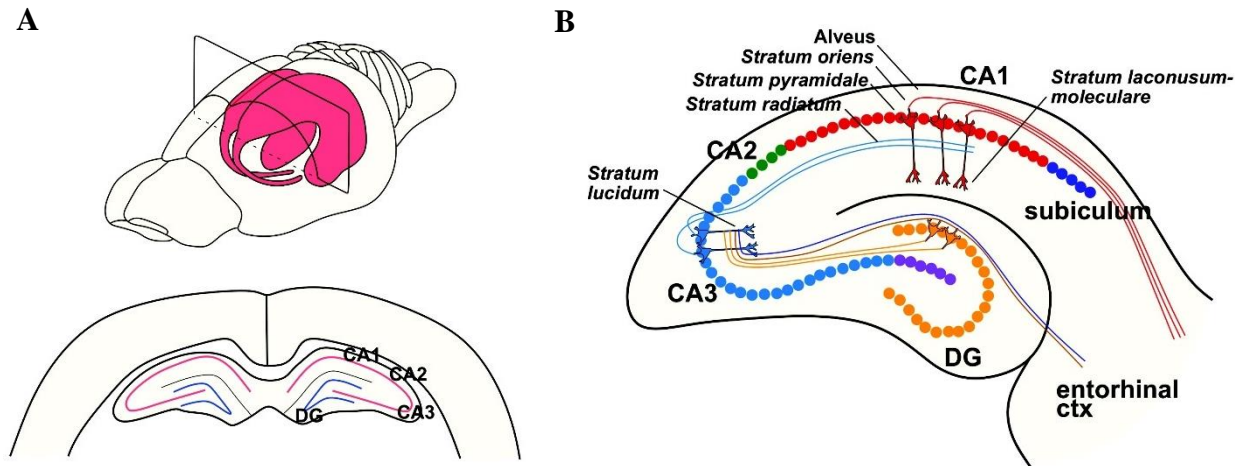


Fig. 1.4. Hippocampal anatomy and circuitry. **A)** Top: schematic representation of the hippocampal formation (in red) in the mouse brain. Bottom: coronal section of the hippocampus shows the main regions. **B)** Details of hippocampal anatomy and trisynaptic circuitry. Here mossy fibers (in yellow) from the dentate gyrus (DG) reach neurons in CA3 stratum lucidum, after receiving input from the entorhinal cortex. Then, Schaffer collaterals (in blue) reach CA1 neurons which in turn project back to the entorhinal cortex, closing the hippocampal synaptic loop. CA: Cornu Ammoni. (Temido-Ferreira *et al.*, 2019).

Basal dendrites of pyramidal cells and distinct types of interneurons are located in the stratum oriens (SO). Superficially to the pyramidal cell layer there are, in order of depth, the stratum lucidum (present only in CA3), the stratum radiatum (SR) and the stratum lacunosum moleculare (SLM), which is the most superficial portion towards the hippocampal fissure (Schultz and Engelhardt, 2014). The SR and the SLM contain the apical dendrites of pyramidal neurons but also interneurons and glial cells. Unidirectional excitatory projections connect all the components of the hippocampal formation (Fig. 1.4B). Indeed, neurons located in layer II and III but also V and VI of the entorhinal cortex send axons to the dentate gyrus forming the perforant path (van Strien, Cappaert and Witter, 2009). This path is necessary for cognitive functions like place learning and spatial memory (Quirk *et al.*, 1992; Ferbinteanu, Holsinger and McDonald, 1999). From the dentate gyrus, mossy fibres of granule cells project towards the stratum lucidum of CA3. There, glutamatergic fibers named Schaffer collaterals (SCs) originate and project to the SO and SR of CA1. This polysynaptic pathway continues from CA1 to the subiculum and finally back to the entorhinal cortex (Finch, Nowlin and Babb, 1983). This has reciprocal projections with the surrounding multimodal sensory association cortices and the olfactory bulb (Krettek and Price, 1977; Insausti, Amaral and Cowan, 1987). The hippocampal formation is also connected to other subcortical structures, like the amygdala, thalamus and hypothalamus (Amaral and Cowan, 1980).

1.2.1 Hippocampal glia

Astroglia is widely distributed in the hippocampus, with varying morphologies throughout the different layers (see Seifert and Steinhäuser, 2018). Astrocyte processes overlap more than half of the neuronal synapses in CA1 SR (Ventura and Harris, 1999), regulating neurotransmitter diffusion and the time course of synaptic transmission. Indeed, astrocytes express both glutamate and γ -aminobutyric acid (GABA) transporters. Glutamate transporters, namely EAAT1/2, uptake glutamate from the synaptic cleft. Astrocytes then convert it into glutamine and release it to neurons through glutamine transporters. Glutamate uptake is associated with influx of Na^+ ions which depolarizes the cell and stimulates the efflux of glutamine (Todd *et al.*, 2017). Glutamine is again converted into glutamate in presynaptic excitatory neurons or, in case of interneurons, it can be converted into GABA (Bröer and Brookes, 2001). Thus, through this shuttle system, astrocytes are able to control both inhibitory and excitatory neurotransmission. Moreover, astrocytes are also deeply involved in the maintenance of ion homeostasis, in particular of K^+ , Cl^- and Ca^{2+} (Kofuji and Newman, 2004; Torres *et al.*, 2012; Egawa *et al.*, 2013). Gap-junction coupling between astrocytes allows the spatial buffering of extracellular K^+ : indeed, astrocytes K^+ -channels can uptake excess extracellular K^+ and redistribute it through the gap-junctional network to more distant sites. Astrocytes can further modify synaptic transmission by releasing neurotransmitters, or gliotransmitters, e.g. ATP, glutamate, GABA, D-serine and glycine (see Verkhratsky and Nedergaard, 2018). Microglia in the hippocampus has also a significant role in regulating the functions of the network. Indeed, the dynamic processes of microglia can directly contact neurons and contribute to the shaping of the neural network during development (Schafer *et al.*, 2012) and adulthood, by pruning excess synapses (Paolicelli *et al.*, 2011) or by modifying synapse activity through crosstalk with astrocytes (Akiyoshi *et al.*, 2018; Du *et al.*, 2022). Lastly, oligodendrocytes in the hippocampus also play a role in learning and memory. Indeed, myelin formation mediated by these cells is modulated by neuronal inputs. Upon sensing signals from neurons, oligodendroglia can modify myelin structure, altering the speed of AP transmission during learning (see Munyeshyaka and Fields, 2022).

1.3 NG2 glia

NG2 glia is a heterogeneous cell type widely and homogeneously distributed in the CNS, both in grey and white matter, both during development and in adulthood. These cells have been elusive for many decades and nowadays their roles are just partially unveiled. Their name derives from the expression of neuron-glia antigen 2 (NG2) chondroitin sulphate proteoglycan,

which is typically present in parenchymal precursors which give rise to myelinating oligodendrocytes in the first 10 weeks of postnatal development in mice and in the first 5-10 years in humans (Sturrock, 1980; Yeung *et al.*, 2014). For this reason, these cells are also named oligodendrocyte precursors (OPCs, Stallcup and Beasley, 1987), but they have also been termed complex cells because of their distinct whole-cell current pattern (Steinhäuser *et al.*, 1994), GluR cells because of the expression of glutamate receptors (see Bergles *et al.*, 2010), synantocytes due to their proximity to neurons (Butt *et al.*, 2002) and ploidendrocytes based on their fine and highly branched processes that give them a stellate morphology (Nishiyama *et al.*, 2009). Indeed, NG2 glial cell processes can contact neuronal dendrites and soma, but also axonal nodes of Ranvier and synapses (Serwanski, Jukkola and Nishiyama, 2017). However, being the most proliferative cell type in the CNS (Dawson *et al.*, 2003), NG2 glia contributes to generation of oligodendrocytes not only during development but also throughout adulthood where they can actively participate in experience-dependent myelination. Indeed, NG2 glia proliferation and differentiation increases up to 4 months of age in mice (Hughes *et al.*, 2018) contributing to early and late phases of motor skill learning (Xiao *et al.*, 2016). Importantly, in case of injuries or demyelinating disorders, NG2 glia increases proliferation and migrates to the lesion site (see Levine, 2016; Valny *et al.*, 2018). This reactive NG2 glia can respond to several factors released by the damaged tissue or other NG2 glial cells present in the area which in turn induce a change in NG2 glia transcription profile increasing its contribution to remyelination (see Gallo and Deneen, 2014; Moyon *et al.*, 2015). On the other hand, it is debated whether all NG2 glial cells contribute to this insult-induced behaviour or rather only a transcriptionally-defined subpopulation (see Viganò and Dimou, 2016). Nevertheless, NG2 glia proliferation and differentiation activities seem independent from the presence of myelinated fibers (see Parolisi and Boda, 2018) and most of the cell population in the healthy grey matter tissue maintains its phenotype throughout adulthood (Dimou *et al.*, 2008), with a low rate of apoptotic cells (Dawson *et al.*, 2003). Interestingly, also the typical spatial distribution of NG2 glia in non-overlapping domains is maintained in a very precise manner (Hughes *et al.*, 2018). Another remarkable evidence for the fact that these cells might serve additional roles in the CNS, is their peculiar and unique ability among glial cells to make functional synapses with both glutamatergic and GABAergic neurons in several brain regions (Bergles *et al.*, 2000; Lin and Bergles, 2004; Jabs *et al.*, 2005; Lin *et al.*, 2005; Müller *et al.*, 2009). Indeed, NG2 glia can sense neuronal activity thanks to the expression of several receptors and channels: e.g. AMPA receptors (see chapter 1.4.1) which display an intermediate Ca^{2+} permeability (Bergles *et al.*, 2010) and mediate signals leading to a decrease of NG2 glia proliferation and an increase in

branching of the cell processes (Fannon *et al.*, 2015; Yuan *et al.*, 1998; Fig. 1.5A); GABA receptors (see chapter 1.4.2), which form synapses with interneurons and might increase Ca^{2+} concentration in NG2 glial cells (Tong *et al.*, 2009); voltage-gated Na^{2+} channels which participate in NG2 glia depolarization and might have a role in the glucocorticoid-induced response to early-life stress (Treccani *et al.*, 2021); voltage-gated Ca^{2+} channels which modulate cell proliferation and are thought to have a role in the regulation of long-term neuronal plasticity in the hippocampus (Zhao *et al.*, 2021); K^+ channels, which constitute the main conductance of these cells (see chapter 1.4.3). All these channels mediate a complex electrophysiological pattern (Steinhäuser *et al.*, 1992, Fig. 1.5B). In the cerebellum, NG2 glia establishes functional synapses with both CFs and PFs. CF-NG2 glia synapses have high efficiency, giving rise to post-synaptic currents ranging from 60 pA to 900 pA and showing paired-pulse depression (Fig. 1.5C and section 1.5.1). A single NG2 glial cell is innervated by multiple CFs, each making up to 70 synaptic contacts (Lin *et al.*, 2005). In the hippocampus, SC-NG2 glia synapses are well characterized and they show a much lower innervation compared to their cerebellar counterpart. Moreover, NG2 glia can respond to signalling from cytokines, hormones like glucocorticoids (Matusue *et al.*, 2014) and neurotrophic factors like BDNF (VonDran *et al.*, 2011) thanks to surface expression of the correspondent receptors (see Dimou and Gallo, 2015). Thus, depolarization and Ca^{2+} elevations induced by neuronal inputs or by other extracellular molecules could trigger proliferation, migration or differentiation of NG2 glial cells. Additionally, interesting evidences show that NG2 glia can release many soluble factors which could potentially influence neuronal activity (see Parolisi and Boda, 2018). Furthermore, overlapping domains between NG2 glia with astrocytes and microglia suggest a crosstalk with these glial cell types (Wigley and Butt, 2009; Du *et al.*, 2021). On this note, ablation of NG2 glia impairs the homeostatic state of microglia and could have profound implications for neurodegeneration (Liu and Aguzzi, 2020). Other intriguing roles for NG2 glia have been recently investigated, like their involvement in synapse remodelling upon sensory stimulation (Auguste *et al.*, 2022) or the possibility that subpopulations of NG2 glial cells act as astrocyte or neuronal progenitors under specific sets of conditions (Richardson *et al.*, 2011).

Thus, NG2 glia is a very versatile cell type with exciting and diverse functions which still need to be further clarified.

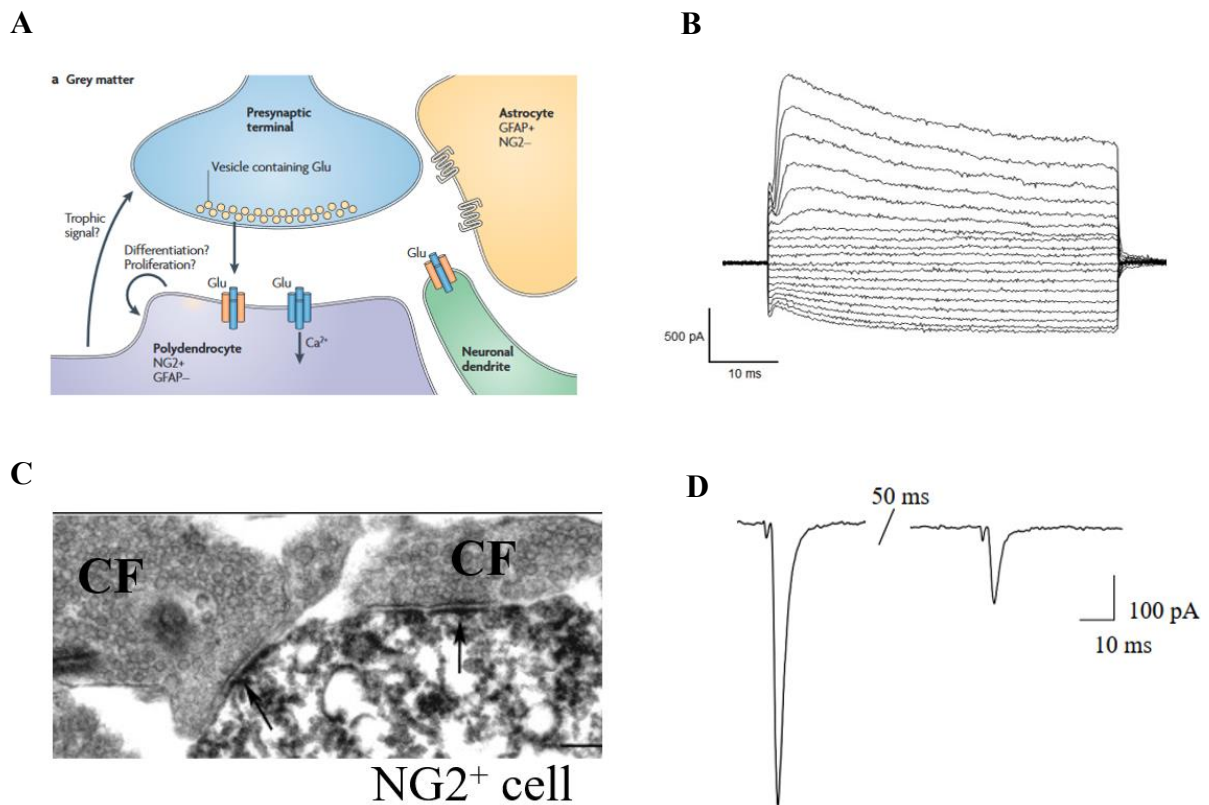


Fig. 1.5. NG2 glia forms functional synapses with neurons. **A)** Schematic representation of a NG2-neuron synapse. Glutamate released from presynaptic neurons is sensed by AMPA receptors on NG2 glia, which in turn mediate entry of Ca^{2+} ions. This can eventually lead to signals for NG2 glia differentiation or proliferation or the release of trophic factors (Nishiyama *et al.*, 2009). **B)** Whole-cell current pattern of hippocampal NG2 glia. Current responses derive from a 10 mV step protocol, ranging from -160 mV to +20 mV. **C)** Innervation of a cerebellar NG2 glial cell from two climbing fiber (CF) axons. Arrows indicate NG2 glia post-synaptic density (Lin *et al.*, 2005). **D)** Post-synaptic AMPA receptor-mediated currents in cerebellar NG2 glia upon stimulation of CFs. Paired-pulse protocol, with inter-pulse interval of 50ms, shows short-term depression (chapter 1.5.1).

1.4 Neurotransmitter receptors and ion channels

1.4.1 AMPA receptors

AMPA receptors (AMPA receptors) are ionotropic glutamate receptors and the main mediators of fast excitatory synaptic transmission in the brain. They are homo- or heterotetrameric structures composed of subunits GluA1-4 (Fig. 1.6). Each subunit is made of four domains:

- an intracellular C-terminus which is subject to phosphorylation and regulates AMPAR trafficking and channel conductance (Derkach, Barria and Soderling, 1999; Kristensen *et al.*, 2011);
- a transmembrane domain composed of four segments, M1-M4. The M2 segment is found at the base of the pore and it contains a Q/R editing site;
- a ligand-binding domain, which has a significant role in channel gating and in regulating AMPAR desensitization (Stern-Bach *et al.*, 1998);
- an extracellular N-terminal domain, which plays a role in the assembly of AMPARs and their synaptic localization (Herguedas, Krieger and Greger, 2013; Watson, Ho and Greger, 2017).

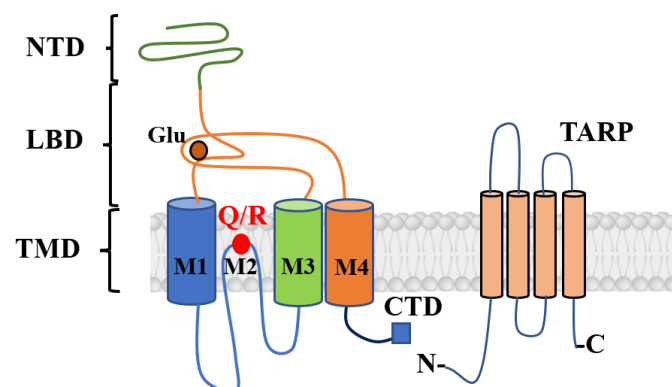


Fig. 1.6. Schematic structure of AMPA receptor subunits. Each subunit has four domains which contain: a large N-terminal extracellular domain (NTD); an extracellular ligand-binding domain (LBD); a transmembrane domain (TMD) containing four segments (M1–4). The M2 segment additionally contains a Q/R editing site and a C-terminal intracellular domain (CTD). AMPARs are usually assembled with transmembrane AMPA receptor regulatory proteins (TARPs) which control many aspects of receptor physiology. Glu: glutamate.

Depending on the subunit composition, AMPARs possess different kinetic properties and ion selectivity. In particular, they can be subdivided into two main classes: Ca^{2+} -permeable AMPARs (CP-AMPA) or Ca^{2+} -impermeable AMPARs (CI-AMPA). CI-AMPA include the GluA2 subunit in which, during RNA editing, a positive arginine (R) replaces a neutral glutamine (Q) at the level of the Q/R site: thus, these receptors are not permeable to

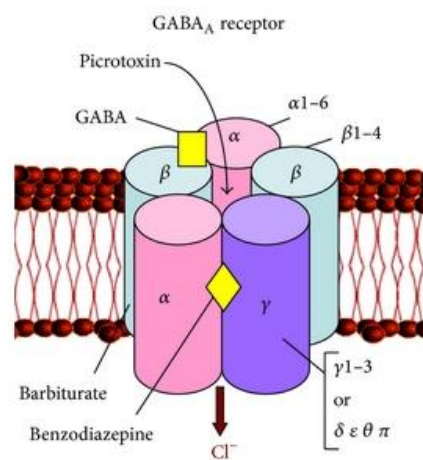
Ca^{2+} ions and they are resistant to intracellular block by polyamines, positively charged molecules present in the cytoplasm which confer AMPARs a characteristic inwardly rectifying current-voltage relationship (Bowie and Mayer, 1995). Principal neurons in the mature brain contain mainly CI-AMPARs (Geiger *et al.*, 1995), while the expression of CP-AMPARs is present in varying proportions in glial cells, like Bergmann glia and NG2 glia (Seifert and Steinhäuser, 1995; Iino *et al.*, 2001). However, the AMPAR composition is dynamically regulated during development or by neuronal activity (Liu and Zukin, 2007). Another peculiar property of AMPARs is their assembly with a variety of auxiliary subunits which regulate every aspect of receptor physiology, from channel kinetics to its localization (see Cull-Candy and Farrant, 2021). The main families of these proteins are the transmembrane AMPAR regulatory proteins (TARPs) and cornichons (CNIH). TARPs are also important regulators of Ca^{2+} -permeability of AMPARs, increasing single-channel conductance and shaping synaptic transmission (Tomita *et al.*, 2005). Importantly, TARP γ 2 also relieves the block by intracellular polyamines, influencing the inward rectification of AMPARs (Soto *et al.*, 2007). Cerebellar BGs express solely CP-AMPARs mainly associated with TARP γ 5 which confer to these cells the ability to properly isolate PC dendritic synapses and ensure functionality of the network (Saab *et al.*, 2012). GluA2-lacking AMPARs in NG2 glial cells have been implicated in cell differentiation and proliferation. In particular, proliferation of NG2 glia increases upon activation of AMPARs both in vivo and in vitro together with elongation and branching of cell processes (Yuan *et al.*, 1998; Mangin *et al.*, 2012). Multiple TARP subunits are assembled with these receptors: for example, TARP γ 2 is associated with membrane delivery of CP-AMPARs to NG2 glia plasma membrane (Zonouzi *et al.*, 2011). In the hippocampus, NG2 glia abundantly express TARPs γ 4, γ 7 and γ 8 and CNIH-2.

1.4.2 GABA receptors

GABA receptors (GABARs) mediate most of the inhibitory transmission in the adult CNS and they are linked to many neurodevelopmental, neurological and psychiatric disorders including epilepsy and anxiety (Korpi and Sinkkonen, 2006; Macdonald, Kang and Gallagher, 2010). GABARs can be divided into two groups: ionotropic ligand-gated GABA_A and metabotropic G protein-coupled GABA_BRs (Olsen and Sieghart, 2008). GABA_ARs are pentameric structures, permeable to chloride, which can be composed of a combination of 19 different subunits: six α , three β , three γ , three ρ , one δ , one ϵ , one π and one θ (see Ghit *et al.*, 2021, Fig. 1.7). Each subunit is composed of four domains: a small extracellular C-terminus; four transmembrane domains which contain the channel pore and allosteric binding sites for barbiturates; an

intracellular domain; an extracellular N-terminus which is the binding site for GABA and drugs like benzodiazepines (BZDs, Sigel and Luscher, 2011). GABA_ARs composed of subunits α 1–3, β 1–3, and γ 2 are localized at the synapse and mediate “phasic inhibition” through a fast membrane hyperpolarization. In contrast, if GABA_ARs contain α 4–6, β 2/3 and δ or ϵ subunits they are localized extra- or peri-synaptically and mediate “tonic inhibition” in which the receptors are activated through GABA spillover (Farrant and Nusser, 2005) mediating long-term hyperpolarization.

Fig. 1.7. GABA_AR structure. GABA_ARs have a pentameric structure. Subunits have binding sites for



GABA but also for antagonists like picrotoxin and different modulators like barbiturates and benzodiazepines. Popova, 2014.

Spillover of GABA is dependent on the expression and activity of GABA transporters (GATs) present in either presynaptic neurons, which express mainly GAT-1, or in astrocytes, mainly expressing GAT-3 (Zhou and Danbolt, 2013). Interestingly, in the immature brain, GABA_ARs mediate excitatory transmission. During the first two weeks of postnatal development, overexpression of a KCl co-transporter (KCC2) changes the Cl⁻ equilibrium potential leading to a shift to a hyperpolarizing effect of GABA (Rivera *et al.*, 1999). NG2 glia has also been found to express GABA_ARs (Lin and Bergles, 2004; Jabs *et al.*, 2005). However, given the lack of expression of KCC2 in these cells, GABA transmission has a depolarizing effect also in the adult brain. Moreover, GABAergic transmission to NG2 glia in the barrel cortex is mainly synaptic in the juvenile brain but it switches to an extrasynaptic mode of transmission in the adult mediated by pure GABA spillover (Vélez-Fort *et al.*, 2010). This switch is due to the downregulation of the γ 2 subunit, present in the juvenile NG2 glia postsynaptic density (Passlick *et al.*, 2013).

1.4.3 Inwardly rectifying potassium (Kir) 4.1 channels

K^+ channels are the main mediators of the repolarization phase of neuronal action potentials. Indeed, thanks to the very negative equilibrium potential for K^+ (E_k), around -85 mV, and the less negative resting potential, these channels allow for the efflux of K^+ from the cytoplasm, after a Na^+ -mediated depolarization, following its electrochemical gradient and quickly bring the cell back to its resting membrane potential. These K^+ channels are also termed outwardly rectifying since they open at depolarized potentials. However, another subtype of K^+ channels activates at negative potentials around E_k , allowing also an influx of K^+ in the cytoplasm (Hagiwara and Takahashi, 1974): these are inwardly rectifying potassium channels (Kir). Kir channels are present in many cell types (see Hibino *et al.*, 2010), including glial cells like retinal Müller glia (Newman, 1993), astrocytes (Higashi *et al.*, 2001), oligodendrocytes (Neusch *et al.*, 2001), BGs (Thomzig *et al.*, 2001) and NG2 glia (Song *et al.*, 2018). They can be classified into seven families, from Kir 1-7. In the brain, Kir channels containing the 4.1 subunit are expressed solely by glial cells. These Kir 4.1 containing channels are homotetramers constituted by two transmembrane domains containing an extracellular loop for ion selectivity (Ohno *et al.*, 2018, Fig. 1.8). Thanks to the expression of these channels, glial cells can maintain their resting membrane potential close to E_k . In astrocytes, Kir 4.1 channels are key players in spatial K^+ buffering (Neusch *et al.*, 2006) influencing neuronal excitability and keeping a low level of K^+ ions in the extracellular space (Djukic *et al.*, 2007). In the spinal cord, Kir 4.1 channels are important for the correct maturation of oligodendrocytes (Neusch *et al.*, 2001). In NG2 glia, Kir 4.1 expression increases during development, eventually becoming the main membrane conductance of these cells (see Seifert and Steinhäuser, 2018).

1.5 Synaptic transmission and plasticity

In the CNS, information flows through the release of neurotransmitters from a presynaptic neuron to the synaptic cleft. Here, neurotransmitters bind to specific receptors on a postsynaptic membrane activating a series of responses. Temporal and spatial summation of signals coming from multiple presynaptic neurons will alter the membrane potential of the postsynaptic cell, leading to the generation of APs at the axon hillock. APs then travel along the axon until the presynaptic terminal, where the depolarization will induce opening of Ca^{2+} channels. Ca^{2+} ions then bind to specific Ca^{2+} -dependent molecules (Perin *et al.*, 1990), which in turn lead to the fusion of neurotransmitter-filled vesicles at the release sites. Most interestingly, vesicle fusion is a probabilistic phenomenon strictly dependent on intracellular Ca^{2+} concentrations. Given the stochastic nature of synaptic release, exocytosis of a single vesicle, called quantum, can happen also in the absence of presynaptic APs. These spontaneous events, called miniature events, can give a lot of information on the properties of the synapse: from the total number of release sites and the probability of neurotransmitter release (P_r) to the amplitude of the post-synaptic response upon the release of a single quantum of neurotransmitter (Lanore and Silver, 2016). The stimulation pattern of a presynaptic neuron will eventually lead to plastic changes in the synapses. Synaptic plasticity is defined as a variation in synaptic strength or efficacy of synapses which is induced by a specific pattern of neuronal activity and it plays a fundamental role in learning and memory formation. Two main forms of plasticity exist in the brain, which differ in the duration of the structural changes that they induce: short-term and long-term plasticity.

1.5.1 Short-term plasticity

In short-term plasticity (STP), changes in synaptic transmission due to repeated stimuli can last from milliseconds to several minutes. STP influences synaptic strength either by modifying the amount of neurotransmitter released from the presynaptic neuron or by changing the response of postsynaptic receptors. The change in synaptic strength can produce either an enhancement or a reduction of the post-synaptic response. If the enhancements last hundreds of milliseconds, STP is termed facilitation and can easily be observed when stimulating the fiber with a pair of stimuli (paired-pulses) separated by an inter-stimulus interval ranging from 50 ms to 200 ms (see Zucker and Regehr, 2002). When enhancements of the post-synaptic response last from a few seconds to several minutes and they are induced by many repeated pulses, we refer to augmentation or post-tetanic potentiation (PTP). All these enhancement mechanisms are due to an increase in the number of vesicles fusing at the presynaptic side (Fisher, Fischer and Carew,

1997). Indeed, every time an AP invades the axon terminal, Ca^{2+} channels open and induce a Ca^{2+} -induced fusion of vesicles containing neurotransmitters. The higher the Ca^{2+} concentration in the presynaptic terminal is, the higher is P_r . After release, Ca^{2+} -buffering mechanisms will bring the Ca^{2+} concentration back to its basal levels. When two APs come temporally close to each other, Ca^{2+} ions which were not completely extruded from the terminal (residual Ca^{2+}) summate to the ions coming upon the next AP, increasing the probability of neurotransmitter release (Fig. 1.8A). Facilitation is typical in brain regions with low-probability of release, like in synapses between Schaffer collaterals and CA1 pyramidal neurons in the hippocampus. However, STP comes also in the form of a reduction of the post-synaptic response and it is named short-term depression or, in case it is generated experimentally by two closely spaced stimuli, paired-pulse depression (PPD, Fig. 1.8B). In this case both pre- and post-synaptic mechanisms can contribute. A classic example of presynaptic mechanisms for PPD is vesicle depletion: here, the first stimulus induces the release of a large amount of neurotransmitter, depleting the total amount of vesicles available. Since the replenishing of the pool can range from hundreds of milliseconds to many seconds (Betz, 1970; Ryan and Smith, 1995), when the second stimulus arrives, a lower number of vesicles will be ready for release and the post-synaptic response will be smaller. Other presynaptic factors can contribute to PPD, like presynaptic calcium channel inactivation (Forsythe *et al.*, 1998), failure of AP initiation or conduction failure (Muñoz-Cuevas, Vara and Colino, 2004) and negative feedbacks through autoinhibitory metabotropic receptors (Davies and Collingridge, 1993; Scanziani *et al.*, 1997). An example of synapse showing PPD is the CF-PC synapse in the cerebellum: here, PPD is due mainly to vesicle depletion (Hashimoto and Kano, 1998). Nevertheless, also postsynaptic receptors can have a role in shaping the final postsynaptic response. In fact, after the first AP, most ionotropic receptors enter a non-conductive state called desensitization (Katz and Thesleff, 1957). Since recovery from desensitization can occur in a brief time (10 ms – 50 ms), depending on the receptor subtype (Hestrin, 1992; Raman and Trussell, 1995), this does not always influence PPD. Another postsynaptic mechanism contributing to PPD is the saturation of postsynaptic receptors after exposure to a high amount of neurotransmitter. Desensitization and saturation are strictly dependent on the structural properties of the synapse: indeed, in CF-PC synapses these mechanisms were not detected since the excess glutamate is readily taken up by transporters present in BGs, which tightly enwrap the synapses and regulate the dynamics of neurotransmitter clearance (see Xu-Friedman and Regehr, 2004) avoiding glutamate spillover (Wadiche and Jahr, 2001). Contrary to PPF, PPD is predominant in synapses with high P_r .

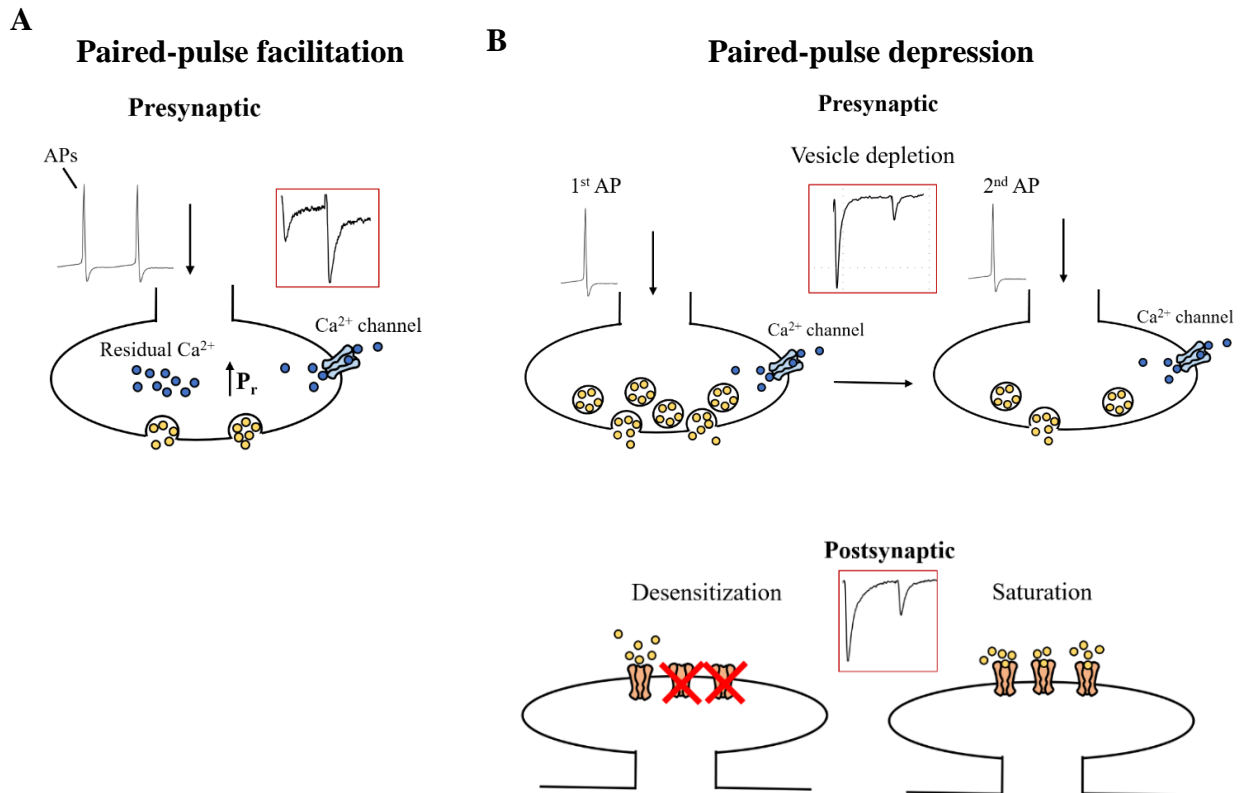


Fig. 1.8. Short-term plasticity. Different forms of short-term plasticity, involving both presynaptic and post-synaptic components. **A)** Residual Ca^{2+} hypothesis for paired-pulse facilitation: when the first AP arrives, Ca^{2+} entry through voltage-gated Ca^{2+} channels induces neurotransmitter release from vesicles at presynaptic sites. If the 2nd stimulus comes in a brief time (50-200 ms), Ca^{2+} that could not be extruded from the terminal will summate to Ca^{2+} entering upon the 2nd AP, increasing P_r . **B)** Top: in areas with high probability of release (P_r), most of neurotransmitter-filled vesicles are depleted on the first stimulus, leading to reduced vesicle availability on the second AP and depression. Bottom: desensitization or saturation of postsynaptic receptors can also lead to paired-pulse depression. Insets in red represent post-synaptic responses in each case.

1.5.2 Long-term plasticity

Changes of the postsynaptic strength following a repetitive stimulation can also endure for a period ranging from tens of minutes to years (Abraham *et al.*, 2002). This is called long-term plasticity, which is thought to be the main process leading to long-lasting memory formation. These long-term changes can come in the form of a potentiation (LTP, Bliss and Lømo, 1973) or a depression (LTD, Dudek and Bear, 1992; Ito and Kano, 1982). In the hippocampus, both these mechanisms are thought to be important for spatial learning and memory (Ferbinteanu, Holsinger and McDonald, 1999; Whitlock *et al.*, 2006; Ge *et al.*, 2010) while in the cerebellum they are the basis for motor learning. Both LTP and LTD share similar molecular mechanisms. Indeed, AMPAR-mediated depolarization of the post-synaptic cell lifts the Mg^{2+} block of N-

Methyl-D-aspartic acid (NMDA) receptors and promotes Ca^{2+} entry into the cell. Ca^{2+} ions will then activate intracellular Ca^{2+} -dependent molecules like Ca^{2+} /calmodulin protein kinase II (CaMKII). At early-LTP (e-LTP) stages, CAMKII binds to NMDARs and increases AMPAR conductance through their phosphorylation (Incontro *et al.*, 2018) but also promotes the insertion of more AMPARs into the plasma membrane (see Malenka, 2003). After this transient e-LTP phase, a late phase of LTP (l-LTP) leads to changes in gene expression and protein synthesis which will promote long-term structural and functional changes of the synapse (see Bramham, 2008). While the mechanisms described above involve only the post-synaptic cell, it is important to note that LTP or LTD can also be mediated by presynaptic changes, e.g., an alteration of neurotransmitter release (Ahmed and Siegelbaum, 2009). Whether pre- or post-synaptic changes predominate is still under debate but it is thought to depend on the LTP induction protocols and on the properties of the synapses considered (MacDougall and Fine, 2014).

1.5.3 Long-term plasticity in the cerebellum

Long-term plasticity can occur in all layers of the cerebellar cortex, involving both interneurons and glutamatergic neurons (see D'Angelo, 2014). The PC-PF synapse in the molecular layer is the most widely studied, since it has always been the main target to explain the cerebellar motor learning theory (Marr, 1969; Albus, 1971). This synapse can undergo several types of plasticity, which can involve either pre- or the post-synaptic neurons. The first mechanism which has been described to be implicated in motor learning is postsynaptic PF-LTD (Ito and Kano, 1982). This requires an elevated level of intracellular Ca^{2+} (Hansel and Linden, 2000), obtained through activation of AMPARs and metabotropic glutamate receptors (mGluR), and it is dependent on factors like $\text{PKC}\gamma$, nitric oxide, NMDARs and endocannabinoid receptors (see Smeets and Verbeek, 2016). Another form of plasticity, postsynaptic PF-LTP, counteracts the effects of PF-LTD (Han, Grant and Bell, 2000). While PF-LTP is not dependent on NMDARs and mGluRs, it still shares many signalling cascades with PF-LTD (Titley and Hansel, 2016). Importantly, PF-LTP requires lower levels of intracellular Ca^{2+} than PF-LTD. Whether LTP or LTD is induced depends on multiple factors, one of the most important being CF innervation of PCs, which act as “control switch” (Smeets and Verbeek, 2016). Indeed, CFs make several synapses on one PC leading to a strong depolarization induced by the complex spike which allows the cell to reach the threshold for PF-LTD. On the contrary, if the input from the CFs is weak, PF-LTP will predominate. Briefly, the higher the intracellular $[\text{Ca}^{2+}]$ is, the higher is the probability for PF-LTD induction, while a low $[\text{Ca}^{2+}]$ promotes PF-LTP. Interestingly, this scheme of

bidirectional plasticity has also been observed in the hippocampus (Jörntell and Hansel, 2006). Therefore, to induce LTD *in vitro*, it is necessary to stimulate simultaneously PFs and CFs, or to induce a depolarization in PCs while stimulating PFs. On the other hand, LTP can be induced by PF stimulation only, through sets of either high- or low-frequency stimuli (Bouvier *et al.*, 2016; Lev-Ram *et al.*, 2002). Both PF-LTP and PF-LTD can also be presynaptic: the former can be induced by 4-8 Hz PF stimulation and it is dependent on cyclic AMP (Salin, Malenka and Nicoll, 1996), while the mechanisms for the latter are still being investigated (Titley and Hansel, 2016).

1.6 Neurotrophins

Neurotrophic factors, or neurotrophins, are essential molecules that regulate many cellular processes, from neuronal survival and synaptogenesis to synaptic plasticity (see Park and Poo, 2013). While the first neurotrophin to be purified was nerve-growth factor (NGF, Levi-Montalcini, 1987), three other molecules were later discovered: brain-derived neurotrophic factor (BDNF, Barde *et al.*, 1982), and neurotrophin 3 and 4 (NT-3 and NT-4, see Lewin and Barde, 1996).

1.6.1 BDNF

BDNF is a protein encoded by the *bdnf* gene and it is secreted by different cell types, including neurons (Dean *et al.*, 2009), astrocytes (Baumbauer *et al.*, 2009; Zhang *et al.*, 2012; Datta *et al.*, 2018), microglia (Gomes *et al.*, 2013; Zhou *et al.*, 2019) and conceivably NG2 glia (Tanaka *et al.*, 2009; Prasad *et al.*, 2017) upon modulation by neuronal activity. BDNF can be secreted by cells in two main forms: proBDNF and its cleaved counterpart, mature BDNF (mBDNF). These two forms have opposing effects on cell behaviour by activating two different receptors: proBDNF activates p75^{NTR} receptor complex and mBDNF activates the TrkB receptor. Activation of the p75^{NTR} leads to apoptosis (Teng *et al.*, 2005) and promotes long-term depression in CA1 pyramidal neurons upon low-frequency stimulation (Woo *et al.*, 2005) through a NMDAR-dependent mechanism. Moreover, the proBDNF- p75^{NTR} pathway mediates structural changes in synapses of DG neurons and CA1 pyramidal neurons reducing dendritic complexity and spine density (Yang *et al.*, 2014). On the other hand, mBDNF binds to TrkB receptors inducing their dimerization and autophosphorylation of tyrosine residues. Afterwards, multiple molecular pathways can be activated (also see Leal *et al.*, 2017):

- the PLC γ -mediated pathway which induces an increase in intracellular Ca²⁺ (Amaral and Pozzo-Miller, 2012) necessary for l-LTP at CA1 synapses (Minichiello *et al.*, 2002);

- the Ras-MAPK pathway which promotes the transcription of genes promoting cell survival (Tao *et al.*, 1998);
- the PI3K pathway which leads to local protein synthesis in neuronal dendrites through the activation of the mammalian target of rapamycin (mTOR, Takei *et al.*, 2004).

mBDNF is also highly expressed in the cerebellum, where it plays a significant role in circuit development promoting granule cell migration (Segal, Takahashi and McKay, 1992; Zhou *et al.*, 2007) and CF pruning (Johnson, Craig and Yeh, 2007). While its role on PC development is still debated (see Camuso *et al.*, 2022), PF-PC synapses show an impaired short-term plasticity and presynaptic vesicle distribution in BDNF^{-/-} mice (Carter *et al.*, 2002). Since proBDNF and mBDNF exert opposing functions, it is important that their ratio is maintained constant in the extracellular space to ensure correct neurotrophic effects in the region. Therefore, enzymes involved in cleavage of proBDNF, like plasmin or matrix metalloproteinases (MMF), also have an essential role in long-term plasticity (Pang *et al.*, 2004). Interestingly, several evidences implicate mBDNF in both activity- dependent and - independent myelination (see Fletcher *et al.*, 2018; Fig. 1.9). Indeed BDNF^{-/-} mice show reduced levels of important myelin proteins like MBP and PLP in the hippocampus (Djalali *et al.*, 2005). Moreover, mBDNF can induce an increase in glutamatergic transmission to NG2 glia, promoting its differentiation (Gautier *et al.*, 2015).

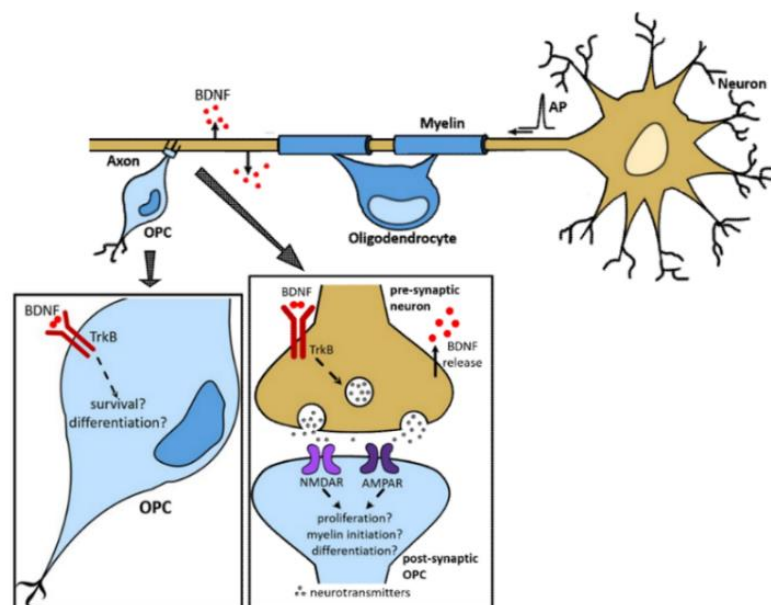


Fig. 1.9. Roles of mBDNF in myelination. Release of BDNF from axons of presynaptic neurons could influence NG2 glia survival and differentiation both through activation of TrkB or glutamate receptors expressed on NG2 glial cell membranes (Adapted from Fletcher *et al.*, 2018).

2 Aim of the Study

Grey matter NG2 glia constitute a heterogeneous glial population whose functions remain incompletely understood. Their ability to form functional synapses with glutamatergic and GABAergic neurons distinguishes them from other glial cell types. However, how these synapses change during development and how their properties differ between brain regions still has to be elucidated. Another fundamental, yet unanswered, question concerns the purpose of these synapses in the CNS, whether they can influence neuronal communication and ultimately behaviour. These points will be addressed in detail in this work.

1) Developmental and regional differences of AMPAR expression in NG2 glia.

In the hippocampus, NG2 glia expresses AMPAR at glutamatergic synapses. Previous studies have shown that in both adult and juvenile mice, AMPARs have an intermediate Ca^{2+} -permeability (Seifert and Steinhäuser, 1995; Seifert *et al.*, 2003). Whether the expression of CP-AMPARs changes during development will be investigated (Hardt *et al.*, 2021). In the adult hippocampus, SC activation of AMPARs in NG2 glia gives rise to small PSCs (Bergles *et al.*, 2000; Jabs *et al.*, 2005). Cerebellar CFs also form synapses with NG2 glia, producing 10-fold larger PSCs (Lin *et al.*, 2005). Whether a different composition of AMPARs or a larger glutamate transient could lead to a higher synaptic efficiency in the cerebellum will be investigated in this section.

2) Impact of AMPARs in hippocampal and cerebellar NG2 glia on neuronal signalling and behaviour.

The physiological impact of AMPARs in NG2 glia will be studied thanks to a previously generated mouse line with an inducible deletion of AMPAR subunits GluA1-4 in NG2 glia. The consequences of this deletion on neuronal plasticity, intrinsic neuronal firing and mouse behaviour will be revealed. Moreover, the mechanisms by which NG2 glia signals back to neurons and the relevance of NG2 glia-expressed CP-AMPARs for neuronal transmission will be investigated.

3) Impact of NG2-glia Kir 4.1 channels in hippocampus and cerebellum.

In a recent work, Timmermann *et al.* (2023) has shown that a proper Kir4.1 signalling in NG2 glia is also a prerequisite for normal neuronal transmission in the hippocampus. Indeed, inducible deletion of Kir 4.1 channels in NG2 glia leads to reduced plasticity in hippocampal pyramidal neurons together with increased myelination and behavioural alterations. The

mechanisms by which NG2 glia might influence neuronal plasticity is unclear. In this part, the BDNF-TrkB pathway (chapter 1.6.1) will be targeted to check whether LTP can be rescued in these transgenic mice. Additionally, synaptic properties of hippocampal and cerebellar NG2 glia in Kir 4.1 ko mice as well as possible dysfunctions of cerebellar PF-PC LTP will be investigated.

4) Developmental switch of GABAR signalling in hippocampal NG2 glia.

Previous studies have shown that GABA_AR-mediated signalling to NG2 glia in the barrel cortex becomes mainly extrasynaptic in adult mice (Vélez-Fort *et al.*, 2010). Whether this developmental switch in GABAergic transmission occurs also in the hippocampus is unclear. Therefore, in this section, experiments have been performed to test whether GABA_AR-mediated transmission to NG2 glia occurs through a pure spillover mechanism.

3 Materials

3.1 Substances

Substance	Company
7,8 dihydroxyflavone	Sigma-Aldrich, München, Germany
Acetic acid	Roth, Karlsruhe, Germany
Agarose	Invitrogen, Darmstadt, Germany
BAPTA	Sigma-Aldrich, München, Germany
BaCl ₂	Sigma-Aldrich, München, Germany
CaCl ₂ ·6H ₂ O	Honeywell international Inc.
Carbogen	Linde, Pullach, Germany
CGP 55845 hydrochloride	Biotechne Tocris Bioscience, Bristol, UK
Cyclothiazide	Abcam, Cambridge, UK
D-AP5	Biotechne Tocris Bioscience, Bristol, UK
DMSO	Sigma-Aldrich, München, Germany
dNTPs	Applied Biosystems, Darmstadt, Germany
DTT	Thermo Fisher, Waltham, USA
Dynabeads Oligo (dT) ₂₅	Invitrogen, Darmstadt, Germany
EDTA Na ₂	Sigma-Aldrich, München, Germany
EGTA	Sigma-Aldrich, München, Germany
Ethanol >99.5%	Roth, Karlsruhe, Germany
Ethidium bromide	Roth, Karlsruhe, Germany
First-Strand Buffer	Invitrogen, Darmstadt, Germany
Gamma-DGG	Biotechne Tocris Bioscience, Bristol, UK
GYKI 53655 hydrochloride	Biotechne Tocris Bioscience, Bristol, UK
Glucose	AppliChem GmbH, Darmstadt, Germany
HEPES	AppliChem GmbH, Darmstadt, Germany
IEM-1460	Biotechne Tocris Bioscience, Bristol, UK
Isofluran	Piramal Healthcare, Morpeth, UK
Kainic acid	Abcam, Cambridge, UK
KCl	AppliChem GmbH, Darmstadt, Germany
K-gluconate	Sigma-Aldrich, München, Germany
Low Molecular Weight DNA Ladder	New England BioLabs, Ipswich, USA

Substance	Company
Lysis/binding buffer	Invitrogen, Darmstadt, Germany
Na ₂ -ATP	Sigma-Aldrich, München, Germany
Na-Azide	Sigma-Aldrich, München, Germany
NaCl	AppliChem GmbH, Darmstadt, Germany
NaH ₂ POH ₄	AppliChem GmbH, Darmstadt, Germany
NaHCO ₃	AppliChem GmbH, Darmstadt, Germany
Naspm trihydrochloride	Alomone labs, Jerusalem, Israel
NBQX	Biotechne Tocris Bioscience, Bristol, UK
Neural Dissociation Kit	Miltenyi, Germany
NNC 711	Biotechne Tocris Bioscience, Bristol, UK
MgSO ₄ .7H ₂ O	AppliChem GmbH, Darmstadt, Germany
MinElute PCR Purification Kit	Qiagen, Hilden, Germany
oligo-dT ₂₄ -primer	Eurogentec, Lüttich, Belgien
PCR Buffer	Thermo Fisher, Waltham, USA
Picrotoxin	Abcam, Cambridge, UK
Platinum® Taq Polymerase	Thermo Fisher, Waltham, USA
Quinine	Sigma-Aldrich, München, Germany
Random Hexamer Primer	Roche Applied Science, Mannheim, Germany
RNasin® RNase Inhibitor	Promega, Madison, USA
Saccharose	AppliChem GmbH, Darmstadt, Germany
(S)-SNAP 5114	Biotechne Tocris Bioscience, Bristol, UK
Sunflower seed oil from Helanthius annus	Sigma-Aldrich, München, Germany
Superscript® III Reverse Transcriptase	Invitrogen, Darmstadt, Germany
Takyon real-time PCR mastermix	Eurogentec, Lüttich, Belgien
Tamoxifen	Sigma-Aldrich, München, Germany
Taq DNA Polymerase	Thermo Fisher, Waltham, USA
Taqman primer/probe mix	Applied Biosystems, Darmstadt, Germany
DL-TBOA	Biotechne Tocris Bioscience, Bristol, UK
Tris	AppliChem GmbH, Darmstadt, Germany
TTX	Abcam, Cambridge, UK

3.2 Devices

Device	Company
A/D converter (patch clamp)	ITC-16, HEKA Elektronik, Lambrecht, Germany
A/D converter (fEPSP recordings)	USB-6221 (National Instruments, Austin, USA)
Amplifier (patch-clamp)	EPC-800, HEKA Elektronik, Lambrecht, Germany
Amplifier (fEPSP recordings)	EXT-02B, npi electronic GmbH, Tamm, Germany
Bath chamber/shifting table	Base plate 500B, shifting table V240, bridge 500 with SM-5 control unit, Luigs & Neumann, Ratingen, Germany
CCD camera	VX45, Optronis, Kehl, Germany
Concentric bipolar electrode (fEPSP recordings)	FHC, Bowdoin, USA
Current stimulator	DS3, Digitimer Ltd, Hertfordshire, UK
De-noise device (fEPSP recordings)	HumBug Noise eliminator, Quest Scientific Instruments Inc
Differential amplifier	DPA-2FS, npi electronic GmbH, Tamm, Germany
Electrophoresis	E0763 (Sigma-Aldrich, Munich, Germany)
Flow cytometer	FACS Aria III 70 μ m nozzle, BD Biosciences, Heidelberg, Germany
Fluorescence system	Polychrome II, 75W xenon lamp (Till Photonics, Martinsried, Germany)
Glass pipettes	Borosilicate glass GB150F-10 and GB150F-10P (Science Products, Hofheim, Germany)
Chamber heating device	Temperatur controller V, Luigs & Neumann
Interface-type recording chamber (fEPSP recordings)	custom-made by AG Heinemann, Charité, Berlin, Germany
Magnet stirrer	RCT basic (IKA Labortechnik, Staufen, Germany)
Magnet stirrer, heating	VELP Scientifica, Usmate, Italy
Micromanipulator	Micromanipulator 6540 R094 with control unit 5171, Eppendorf, Hamburg, Germany LN mini 25, Luigs & Neumann, Ratingen, Germany
Microscope (patch-clamp)	Axioskop FS2, Zeiss, Oberkochen, Germany

Device	Company
Microscope objectives (patch-clamp)	CP-Achromat (5x; NA: 0.12), Zeiss, Oberkochen, Germany LUMPlan FI/IR (60x; NA: 0.90), Olympus, Tokio, Japan
Oscilloscope	HM 507, Hameg, Mainhausen, Germany
PCR-Cycler	PTC-200, Biozym, Hessisch Oldendorf, Germany
PCR-Cycler (RT-PCR)	CFX 384, Biorad, Munich, Germany
pH meter	766 Laboratory pH Meter, Knick, Berlin, Germany
Sonificator	Transonic 5520, Elma-Ultrasonic, Singen, Germany
Pump	ISM 930C, Ismatec/Idex, Wertheim, Germany
Vortexer	VWR, Darmstadt, Germany
Vibration isolation table	Vision Isostation VIS-3036, Newport, Irvine, USA
Vibratome	Leica VT1200S, Leica Microsystems, Wetzlar, Germany
Water bath heater	Gesellschaft für Labortechnik (GFL), Burgwedel, Germany
Weighing scales	Acculab vicon (Bradford,USA) Sartorius Practum 3102-1S, Sartorius, Göttingen, Germany BP121S, Sartorius, Göttingen, Germany

3.3 Software

Software	Company
Easy electrophysiology 2.5.2	Easy Electrophysiology Ltd, London, UK
EthoVision XT tracking system	Noldus, Wageningen, Netherlands
IGOR Pro 7, 8, 9	WaveMetrics, Lake Oswego, USA
Office 2016	Microsoft, Redmond, USA
Origin Pro 9.1	OriginLab, Northampton, USA
pClamp 10, 11	Molecular Devices, Union City, USA
TIDA 5	HEKA Elektronik, Ludwigshafen, Germany
R	R Core Team, General Public License
R Studio	Posit Software, PBC formerly RStudio, Boston
Zotero	Corporation for Digital Scholarship, USA
WinWCP 4.6.1	University of Strathclyde, Scotland,UK
Kdenlive 22.12.1	KDE

3.4 Solutions

3.4.1 Intracellular solutions

Intracellular solution 1

Substance	mM
KCl	130
MgCl ₂	2
CaCl ₂	0.5
BAPTA	5
HEPES	10
Na ₂ -ATP	3

Intracellular solution 2

Substance	mM
CsCl	120
MgCl ₂	2
CaCl ₂	0.5
BAPTA	5
HEPES	10
Na ₂ -ATP	3
TEA	10

Intracellular solution 3

Substance	mM
KCl	130
MgCl ₂	2
CaCl ₂	0.5
BAPTA	5
HEPES	10
Na ₂ -ATP	3
Naspm	0.1

Intracellular solution 4

Substance	mM
KCl	130
MgCl ₂	2
CaCl ₂	0.5
BAPTA	5
HEPES	10
Na ₂ -ATP	3
Spermine	3

Intracellular solution 5

Substance	mM
K-gluconate	125
MgCl ₂	2
EGTA	0.5
Hepes	10
KCl	20
NaCl	3
Na ₂ -ATP	3

3.4.2 Extracellular solutions

Preparation solution

Substance	mM
NaH ₂ PO ₄	1,25
NaCl	87
KCl	2.5
MgCl ₂	7
CaCl ₂ *6H ₂ O	0.5
Glucose	25
NaHCO ₃	26
Saccharose	61.3

aCSF for 35°C

Substance	mM
NaH ₂ PO ₄	1.25
NaCl	132
KCl	3
MgCl ₂ *6H ₂ O	2
CaCl ₂ *6H ₂ O	2
Glucose	10
NaHCO ₃	20

During preparation and use, all extracellular solutions were gassed with carbogen (95%O₂/5%CO₂). aCSF was made freshly every day or kept in the fridge to be used for a maximum of 2-3 consecutive days.

4 Methods

4.1 Animals

In this study, both adult (p50-70) and young mice (p7-12) have been used. Mice were kept under standard housing conditions (12/12 h light/dark cycle, food and water ad libitum). All experiments were carried out in accordance with local, state and European regulations (veterinary licenses 84-02.04.2015.A411, 81-02.04.2017.A437, 81-02.04.21A189). Efforts were made to minimize the use of animals in all procedures.

4.1.1 NG2-YFP knock-in mouse line

In this mouse line, NG2 glia expresses the enhanced yellow fluorescent protein (EYFP) allowing fast recognition and localization of NG2-positive cells under fluorescent light. This genotype, based on a C57Bl/6N background, was generated through homologous recombination in which the cDNA for EYFP was inserted into the first exon of the NG2 gene allowing EYFP expression under the NG2 promoter (Karram *et al.*, 2008).

4.1.2 NG2-CreERT2 x Rosa26-EYFP

In this line, the CreERT2 sequence (see section 4.2) was inserted into the first exon of the NG2 gene so that the NG2 promoter drives CreERT2 expression. CreERT2 is a modified version of the human estrogen receptor (ERT2) which allows regulation of Cre activity by estrogen analogs such as tamoxifen (Huang *et al.*, 2014). To visualize Cre activity, the NG2-CreERT2 mouse line was crossbred with a reporter line TgH(Rosa26-floxed-stop-EYFP) (Rosa26-EYFP). Thus, the Rosa26 promoter, which is ubiquitously expressed, controls expression of EYFP. Since these mice were used as controls in the experiments, they will be named control mice.

4.1.3 NG2-CreERT2 x GluA1/fl x Rosa26-EYFP

Here, the previously described control mice (section 4.1.2) were crossbred with lines having genes corresponding to the four AMPARs subunits flanked by loxP sites (NG2-CreERT2 x GluA1fl/fl; GluA2fl/fl; GluA3fl/fl; GluA4fl/fl x Rosa26-EYFP). Therefore, injection of tamoxifen will induce AMPARs deletion in NG2 glia. These mice are herein after termed GluAko mice. GluAko mice expressing only the GluA3 subunit of AMPARs are named GluA3WT.

4.1.4 NG2-CreERT2 x Kir4.1fl/fl x Rosa26-EYFP

In this case, mice with the floxed Kir4.1 gene (Kir4.1 fl/fl) were crossbred with the control line, generating progeny lacking Kir4.1 channels in NG2 glia after tamoxifen injection. These mice will be called Kir4.1 ko.

4.2 Inducible CreERT2-loxP recombination system

The Cre-LoxP system is a site-specific recombination system which allows for targeted insertion, deletion or exchange of DNA sequences in a cell (see Álvarez-Aznar *et al.*, 2020). The system relies on the Cre recombinase enzyme, which recognizes and binds to specific LoxP sequences in the genome. The LoxP sequence is a 34-base-pair sequence containing two 13bp palindromic sequences which flank a central 8bp non-palindromic sequence. When the Cre recombinase binds to two LoxP sites, it mediates recombination of the DNA between the two sites, resulting in deletion or inversion of DNA sequences, depending on the orientation of the flanking loxP sites. Conditional gene deletion is accomplished through the regulation of Cre recombinase by a promoter specific to a tissue or cell type. If a gene or a reporter is located next to a loxP-flanked STOP codon, activation of Cre will promote overexpression of that gene. In order to achieve a time-sensitive deletion or overexpression of a gene, Cre can be combined to a modified estrogen receptor (ERT2, Feil *et al.*, 1997). Indeed, CreERT2 is usually unable to enter the nucleus by itself. However, the estrogen receptor agonist tamoxifen can bind to ERT2 and aids its translocation to the nucleus, where it will bind loxP-flanked target genes. For this study, mice containing LoxP sequences (control, GluAko, GluA3WT and Kir4.1 ko mice) were given tamoxifen through intraperitoneal injection at around 3-4 weeks of age. Tamoxifen protocols were optimized to reach the highest recombination rate with the lowest concentration, which, for each mouse, consisted of 1.5mg of tamoxifen dissolved in ethanol (10µl) and sunflower seed oil (90µl) given once a day for three consecutive days. Electrophysiological recordings and behavioural tests were performed at least three weeks after tamoxifen injection.

4.3 Electrophysiology

4.3.1 Acute brain slice preparation

For slice preparation, mice were anesthetized with isoflurane and decapitated. The brain was surgically removed and placed into ice-cold preparation solution. Depending on the brain region and the section to be studied, cutting procedures were different:

-
- Parasagittal cerebellar slices: in this case the brain was cut off at the level of the midbrain. The cerebellar vermis and paravermal regions were isolated by cutting off the cerebellar hemispheres at the level of the primary fissures. The tissue was then put on one side and transferred to a glue-covered specimen holder;
 - Transverse cerebellar slices: the brain was cut off at the level of the midbrain. The cerebellum, kept upright, was then glued to a specimen holder;
 - Coronal hippocampal slices: the cerebellum and part of the frontal lobe of the brain were cut off. The brain was then glued on its frontal part;
 - Horizontal hippocampal slices: the cerebellum, part of the frontal lobe and a thin part of the dorsal brain were cut off. The brain was glued on its dorsal part. This cutting section was used only for field potential recordings.

The specimen holder was then placed in a vibratome buffer tray, filled with ice-cold preparation solution and surrounded by ice. Slice thickness was 300 μm for the hippocampal coronal or horizontal slices and 250 μm for cerebellar transverse and sagittal slices. After cutting, slices were transferred to the preparation solution kept in a bath heater at 35°C. After 15 min, slices were moved again to warm aCSF which was left to gradually cool down to room temperature. Slices were ready to be used for recordings around one hour after cutting.

4.3.2 Patch-clamp setup

The patch clamp setup consisted of an upright microscope (Axioscope FS) placed on top of an anti-vibration table. The microscope had two objectives, a 10X objective to visualize most of the slice and select the region of interest and a 60X immersion objective to localize single cells. Slices were placed on a slice holder into the recording chamber of the microscope and were continuously perfused with aCSF or aCSF-based solutions at a rate of 1.40 ml/min through a tubing system connected to a pump. A valve-based connection allowed for a fast and air bubble-free exchange of solutions during the recordings. In some experiments, used solutions were filtered and recycled. The recording chamber was also connected to a heating device which kept bath temperature at 35°C. A CCD camera allowed visual signals to be shown on an external monitor. To enhance contrast of the images, differential interference optics (DIC) were connected to the microscope. A fluorescent xenon lamp system with a manually set wavelength of 490 nm helped visualization of fluorescent EYFP cells. The regions of interest could be clearly visualized thanks to a motorized focus system and an electrical shifting stage. Two electrically-driven micromanipulators were used to move both the recording and the stimulation electrodes. Both electrodes were made of teflon-coated silver material, with a manually

chlorinated tip. The recording electrode was connected to a headstage (preamplifier), in turn connected to the patch-clamp amplifier (EPC-800). A reference electrode, made of a silver/silver chloride pellet, was also connected to the headstage, and placed in the recording chamber. Analogue signals from the amplifier were digitized through an A/D converter in order to be visualized through the computer software (Tida). The same signals could also be independently visualized on an oscilloscope connected to the amplifier. Since low background noise is critical for useful patch-clamp recordings, microscope, heating system, amplifier, oscilloscope, stimulation device and microscope stage were all grounded to a single point on the anti-vibration table surface to reduce electrical noise during recordings. The stimulation electrode was further connected to the reference electrode and to the headstage.

4.3.3 Patch-clamping protocol

The whole-cell patch-clamp technique was used in this study to record electrical signals from cells (Neher and Sakmann, 1976). This technique can be used in two different modes: voltage-clamp and current-clamp. In the former, the experimenter can set a voltage for the cell (command potential) and measure the currents flowing through the membrane. The amplifier can keep the selected voltage thanks to a feedback circuit present in the headstage. On the other hand, current-clamp is used in this study to measure spontaneous activity of the cells when no current is injected and cells can maintain their physiological membrane potential. To patch the selected cells, glass pipettes were pulled from a borosilicate glass filament and their small tip was filled with intracellular solution using a microloader pipette. Pipette tip sizes are usually in the micrometer range and their resistance is between 2 and 4 M Ω . The chlorinated tip of the recording electrode (Ag/AgCl-electrode) was then inserted into the pipette. A pressure system connected through tubes to the pipette holder ensured a continuous positive pressure on the pipette tip, which helped in keeping it clean and in blowing away the tissue while approaching the selected cell. To monitor changes in the pipette resistance, 10 mV depolarizing steps were continuously applied. After coming in contact with the membrane of the cell with the pipette tip, positive pressure was released and a patch of the cell membrane would be directly pulled into the tip accompanied to a sudden increase in pipette resistance (which should eventually reach at least 1 G Ω). If necessary, negative pressure was applied to easily obtain a gigaOhm seal (gigaseal). In the meantime, the holding potential is decreased from 0 to -70 or -80 mV. Next, capacitive artefacts were compensated. Finally, by applying short pulses of negative pressure, the cell membrane was ruptured to gain electrical access to the entire cell (whole-cell patch-clamp mode). NG2 glia was recorded in the molecular layer of lobule VI in the

cerebellum and in the stratum radiatum of the CA1 region of the hippocampus. Purkinje neurons were located in lobule VI, either in Z- or Z+ areas. Discrimination between different zebrin regions (see chapter 1.1.3) was first made through visual localization based on literature data shown in Fig. 1.3B. Subsequent to functional analyses, the respective cells were harvested for further RT-PCR analysis of Zebrin mRNA (chapter 4.5.3).

4.3.4 Liquid junction potential

A liquid junction potential (LJP) occurs when two solutions of different ionic concentrations are brought into contact with each other. In a typical patch-clamp experiment, the patch electrode is filled with a solution that has an ionic concentration different from the extracellular fluid. When the patch electrode is positioned in close proximity to the cell membrane, a liquid junction is formed between the two solutions, which creates a potential difference. The LJP interferes with the measurement of the cell's membrane potential and can cause errors in the interpretation of the electrical signals. LJP can be calculated based on the mobility of ions present in the solutions. For this study, LJP was calculated with the Patcher's Power Tools of IGOR Pro. LJP was then compensated during experiments.

4.3.5 Passive membrane properties

The first parameters that could be calculated during patch-clamp experiments are passive membrane properties, i.e., membrane resistance (R_m) and membrane capacitance (C_m). Indeed, the cell represents an electrical circuit (Fig. 4.1A) in which a capacitor is connected in parallel with a resistor. In this model, the plasma membrane of the cell acts as a capacitor because it can store electrical charge in response to changes in voltage. The capacitor can store an amount of charge (C_m) which is proportional to its size. Therefore, in the case of the cell membrane, C_m could be considered as a measure of the cell surface area. The ion channels are modeled as resistors in electrical circuit models because they control the flow of ions in and out of the cell. The different properties of ion channels determine R_m . While performing whole-cell recordings, the resistance between the electrode and the cytoplasm is in series with R_m and it is called series resistance (R_s). R_s depends on the shape of the pipette tip and on the conductance of the pipette solution. Since R_s can lead to voltage measurement errors, it was constantly monitored during recordings and cells were discarded when R_s values were exceeding 20 M Ω or showed a great variation in time.

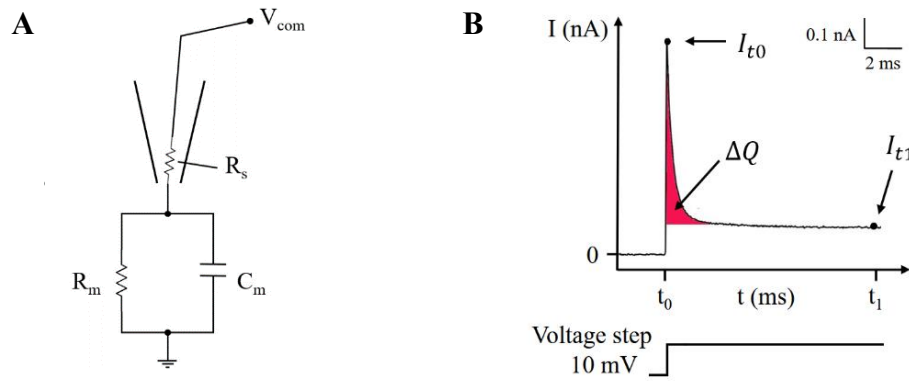


Fig. 4.1. Calculation of passive membrane properties. **A)** Schematic representation of a model cell circuit. V_{com} =command voltage given by the amplifier; R_s : series resistance; R_m : membrane resistance; C_m : membrane capacitance. **B)** Sample trace obtained by the average of 10 depolarizing pulses of 10 mV. Current flow first charges the capacitor (I_{t0}) then reaches a steady-state (I_{t1}). The electrical charge stored by the capacitor is calculated through the integral of the capacitive current (ΔQ , in red).

Calculation of passive membrane parameters was made after giving depolarization pulses of 10 mV (50 ms duration) to cells in whole-cell mode. This would evoke current responses as shown in Fig. 4.1B. As in a RC circuit, the current change would first recharge the capacitor (capacitive current, I_{t0}) then pass through the resistors and reach a steady state (I_{t1}). Since I_{t0} is only dependent on R_s , this latter can be calculated through the first Ohm's law:

$$R_s = \frac{\Delta V}{I_{t0}} \quad (1)$$

I_{t1} depends instead on both R_m and R_s :

$$I_{t1} = \frac{\Delta V}{R_s + R_m} \quad (2)$$

Therefore, R_m can be obtained as:

$$R_m = \frac{\Delta V}{I_{t1}} - R_s \quad (3)$$

The exponential function $I(t)$ between I_{t1} and I_{t0} , is defined as follows:

$$I(t) = I \cdot e^{-\frac{t}{\tau}} + I_{t0} \quad (4)$$

$$\text{with } \tau = R_s \cdot C_m$$

The capacitor charge change (ΔQ) in response to the voltage step is equal to the capacitive area under the curve:

$$\Delta Q = \int_{t_0}^{t_1} I(t) dt - \int_{t_0}^{t_1} I_{t1} dt \quad (5)$$

Therefore, C_m is given by the change of charge in response to the voltage step:

$$C_m = \frac{\Delta Q}{\Delta V} \quad (6)$$

Calculations could be easily and quickly made during recordings thanks to a custom-written macro on IGOR Pro programmed by Dr. Ronald Jabs.

4.3.6 Bath application of kainate

During experiments 5.1.1 and 5.1.2, AMPARs were activated through bath application of kainate (250 μM). To isolate AMPAR currents, other ion channel or receptor conductances in NG2 glial cells had to be blocked. Therefore, we applied tetrodotoxin (TTX, 0.5 μM) to block Na^+ channels, barium chloride (BaCl_2 , 100 μM) and quinine (200 μM) to block K^+ channels and picrotoxin (100 μM) to block GABA_A receptors. Importantly, in these experiments, the intracellular solution contained 1-Naphthyl acetyl spermine (Naspm, 100 μM , intracellular solution 3). Naspm belongs to the family of polyamines, positively charged molecules able to block selectively CP-AMPARs from the inside when cells are held at positive potentials (Fig. 4.2). Efficacy of blockers was monitored with a stimulation protocol in which cells were repetitively clamped at potentials ranging from -100 mV to +100 mV (-70, -40, -20, 0, 20, 40, 70, 100, and -100 mV, interstimulus interval of 100 ms). This sequence of depolarization steps was applied every 3 s. Blockers were perfused for at least 5 min then kainate was additionally washed-in for 30-40 s. Current density (CD) before and after the blockers could be calculated as:

$$CD = \frac{I_{-70\text{mV}}}{C_m} \quad (7)$$

Moreover, a current/voltage (I/V) relationship was determined to verify rectification properties of AMPARs (see also chapter 1.4.1). To do this, the difference between currents evoked after and before kainate application was calculated for every voltage step.

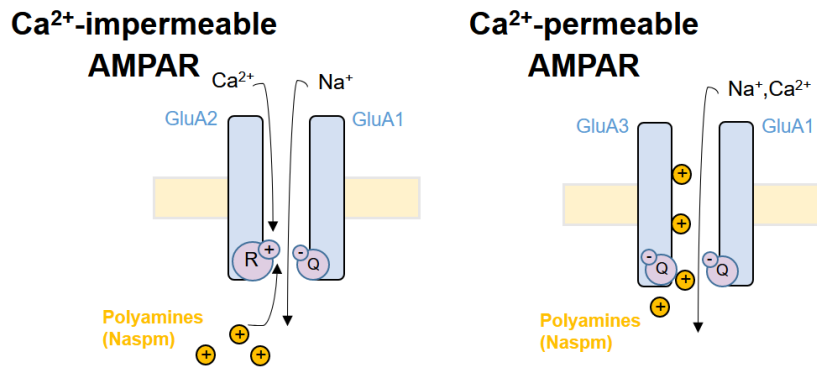


Fig. 4.2. Schematic representation of intracellular polyamine block. Ca^{2+} -impermeable AMPARs (top left) contain the GluA2 subunit in which a positive arginine residue (R) makes AMPARs insensitive to intracellular polyamine block and mainly permeable to Na^+ ions (left) leading to a linear or slightly outward I-V relationship. AMPARs that lack GluA2 are permeable to Ca^{2+} and, at positive holding potentials, they are subject to polyamine block from the intracellular side (right). This leads to a characteristic inward rectification of the I-V relationship as less current can flow through AMPARs at positive voltages. Q: glutamine residue.

The corresponding rectification index (RI) was derived by measuring the chord conductance of agonist/blocker-sensitive currents at -70 and $+40$ mV following the equation:

$$RI = \frac{I_{+40\text{mV}}/40 \text{ mV} - E_{rev}}{I_{-70\text{mV}}/-70 \text{ mV} - E_{rev}} \quad (8)$$

where E_{rev} is the reversal potential obtained by visual analysis of I/V relationships, i.e., when I-V curves crossed the x-axis. Based on equation 8, AMPARs show inward rectification for RI values < 1 and outward rectification for values > 1 .

To compare multiple I-V relationships of cells between different mouse genotypes, they were normalized to the minimum current (at -100 mV).

4.3.7 Evoked post-synaptic current (ePSC) recordings

Postsynaptic currents were evoked in NG2 glia through stimulation of presynaptic fibers or local interneurons in the cerebellum and hippocampus. Stimulation electrode was a monopolar chlorinated silver wire inserted in a glass pipette ($< 1 \text{ M}\Omega$) filled with aCSF. Stimulation pulses were biphasic ($100\mu\text{s}$ in duration), delivered in voltage mode by a pulse stimulator. Cells were usually stimulated with at least 20 pulses at a frequency of 0.6 Hz. Stimulation pulse intensity was chosen as the minimal stimulation intensity needed to evoke a postsynaptic response interspersed with synaptic failures (i.e., stimuli that do not induce a response). In paired-pulse recording experiments, the interstimulus interval was 50 ms. Intracellular solution 2 was used in these recordings: this solution is based on Cs^+ , which is known to block K^+ channels

intracellularly improving space-clamp and the quality of recordings (Segev, Garcia-Oscos and Kourrich, 2016). Blockers were applied after performing control stimulation for at least 10 min. To calculate the blocking effect (block %), the ratio between the median current amplitude after and before wash-in of blockers was performed. All recordings were sampled at 10 kHz and filtered at 1 kHz.

4.3.7.1 Glutamatergic ePSCs in the cerebellum

In the cerebellum, test pulses were delivered while recording NG2 glia in the molecular layer in the whole-cell patch clamp mode. During these test pulses, the stimulation electrode was moved under optical control in the granular layer to find the optimal position for the stimulation of CFs. CFs-evoked responses were identified due to both their fast kinetics and strong PPD. The stimulation electrode was usually placed 60 μm - 150 μm away from the recorded cell. Recordings were performed in the presence of picrotoxin (100 μM) to avoid the influence of GABAergic inputs.

4.3.7.2 Glutamatergic ePSCs in the hippocampus

In the hippocampus, the stimulation electrode was placed in the stratum radiatum of CA1, usually 60 μm distant from the cell. Also in this case, we used a minimal stimulation protocol. However, this procedure was not always successful due to the small response amplitude and a low signal-to-noise ratio in some of the experiments, leading to an increased pulse intensity and a low failure rate. Recordings were performed in the presence of picrotoxin (100 μM) to avoid the influence of GABAergic inputs.

4.3.7.3 GABAergic ePSCs in the hippocampus

Stimulation of GABAergic interneurons was performed by placing the stimulation electrode about 30 μm from the recorded cell. GABA responses were recorded in the presence of 10 μM NBQX and 50 μM D-APV to block AMPAR and NMDAR currents respectively. ePSCs were recognized by their long decay times.

4.3.7.4 Analysis of ePSCs

Analysis of currents evoked in NG2 glia was performed with Igor Pro macros written by Dr. Ronald Jabs. Here, single ePSCs were divided manually into failures or responses. The average of failures was then subtracted to each response trace to get rid of the stimulation artefact and improve the accuracy of subsequent analyses. In case not enough failures could be recorded, TTX (0.5 μM) was applied at the end of each recording. Kinetic properties of ePSCs could be

then calculated: the rise time was obtained from 20%-80% range of the response, while the decay time τ was derived from fitting the following mono-exponential function from which τ could be calculated:

$$I(t) = I_0 \cdot e^{-t/\tau} \quad (9)$$

The PPR was calculated from the amplitude ratio between the second response and the first.

4.3.8 Miniature PSCs

Miniature PSCs (mPSCs) were recorded in the voltage-clamp mode during whole-cell measurements of NG2 glia or PCs in the presence of TTX (0.5 μ M) and picrotoxin (100 μ M), except in chapter 5.3.1 where picrotoxin was omitted. Intracellular solution 5, based on K-gluconate (section 3.4.1), was used for all mPSC experiments. Analysis was performed with pClamp and IgorPro. Original data was uploaded in Clampfit for mPSC detection through a template search protocol. Events were accepted or rejected by visual inspection. Cells with less than two events detected over 7 min were discarded. Data was then transferred to Igor Pro for measurement of kinetic properties and frequency of events with a macro written by Dr. Ronald Jabs. The rise time was calculated from the 20%-80% amplitude range, while the decay time was obtained through a mono exponential fit of current decay (see equation 9). In chapter 5.3.1 AMPAR and GABAR-mediated PSCs were detected through two templates which allowed to calculate currents with fast and slow kinetics, respectively. Events with decay time constants faster than 15 ms were considered AMPAR-mediated. In these experiments, Kir 4.1 ko cells were clamped at -60 mV and control cells at -80 mV since Kir 4.1 ko cells present a depolarized resting potential (Timmermann *et al.*, 2023). Since the holding potential has an influence on the amplitude of the responses, these values were extrapolated to -70 mV assuming to have a linear I/V curve between -80 mV and -60 mV. In recordings from PCs, holding potential was -60 mV.

4.3.9 Field potential recordings

Field excitatory post-synaptic potentials (fEPSPs) for LTP assessment were evoked in an interface-type recording chamber. A bipolar concentric electrode was used for stimulation of the fibers, while the recording electrode consisted of a teflon-coated silver wire whose tip was chlorided. The chamber was heated at 35°C and aCSF was superfused on two layers of filter tissue that helped its homogeneous redistribution. Slices were transferred to the chamber on top of an additional small squared filter tissue. aCSF was pumped at a speed of 2.3 ml/min. Thanks to manually driven manipulators, electrodes could be moved under optical control through a binocular loupe on top of the slice. For cerebellar sagittal slices, electrodes were placed in the

molecular layer of lobule VI. As shown in Fig. 4.3A, the recording electrode was placed deeper into the tissue (around 100-150 μm) while the stimulation electrode was just on top of it. This configuration allows to record fEPSPs from PCs upon PF stimulation. In transverse cerebellar slices, the stimulation electrode could be placed further away in the molecular layer, in parallel to the recording electrode. In the hippocampus, the stimulation electrode was placed between the stratum radiatum of CA3 and of CA1 to stimulate Schaffer collaterals, while recording pyramidal neurons in CA1 (Fig. 4.3C). Signals were cleared from 50Hz noise frequencies through a specific device, sampled at 20 kHz and filtered at 10 kHz. Once recorded with WinWCP 4.6.1 software, fEPSPs were analysed with Clampfit software. Quantification of neuronal activity was performed by analysing fEPSP slopes in the linear rising phase as measures of the postsynaptic responses and the fiber volley (FV) amplitude to quantify presynaptic properties and PPRs (interstimulus interval of 50 ms). Before starting recordings, an input/output (I/O) curve was always registered with stimulation intensities ranging from 25 μA to 400 μA . Stimulation amplitude was chosen as the half maximum of the I/O curve. In hippocampal slices, LTP strength was measured through fEPSPs slopes. In cerebellar slices fEPSPs slope was more variable during recordings. Therefore, since this measure is proportional to the presynaptic FV amplitude, the ratio between fEPSP slope and FV amplitude was always calculated (see Fig. 4.3B). After placing both electrodes, slices were left to stabilize for 20-30 min before starting the measurements. In case of 7,8-DHF application (chapters 5.2.2.1 and 5.3.2), incubation time was 30 min. Baseline recordings of 10 min were made before LTP induction. After LTP induction, recordings lasted additional 30 min. Paired-pulses before and after LTP were given at a frequency of 0.6 Hz. If baseline recordings showed a variability higher than 10%, they were excluded from the analysis. After quantification, fEPSP slope and FV amplitudes were normalized to their average baseline value and plotted.

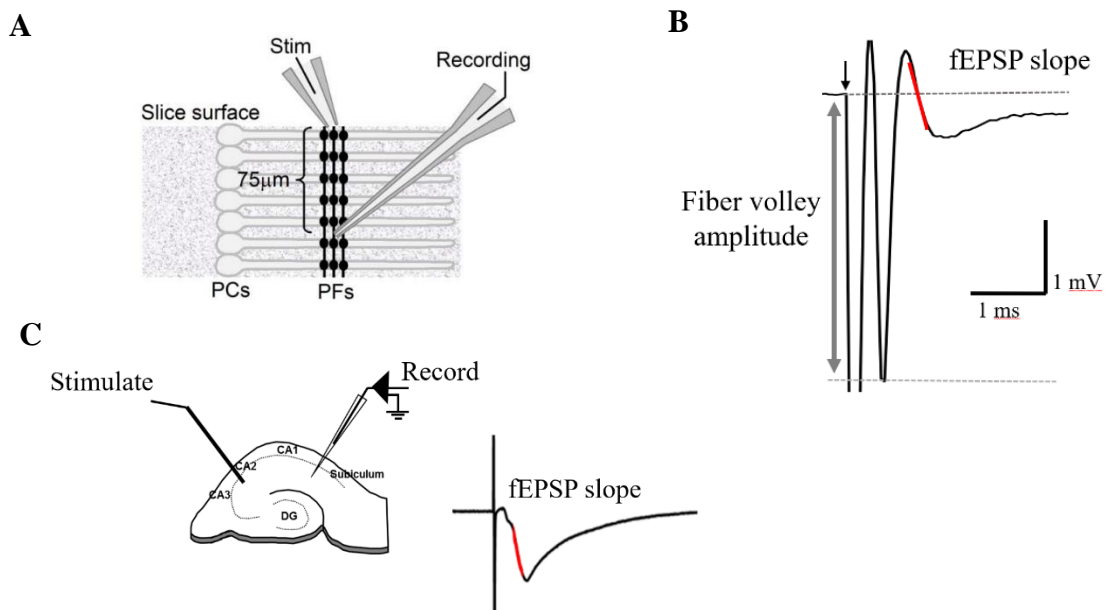


Fig. 4.3. fEPSP recordings in cerebellar and hippocampal slices. **A)** Electrode configuration in a sagittal cerebellar slice. Here, the stimulation electrode is placed above the recording pipette to efficiently stimulate PFs (Bergerot *et al.*, 2013). **B)** Sample of fEPSP generated upon PF stimulation. A large fiber volley precedes the smaller postsynaptic response. The stimulation artefact (black arrow) is due to the close distance between electrodes. **C)** Stimulation of hippocampal Schaffer collaterals coming from CA3 gives rise to a fEPSP recorded in CA1 pyramidal neurons.

4.3.10 Measurement of neuronal intrinsic firing properties

Cerebellar PCs in control and GluAko mice were recorded in the whole-cell patch-clamp mode to assess possible alteration in their electrical activity. Cells were recognized based on their position between the granular and molecular layers and on their size and shape. For these experiments, the intracellular solution contained K-gluconate (intracellular solution 5). Recordings started around 5 min after gaining electrical access to the cytoplasm in whole-cell mode, keeping the cell at a holding potential of -70 mV. At this point, the amplifier was switched to current-clamp mode for recording the neurons spontaneous activity, with a sampling rate of 6 kHz, a gain of 20 kHz and filtering signals at 1 kHz. Recordings lasted 2 min. Afterwards, TTX (0.5 μ M) and picrotoxin (100 μ M) were washed in for mPSC recordings in the voltage-clamp mode. These recordings were made maintaining a holding potential of -60 mV. The sampling rate was 6 kHz, filtering at 1 kHz. In the current-clamp mode, PCs showed three modes of activity: tonic firing, phasic firing or silence. APs were analysed only from tonic firing cells which showed a constant firing frequency. AP parameters considered are shown in Fig. 4.4A and they were:

- AP threshold, calculated as described previously (Sekerli *et al.*, 2004, method III). Briefly, the first derivative of the voltage (dV/dt) was plotted against the membrane voltage, giving rise to a so-called phase-plane plot (Fig. 4.4B). These plots underwent cubic spline interpolation to increase the accuracy. Threshold potentials were defined as membrane potential value corresponding to a first derivative of 20 mV/ms;
- AP amplitude from the most positive to the most negative peak;
- AP half-width, calculated as width at half maximum from AP threshold;
- After-hyperpolarizing potential (AHP), calculated from AP threshold to the most negative peak;
- AP upstroke from AP threshold to the maximum peak;
- AP kinetics: rise time and decay time calculated from 10-90% of the total AP amplitude;
- Interspike interval (ISI), calculated as the time distance between the peak of two consecutive spikes;
- AP frequency, derived from the reciprocal of the ISI;
- Coefficient of variation of the ISI (CV_{ISI}), given by the ratio between the standard deviation of the ISI and the mean ISI ($CV_{ISI} = SD_{ISI}/Mean_{ISI}$). This parameter gives an estimation of the regularity of firing patterns as a higher CV_{ISI} corresponds to a more irregular spike pattern.

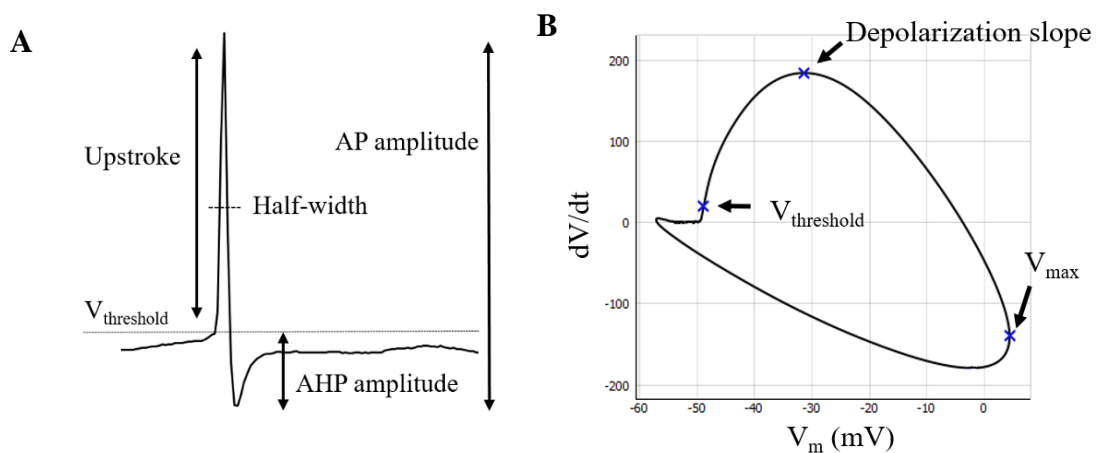


Fig. 4.4. Parameters for AP analysis in cerebellar PCs. **A)** Main parameters calculated for each action potential. **B)** Phase-plane plot of a single AP. The membrane voltage (V_m) is plotted against its first derivative (dV/dt). After cubic spline interpolation to produce a continuous plot even with a low sampling rate, the action potential threshold ($V_{threshold}$) was set at 20 mV/ms. V_{max} : voltage corresponding to spike maximum. AHP: after-hyperpolarizing potential.

Analysis of mEPSCs was performed as described in section 4.3.7.

4.4 Behavioural tests

Behavioural experiments were performed in collaboration with PhD candidate Michela Palmisano, Dr. Andras Bilkei-Gorzo (Department of Molecular Psychiatry, University of Bonn), Dr. Gerald Seifert and PhD candidate Nehal Gebril. Tests were made to assess possible memory or motor impairments in GluAko mice. Memory tests were all based on the general behaviour of mice to prefer a new stimulus, whether it is an object, partner or environment, over a known one. Mice were transferred to a room with reversed 12h day/night cycle at least one week before performing the tests so that experiments could be performed during mice dark phase when they are more active. Three days before starting the tests, mice underwent a habituation period in which they were placed individually into a squared arena (44x44 cm²) for 5 min every day and they were left free to explore. Arenas were covered with 1 cm of sawdust, which helped in retaining the odour of animals. Males and females were always placed in different arenas. Arenas were positioned in a sound-isolated and dimly-illuminated room for memory tests, while brighter illumination was used for the motor test. A camera inside the room was connected with Noldus Ethovision XT software, in order to record, track and evaluate mice behaviour.

4.4.1 Novel object location recognition (NOLR) test

This test is designed to measure hippocampus-dependent episodic memory in mice. Here, three objects with the same shape but distinct colors (LEGO pieces around 2x2cm) were placed in a fixed location on the side of the arenas (Fig. 4.5). Mice could then explore the area and objects for 6 min. After this time, they were placed back in the cages for 30 min. In the meantime, one of the three objects was placed in the opposite corner of the arena. Later, mice were left to explore again for additional 3 min. The time in which mice were interacting with each object was calculated when the mice nose was 2-3 cm close to the object. After testing, the percent of total investigation time was calculated as:

$$\textit{Exploration of novel location (E)} = \frac{t_a}{t_a + t_b + t_c} * 100 \quad (10)$$

where t is the time spent in the investigation of either object a (the object which was moved), b, or c (objects which stayed in the same location). A value above 50% in trial 2 indicates a greater investigation of the novel location.

Preference for the novel location was then determined as:

$$\text{novelty preference } (P) = \frac{E_{Tr2} - E_{Tr1}}{E_{Tr1} + E_{Tr2}} * 100 \quad (11)$$

where Tr indicates the trial. A positive value indicates more time investigating the novel location. A value equal to zero indicates equal time spent with both location. To detect biases from lack of motivation or anxiety, total walking distance and velocity of mice were also calculated.

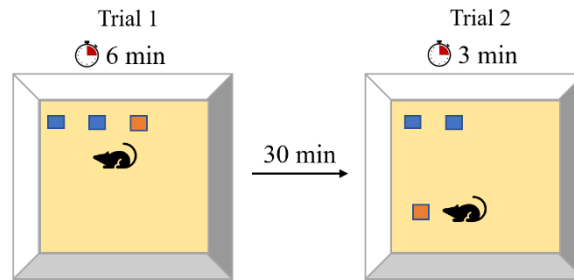


Fig. 4.5. Schematic representation of NOLR test. Mice were placed in an arena containing 3 identical objects. On the first trial, lasting 6 min, mice spent time with all the objects, recognizing shapes and location. On the second trial, lasting 3 min, one object was moved to a new location. Time spent exploring each object was calculated. As an innate instinct, healthy mice should spend more time in the novel location during the second trial.

4.4.2 Partner recognition test (PRT)

This test allowed for determination of long-term social recognition memory. In this case, a decrease in the exploration of a known familiar social partner from a previous training session (familiar partner) underlies a memory for the partner. Therefore, PRT consisted on two trials (Fig. 4.6). On trial one, lasting 6 min, mice were placed in arenas where two cylindrical metal grid cages were present: one containing another mouse of same age and sex (familiar partner) and one empty. Cages were placed on opposite sides of the arenas and both were 6-7 cm away from the walls. Novelty preference, underlying recognition of the familiar partner in trial 2, is:

$$\text{novelty preference } (P) = \frac{t_{\text{unfamiliar}} - t_{\text{familiar}}}{t_{\text{unfamiliar}} + t_{\text{familiar}}} * 100 \quad (12)$$

where t is the time spent with either the familiar or the unfamiliar partner during trial 2.

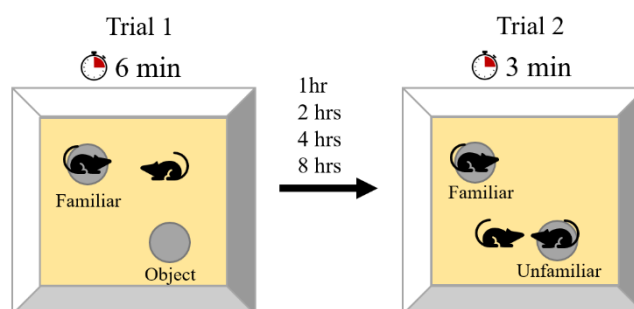


Fig. 4.6. Representation of PRT paradigm. On trial one, mice are placed in the arena together with a partner mouse (familiar partner) in a metal grid cage and an empty grid cage (object). Healthy mice should spend more time interacting with the partner than with the object. On trial two, after an amount of time varying on each experimental day, a new partner (unfamiliar) was placed in the empty cage. Mice with good long-term memory would remember the familiar partner and spend more time with the unfamiliar one.

4.4.3 Y-maze test

Spatial working memory abilities of GluAko mice and controls could be assessed through the Y-maze test. Here, mice were placed for 10 min in a Y-shaped maze composed of three arms of equal length set at 120° (Fig. 4.7). When mice enter all three arms in a consecutive way without going back to a previously visited arm, they complete a so-called alternation. Another important parameter, the total number of arm entries, represents the activity and locomotion and it is needed to calculate the percentage of spontaneous alternations, which relate to working memory (equation 13). The maze was thoroughly cleaned after each mouse to avoid odour cues.

$$\text{Spontaneous alternation \%} = \frac{\# \text{ of alternations}}{\text{total number of arm entries} - 2} * 100 \quad (13)$$

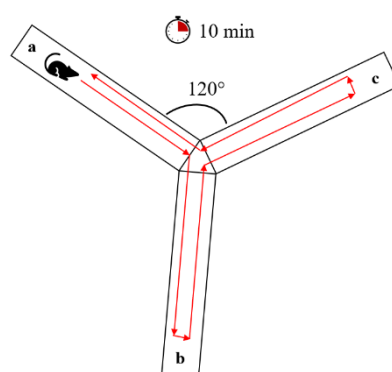


Fig. 4.7. Y-maze test. Mice were placed in a Y-shaped maze and were free to explore each arm. If working memory abilities were functional, animals would tend to always explore an unexplored arm, e.g., following red arrows, completing an alternation. Locomotor activity was measured as total number of arm entries.

4.4.4 Beam-walking test

This test measures motor coordination abilities of mice, associated with cerebellar functions. Here, a 100 cm rod was fixed to a shelf at a height of 70cm. At the end of the rod, an escape chamber (7x10x10 cm³), made of dark plastic and with the bottom covered in sawdust, served as safehouse (Fig. 4.8). Four sawdust covered arenas were placed under the rod, so that mice could fall on a soft ground. The test consisted of two days of experimental sessions. On day one, mice were placed on a 28 mm-thick rod and left walking to reach the safehouse. Each mouse repeated the test for three times, resting for one min after each trial. In case mice fell from the rod, they were placed back on the original position. At the end of the first training day mice were able to quickly walk from one end of the rod towards the safehouse. On the second day, the real test started as described above. Each mouse was timed while walking from the start of the rod to the safehouse. Animals had to enter the safehouse with all four limbs to complete the test. Three rods were used, which differed in their diameter: a thicker rod of 28 mm, an intermediate rod of 14 mm and a smaller rod of 8 mm. For the analysis, data was obtained by taking the average of three consecutive trials per beam for each animal. Trials in which mice fell from the rod or that lasted more than 70 sec were excluded from the analysis. Parameters for the evaluation of motor abilities were the time elapsed to reach the safehouse (latency), number of hindlimb slips. Recorded videos were analysed with the open-source software Kdenlive.

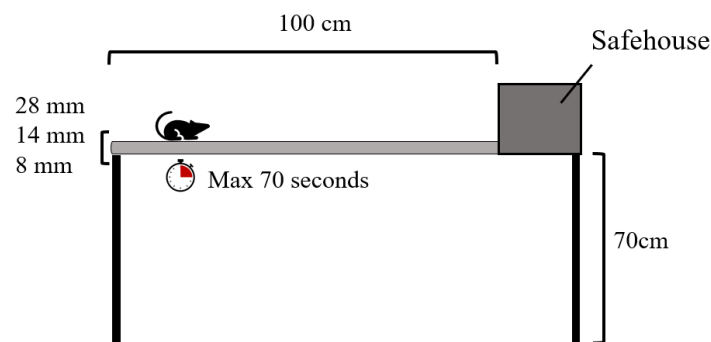


Fig. 4.8. Scheme of the beam-walking test setup. Mice were placed on a rod of variable diameter (28mm, 14 mm or 8 mm) and they walked until reaching a safehouse at the end of the beam. Total time for completing the task, as well as the number of hindlimb slips, were the parameters used to assess motor coordination abilities of the animals.

4.5 Molecular analyses

Molecular analyses were performed by Dr. Gerald Seifert.

4.5.1 FAC sorting

Analyses of mRNA expression of AMPA receptor accessory proteins in hippocampal NG2 glia was quantified by semi quantitative RT-PCR (see below). For this purpose, yellow fluorescent NG2 glia were isolated from brain tissue of NG2-EYFPki mice and NG2creERT2 x Rosa26EYFP mice (p60) by fluorescence activated cell sorting (FACS). Mice of both sexes were anesthetized with isoflurane and decapitated. The brains were dissected and whole hippocampi and cerebella were isolated under microscopic control. The tissue was mechanically ruptured and digested in papain for 15 min 37 °C. To degrade the DNA the tissue was incubated for 10 more minutes with DNase and further dissociated by Pasteur pipettes and filtered through a 70 µm cell strainer. After adding 10 ml HBSS (Hanks' Balanced Salt Solution) supplemented with Ca²⁺ and Mg²⁺, the solution was centrifuged for 10 min (300 x g) and the respective pellet re-suspended in 1 ml HBSS without Ca²⁺ and Mg²⁺. NG2 glial cells of the mouse lines mentioned above expressing the fluorescence protein eYFP either under control of the NG2 promoter (NG2-EYFPki mice) or driven by the artificial Rosa26 promoter after Cre mediated recombination (NG2creERT2 x Rosa26EYFP), NG2 glia could be identified and sorted according to their EYFP specific emission at 527 nm by a flow cytometer (70 µm nozzle). Sorted cells (10.000 to 25.000 cells) were collected in HBSS (without Ca²⁺ and Mg²⁺). The cell suspension was centrifuged for 10 min (2000 x g). The supernatant was discarded and the cells were re-suspended in 200 µl lysis/binding buffer. Samples were frozen in liquid nitrogen and stored at -80 °C until use.

4.5.2 Semiquantitative RT-qPCR

Samples containing the FAC-sorted NG2 glia were incubated in lysis/binding buffer to extract the mRNA from the cells. To specifically isolate the mRNA, the samples were incubated with polymer particles covered with an oligo dT-tail (oligo(dT)25-linked Dynabeads). Here, the poly A-tail of the mRNA binds to the oligo dT sequence and can be separated from the rest of the solution via a magnet. After three wash steps, for first strand synthesis, these beads with the adherent mRNA were suspended in DEPC-treated water (20 µl) and incubated with first strand buffer, DTT (10 mM), dNTPs (4 x 250 µM), oligo-dT24-primer (5 µM), RNase inhibitor (80 U), and SuperscriptIII reverse transcriptase (400 U) for 1 hour at 50 °C. Reaction volume was 40 µl.

The reaction mixture for qPCR contained Taqman mastermix (Takyon, Eurogentec, Belgium), primer/probe mix, and 1 μ l of cDNA was added (reaction volume of 12.5 μ l). A predeveloped primer/probe mixture for each gene was used (Applied Biosystems). The PCR program for qPCR started with denaturation at 95°C for 10 min, followed by 50 cycles of 15 sec denaturation at 95 °C and 1 min primer annealing/elongation at 60 °C. The Taqman probe in the mixture is an oligonucleotide labelled with a fluorescent reporter at the 5' end (6-carboxyfluorescein, FAM) and a non-fluorescent quencher at the 3' end. During the amplification process of the PCR, the DNA polymerase cleaves the probe and disrupts the fluorescence energy transfer. The reporter dye now emitted light that was detected by the qPCR detection system CFX 384 (Holland *et al.*, 1991; Livak *et al.*, 1995; Seifert *et al.*, 2002). Per PCR cycle the emission accumulates and can be measured in real time. The fluorescence intensity is increasing exponentially until plateau phase is reached. In the exponential phase the threshold cycle (CT) can be determined and was used to calculate the amount of RNA that was initially used (Fink *et al.*, 1998; Seifert *et al.*, 2002). The relative quantification of the gene expression ratio of the target gene and β -actin, a housekeeping gene serving as reference, was determined by comparing both CT-values and was calculated as followed:

$$X_{\text{target}} / X_{\beta\text{-actin}} = E^{\beta\text{-actin CT}_{\beta\text{-actin}}} / E_{\text{target}}^{\text{CT}_{\text{target}}} \quad (14),$$

with X being the input copy number, E the efficiency of amplification and CT the threshold cycle. Water was used as a negative control. The amplification efficiency was assessed by serial dilutions of mRNA: for TARP γ 2 it was 1.89, for γ 4 1.90, for γ 7 1.92, for γ 8 1.96, for CNIH-2 1.98, and for β -actin 1.94.

4.5.3 Single-cell RT-PCR

The presence or absence of Zebrin, EAAT4 or metabotropic glutamate receptor 1 (mGluR1b) mRNAs in individual PCs was determined using single cell RT-PCR. To perform this, PCs were first characterized using the patch-clamp technique. The patch pipette, along with the attached cell, was carefully lifted above the tissue slice and the cell cytoplasm was aspirated into the pipette. Subsequently, the pipette was removed and the intracellular solution containing the cell was expelled into a thin-walled Eppendorf tube containing 3 μ l of DEPC water, which is free of RNase and DNA. The tube was then rapidly frozen using liquid nitrogen and the cells were stored at -20°C until further use. Next, a two-step reverse transcription PCR (RT-PCR) was performed. In the first step mRNA was transcribed into cDNA. Each cell collected was treated with a buffer composed of first strand buffer, DTT (10 mM), dNTPs (4 x 250 μ M),

random hexamer primer (50 μ M), RNase inhibitor (20 U), and SuperscriptIII reverse transcriptase (100 U). This reaction mixture was incubated for one hour at 37 °C. Volume of the RT reaction was 10 μ l. As negative control, DEPC water or buffer from the recording chamber was used. RNA isolated from the whole mouse brain served as positive control. In the second step, a two-round multiplex PCR was performed to identify specific cDNA sequences. For the first round, to the 10 μ l of the cDNA were added PCR buffer, MgCl₂ (2.5 mM), primers (200 nM each, Table 1), dNTPs (4 x 50 μ M), Taq DNA-polymerase (2 U, Invitrogen; reaction volume 50 μ l).

Gene	Primer sequence	Product length	Position	Genbank accession number
Calbindin-D 28K	se 5'-GACGGAAGTGGTTACCTGGAAGGA as 5'-ATGAAGCCGCTGTGGTCAGTATCA	278 bp	76 330	NM_009788
Calbindin-D 28K (nested)	se 5'-GCGCGAAAGAAGGCTGGATT as 5'-CCTCGCAGGACTTCAGTTGC	169 bp	136 285	
Zebrin II	se 5'-CAGTGCTGATGACCGTGTGAAAA as 5'-AGAGCCCATCCAGCCCTTGAG	203 bp	192 374	NM_009657
Zebrin II (nested)	se 5'-CCCCTTCGTCCGCACCATC as 5'-GTCGGTCCCAGCTAGAGGCACTAC	85 bp	276 337	
EAAT4	se 5'-CGCTGACCCGAGGCTGAGAC as 5'-ATTAGGATGCCGATGAAAACTGC	460 bp	-23 415	NM_013693
EAAT4 (nested)	se 5'-GCGCCTGCAGACCATGACC as 5'-GCATTCCCATCCGCCCTGTC	272 bp	108 360	
mGluR1b	se 5'-CAGCTCTGTGGCCATTCAAGTCC as 5'-GCGGCGCATGGCACTCA	424 bp	492 899	NM_001114333
mGluR1b (nested)	se 5'-GTTCGACATCCCACAAATC as 5'-AGAAGCAGACCACAACCCT	341 bp	531 853	

Table 1. Primers used for preamplification for qPCR. Position 1 is the first nucleotide of the initiation codon. The length of PCR products was indicated as base pairs (bp). Se: sense primer; as: antisense primer. All sense and antisense primers are located on different exons, respectively.

PCR program consisted of a 3 min initial denaturation (94 °C), followed by 35 cycles of denaturation (25 sec at 94 °C), primer annealing (2 min first 5 cycles, 45 sec last 30 cycles at 51 °C), and primer elongation (1 min at 72 °C, final elongation for 7 min). For the second PCR round, nested primers were used that bind within a specific sequence of the PCR product obtained from the reaction before. 2 µl of the PCR product were added to the substances mentioned above (volume 50 µl) and amplified in a PCR reaction (35 cycles, primer annealing at 54°C). Finally, agarose gel electrophoresis was performed. A 1.5% agarose gel in TAE buffer was employed, supplemented with 20 µl ethidium bromide (1 mg/ml) for visualization of the PCR products under UV-light. Samples were separated in an electric field (240 V for 40-45 min) by their size and charge. A low molecular weight DNA ladder (New England Biolabs) was used to indicate molecular size and to identify cDNA.

4.6 Statistics

Statistical analyses were performed through either self-made R scripts, OriginPro or Microsoft Excel software. First, data was always tested for normality through Shapiro-Wilk test. Parametric data then underwent Levene's test for determining whether variances were homogenous. Parametric data with equal variances was tested with paired-sample or two-sample Student's t-test. t-test with Welch's correction was employed in case of unequal variances. Non-parametric data was analysed with Mann-Whitney U test. For group analyses, two-way ANOVA or repeated measures ANOVA with Tukey or Bonferroni post-hoc tests were performed. One-sample t-tests were also used to assess whether the population mean was different than zero. Gaussian-distributed data was plotted as bar plot with mean \pm SD unless specified. Non-parametric data was plotted as box plots showing median as central line, 25-75% quartiles and whiskers (\pm 1.5 interquartile range). Extreme outliers were defined as \pm 3*interquartile range and removed from the analysis. n refers to the number of cells or slices, while N to the number of mice.

5 Results

5.1 Developmental and regional differences of AMPAR expression in NG2 glia

NG2 glial cells express AMPARs both during development and in adulthood, with varying Ca^{2+} permeability depending on the brain region considered. This heterogeneity of AMPARs depends not only on the presence of the GluA2 subunit but also on regulatory actions of auxiliary subunits (see chapter 1.4.1). In the next sections, it will be first described how Ca^{2+} permeability is developmentally regulated in hippocampal NG2 glia (Hardt *et al.*, 2021), then a comparison will be made with the adult cerebellum. Moreover, additional properties of SC-NG2 and CF-NG2 synapses will be assessed.

5.1.1 CP-AMPArs in developing hippocampal NG2 glia

In order to verify the proportions of CP-AMPArs in hippocampal NG2 glia during development, AMPAR-mediated currents were isolated by bath application of a cocktail of blockers (chapter 4.3.6) in slices from both juvenile and adult mice (NG2-YFP mouse line, chapter 4.1.1; p10 and p60 respectively). When kainate, an AMPAR agonist, was washed-in, AMPAR currents were activated in NG2 glia at both developmental stages (Hardt *et al.*, 2021). The presence of a polyamine, namely spermine (50 μM or 100 μM), in the intracellular solution allowed to check for the presence of CP-AMPArs. Indeed, spermine, like other polyamines, can plug CP-AMPArs from the intracellular side when the cell is held at positive potentials (e.g., +40 mV), determining a characteristic inward rectification (see Fig. 4.2). As shown by Stefan Hardt, rectification index was 1.74 in young NG2 glia compared to 1.24 in the adult, suggesting a developmental increase in CP-AMPAr conductance. However, Hardt and colleagues (2021) have also shown how auxiliary subunit expression differs between the two developmental stages and this could potentially influence Ca^{2+} permeability. Thus, I performed additional experiments by replacing spermine with Nasp (100 μM) in the intracellular solution. Indeed, intracellular Nasp can block CP-AMPArs independently from TARP activity, revealing their actual prevalence (Coombs *et al.*, 2023). Inward rectification of kainate-induced responses with intracellular Nasp was stronger than with spermine and differed

significantly between developmental groups (p10: $RI = 1.44 \pm 0.30$; $p < 0.01$; p60: $RI = 1.03 \pm 0.17$; $p < 0.01$; Fig. 5.1C).

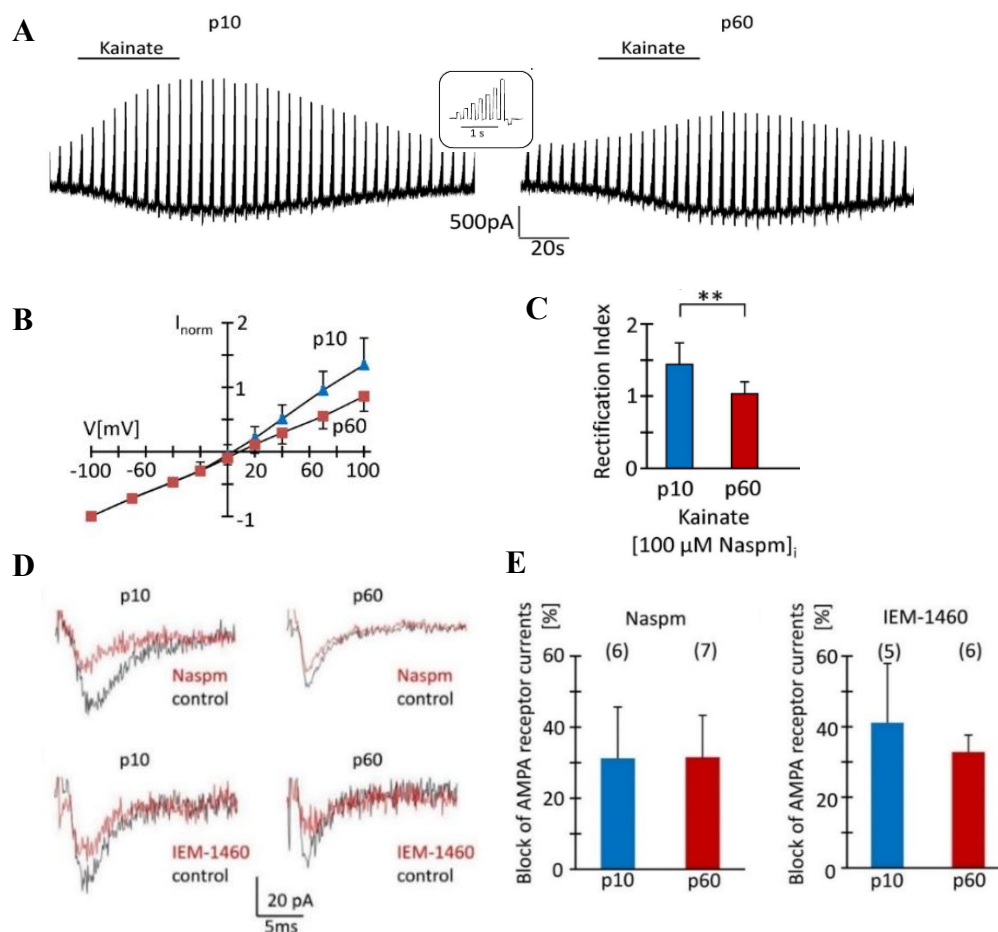


Fig. 5.1. Analysis of CP-AMPA expression in hippocampal NG2 glia. **A)** De- and hyperpolarization steps (-70 , -40 , -20 , 0 , 20 , 40 , 70 , 100 , and -100 mV, shown in inset) in the presence of blockers (200μ M quinine, 100μ M $BaCl_2$, 0.5μ M TTX, 100μ M picrotoxin) and kainate (250μ M) in both juvenile (p10, left) and adult (p60, right) mice. **B)** Normalized I-V relationship obtained in the presence of intracellular Naspam (100μ M). Currents are calculated from the difference between current values before and after agonist application. Responses were normalized to maximum inward currents and averaged. **C)** Bar plot showing a lower RI in adult mice (p10, p60: $N=3$, $n=18$). **D)** Sample traces showing ePSCs recorded in NG2 glia during low-frequency stimulation of Schaffer collaterals. Naspam and IEM-1460 block is shown in red. **E)** Block percentage of AMPAR currents with both Naspam (50μ M) and IEM-1460 (100μ M). Number of cells is given in parentheses. Two-sample t-tests show no difference in CP-AMPA-mediated synaptic currents during development. **: $p < 0.01$. Modified from Hardt *et al.*, 2021.

Next, I assessed the involvement of CP-AMPARs in mediating ePSCs in SC-NG2 synapses. In this case, AMPAR-mediated PSCs were generated in NG2 glia through low-frequency stimulation of SCs (sections 4.3.7 and 4.3.7.2). The average ePSC amplitude on the first pulse was -37.26 ± 8.70 pA (range from -14 pA to -56 pA, N=11 n=19). Cell responses showed rapid kinetics (20%-80% rise time = 0.56 ± 0.12 ms, n=22; decay time = 2.69 ± 0.91 ms, n=24) and paired-pulse facilitation (PPR = 2.03 ± 0.44 , n=18). After at least 15 min of control stimulation in the presence of CTZ (100 μ M) and picrotoxin (100 μ M), either NaspM (50 μ M) or the adamantane derivative IEM-1460 (100 μ M) were washed in for the same duration. These molecules are use-dependent blockers for CP-AMPARs and differ in their affinity for the receptor complex (Twomey *et al.*, 2018). Block of synaptic currents was similar with both molecules and did not differ between juvenile and adult mice (NaspM: p10, by $31.2 \pm 14.4\%$, n = 6, N = 4; IEM-1460: $41.1 \pm 16.8\%$, n = 5, N = 3; p60, by $31.5 \pm 10.8\%$, n = 7, N = 4 and $32.8 \pm 4.8\%$, n = 6, N = 5; Fig. 5.1D, E). These results, taken together, show that CP-AMPARs are expressed in different proportions during development and are overexpressed in adult mice. Nevertheless, the lack of difference in synaptic current block might indicate that the expression of CP-AMPARs is limited to the soma or extra synaptic membrane.

5.1.2 CP-AMPARs in cerebellar NG2 glia

In the adult cerebellum, NG2 glia can make strong synapses with CFs in which around 80% of AMPARs seem to be Ca^{2+} permeable (Lin *et al.*, 2005). Moreover, preliminary sqPCR analyses from our group suggests a higher expression of auxiliary subunit TARP γ 2 in the cerebellum (Fig. 5.2A). Interestingly, TARP γ 2 is associated to membrane delivery of CP-AMPARs in cerebellar NG2 glia (Zonouzi *et al.*, 2011). To confirm this data and to compare CP-AMPAR expression between cerebellum and hippocampus, recordings of CF-NG2 ePSCs were performed (see section 4.3.7.1). These currents showed PPD (PPR = 0.56 ± 0.11) with an average peak amplitude of -338.94 pA \pm 291 pA (range -85 pA to -1106 pA, N=13, n=19). Compared to the hippocampus, the rise time of these currents was shorter (0.40 ± 0.08 ms; two-sample t-test $p < 0.0001$, n=19), while the decay time was longer (3.83 ± 1.80 ; two-sample t-test $p < 0.05$, n=20). To quantify the contribution of CP-AMPARs to ePSCs, NaspM (50 μ M) or IEM-1460 (100 μ M) were applied after 15 min of control stimulation in normal aCSF.

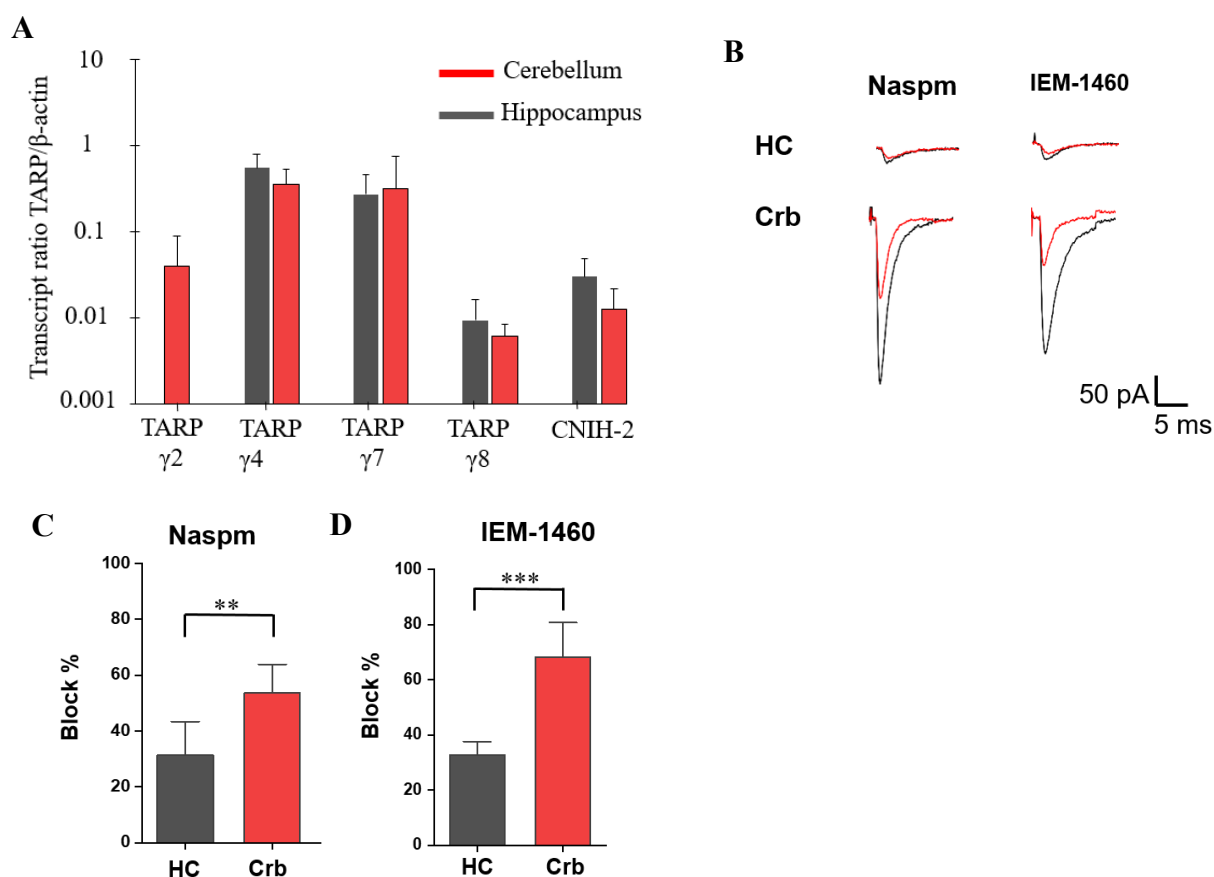


Fig. 5.2. Synaptic CP-AMPA receptor expression in hippocampal and cerebellar NG2 glia.

A) sqRT-PCR of TARP and CNIH-2 in NG2 glia, FAC sorted from hippocampus and cerebellum. TARP γ -2 was found in NG2 glia of the cerebellum, but not in the hippocampus. **B)** Examples of inward currents (ePSCs) elicited in NG2 glia upon stimulation of Schaffer collaterals in the CA1 region of the hippocampus (top) or of climbing fibers in the cerebellar molecular layer (bottom). ePSCs were partially blocked upon application of extracellular polyamines (Naspmm, 50 μ M, left; IEM-1460, 100 μ M, right). **C, D)** Block of ePSCs by Naspmm (C) and IEM-1460 (D) in NG2 glia of hippocampus and cerebellum (Naspmm, left: crb: N=7, n=6, HC: N=4, n=6; IEM-1460, right: crb: N=5, n=8, HC: N=5, n=6; two-sample t-test). Picrotoxin (100 μ M) and CTZ (100 μ M) were always present in the bath. V_h : -70 mV. HC: hippocampus; Crb: cerebellum. **: $p < 0.01$, ***: $p < 0.001$.

This revealed that 88.8% of the cells tested (N=13 n=19) were sensitive to the blockers. Currents were blocked significantly more than in the hippocampus (Naspmm: $53.6 \pm 10.2\%$ vs $31.5 \pm 10.8\%$, $p < 0.01$; IEM-1460: $68.1 \pm 12.5\%$ vs $32.8 \pm 4.8\%$, $p < 0.0001$; Fig. 5.2C, D), with IEM-1460 having a stronger effect than Naspmm ($p < 0.05$). These results show that in the cerebellum, the majority of synaptic AMPARs expressed by NG2 glia is Ca^{2+} -permeable and they contribute more to ePSCs in this region than in the hippocampus. In order to further assess the prevalence of AMPAR expression in cerebellar NG2 glia, independently from TARP expression, AMPAR current was isolated by co-applying a mix of blockers (quinine, 200 μ M; $BaCl_2$, 100 μ M; TTX, 0.5 μ M; picrotoxin, 100 μ M; Fig. 5.3A).

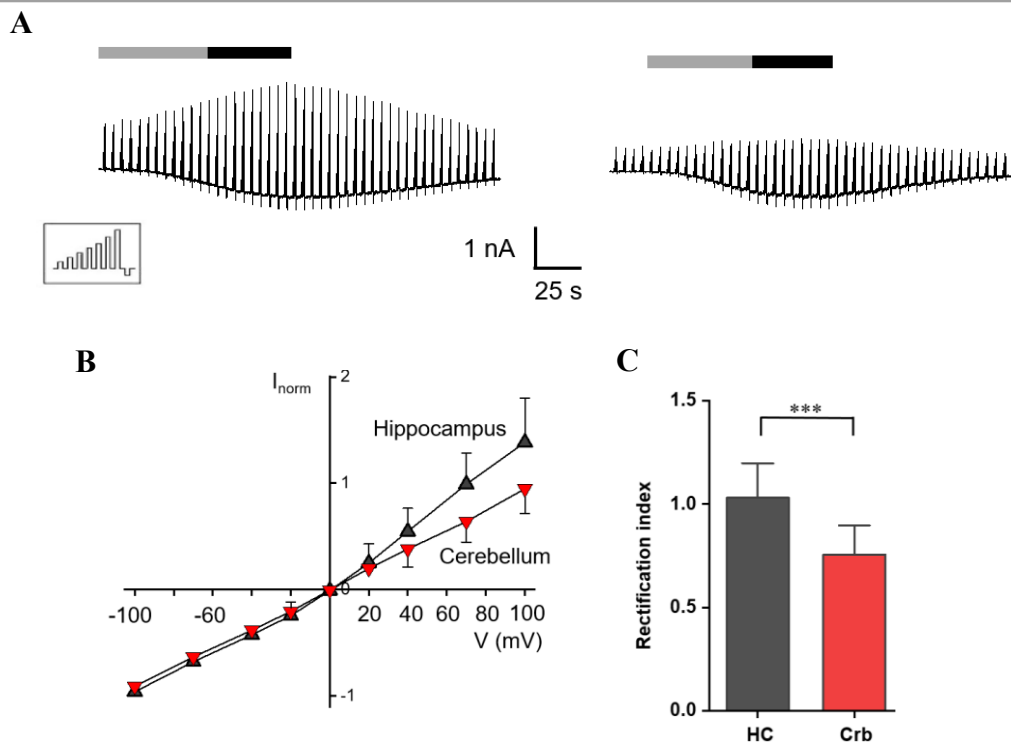


Fig. 5.3. Intracellular polyamine block of CP-AMPA receptors. **A)** NG2 cells were patch-clamped and different voltage steps were applied (-70, -40, -20, 0, 20, 40, 70, 100, -100 mV; duration 100 ms, interval 100 ms, every 4.5 s). The pipette solution contained Naspm (100 μ M) and the extracellular solution blockers of K^+ and Na^+ channels. **B)** I-V curves of kainate-induced responses in cerebellar and hippocampal NG2 glia. Currents before and during agonist application were subtracted at corresponding voltages. Responses were then normalized to the maximum inward currents and averaged (I_{norm} ; hippocampus, grey, N=3, n=18; cerebellum, red, N=3, n=18). **C)** The rectification index differed significantly between cerebellum and hippocampus (hippocampus: N=3, n= 18; cerebellum: N=3 n= 18; two sample t-test). ***: $p < 0.001$.

AMPA receptors in NG2 glial cells were subsequently activated through bath application of kainate (250 μ M) which generated inward currents of 12 pA/pF ($V_h = -70$ mV). The derived current-voltage relationship showed an inward rectification in all cells, which was much stronger than in hippocampal NG2 glia (R.I.: 0.76 ± 0.14 vs 1.03 ± 0.17 ; two sample t-test $p < 0.0001$; Fig. 5.3B, C). These experiments confirm a high prevalence of CP-AMPA receptors in cerebellar NG2 glia, which could be the main reason for a higher synaptic efficiency in this area.

5.1.3 Multivesicular release from CFs contributes to a larger glutamate transient

Differences in ePSC kinetics between cerebellar and hippocampal NG2 glia might underlie further differences in synaptic transmission between the two regions. In particular, shorter rise times are associated with a higher glutamate transient in the synaptic cleft. If glutamate concentration is higher in the cerebellum, this could also concur to the increased efficiency of CF-NG2 synapses. An indirect way to test for the amount of glutamate released is to use a low-affinity antagonist of AMPARs, gamma-D-glutamylglycine (γ -DGG, 1 mM; Wadiche and Jahr, 2001). This molecule competes with glutamate to bind AMPARs: the higher the glutamate concentration, the lower the block of currents by γ -DGG and vice versa. Therefore, γ -DGG was added to the bath during ePSC recordings of both SC- and CF-NG2 synapses. γ -DGG block on ePSC1 was stronger in the hippocampus than in the cerebellum (hippocampus: $73.71\% \pm 12.4$; cerebellum: $58.51\% \pm 8.8$; $p < 0.01$; Fig. 5.4B), suggesting a higher concentration of glutamate in CF-NG2 synaptic clefts. Two main hypotheses might explain this finding: multivesicular release from CFs or spillover and accumulation of glutamate at neighbouring synapses (Wadiche and Jahr, 2001). Multivesicular release happens mainly in brain regions with high P_r where a single AP can lead to the fusion of multiple vesicles (see Xu-Friedman and Regehr, 2004). This mechanism was demonstrated in synapses between CFs and PCs. On the other hand, in low P_r areas univesicular release predominates. In order to test this hypothesis, CF-NG2 PSCs were evoked with a paired-pulse protocol in two conditions: normal P_r , with aCSF containing 2 mM Ca^{2+} , and low P_r in which $[\text{Ca}^{2+}]$ was reduced to 1 mM. In this latter case, $[\text{Mg}^{2+}]$ was increased from 2 mM to 3 mM to maintain the same amounts of bivalent ions in the solution. The rationale behind these experiments is that multivesicular release is dependent on P_r . Therefore, if γ -DGG blocks ePSCs in a stronger way in low P_r conditions than at normal P_r , then it follows that a larger amount of glutamate is released in normal P_r , likely due to multivesicular release. In conditions of low P_r , γ -DGG blocked the first pulse (ePSC1) by $80.85\% \pm 6.8\%$ and the second pulse (ePSC2) by $81.78\% \pm 6.30\%$. This block was significantly higher than at normal P_r (ePSC1: $p < 0.0001$; ePSC2: $p < 0.01$; Fig. 5.4C). Therefore, like in CF-PC synapses, multivesicular release contributes to a large glutamate transient. Nevertheless, it is still not possible to exclude also a contribution of glutamate coming from neighbouring synapses. This idea was discarded in CF-PC synapses, since BGs glutamate transporters are very efficient in isolating these synapses (Wadiche and Jahr, 2001, see also chapter 1.1.4).

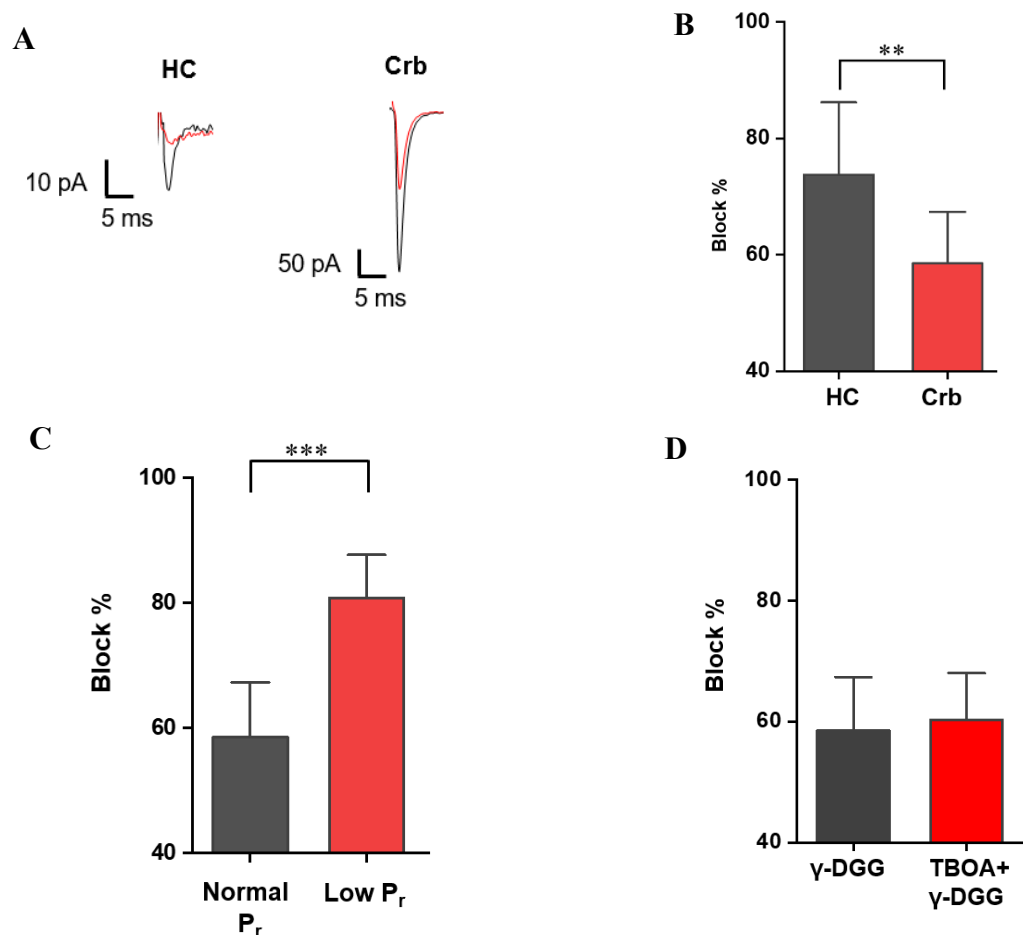


Fig. 5.4. Multivesicular release influences synaptic efficiency of NG2 glia. **A**) Example traces of the application of γ -DGG (1 mM) in hippocampal (left) and cerebellar (right) NG2 glia. **B**) Blocking effect of γ -DGG on ePSC1 in the hippocampus and cerebellum (hippocampus: N=4, n=7; cerebellum: N=5 n=10). **C**) Block by γ -DGG in cerebellar NG2 glia in different P_r conditions, which were simulated by decreasing the extracellular $[Ca^{2+}]$ from 2 mM (normal P_r) to 1 mM (low P_r) while increasing the $[Mg^{2+}]$ from 2 mM to 3 mM. The effect of γ -DGG was significantly higher in normal P_r conditions (ePSC1: N=4, n=9). Block percentage is the ratio between the median peak current amplitude after and before the application of γ -DGG. **D**) Blocking effect of γ -DGG after application of DL-TBOA (ePSC1, TBOA+ γ -DGG: N=6 n=9) suggests that spillover of glutamate does not contribute to AMPAR activation. Data was tested with two sample t-tests. **: $p < 0.01$, ***: $p < 0.001$.

However, BG lamellae are not found close to CF-NG2 synapses (Lin *et al.*, 2005), potentially allowing spillover. To test this, ePSCs were recorded again in the presence of γ -DGG for 10 min. After this time, glutamate transporters were blocked through bath application of DL-TBOA (30 μ M). In case of spillover from neighbouring synapses, γ -DGG-mediated current block would be partially relieved due to a higher concentration of glutamate in the cleft. However, block by γ -DGG did not change in the presence of DL-TBOA (ePSC1 block: $60.32 \pm 7.67\%$; ePSC2 block: $65.88\% \pm 13.31\%$; $p > 0.05$; Fig. 5.4D), even though DL-TBOA

increased the decay of the ePSCs by $16\% \pm 10\%$ (control = 1.02 ± 0.23 ; TBOA = 1.16 ± 0.26 ; paired t-test $p = 0.02$, $N=6$ $n=10$). These results demonstrate that, at CF-NG2 synapses, multivesicular release but not spillover leads to an increase in glutamate concentration in the cleft and contributes to the higher synaptic efficiency.

5.1.4 Short-term plasticity at CF-NG2 synapses

In order to gain a better understanding of cerebellar CF-NG2 synapses, the paired-pulse ratio (PPR) of synaptic responses was analyzed under different experimental conditions to determine the mechanisms of short-term plasticity. It has been established that short-term plasticity mechanisms in CF-PC synapses are primarily presynaptic (Hashimoto and Kano, 1998). During ePSC recordings of CF-NG2 synapses, PPR significantly increased when extracellular $[Ca^{2+}]$ decreased (control PPR = 0.40 ± 0.11 ; low $[Ca^{2+}]$ PPR = 0.53 ± 0.11 , $N=4$ $n=9$; two-sample t-test $p=0.01$; Fig. 5.5A). Additionally, γ -DGG reduced PPR (control: 0.40 ± 0.08 ; DGG: 0.30 ± 0.09 , $p < 0.05$, Fig. 5.5B) suggesting a lower concentration of glutamate released upon the second pulse. Both these evidences indicate that presynaptic Ca^{2+} -dependent mechanisms may be involved in short-term plasticity (Rabl, *et al.*, 2006). Vesicle depletion has been traditionally used to explain presynaptic paired-pulse depression (PPD) at many synapses, including the CF-PC synapse (Liley and North, 1953; Betz, 1970; Zucker and Regehr, 2002). If the depletion model of depression is also applicable to the CF-NG2 synapses, then the amplitude of the second ePSC should depend on the one of the first (Kirischuk *et al.*, 2002). However, linear regression analyses found no correlation between the amplitudes of the two responses ($p = 0.37$, Fig. 5.5C). Next, to test for postsynaptic PPD mechanisms, CF-NG2 synapses were stimulated while applying CTZ ($50\mu M$), which blocks AMPAR desensitization. The modulatory effect of CTZ was significantly higher for ePSC2 than for ePSC1 (ePSC1 = $109.21\% \pm 22.78\%$; ePSC2 = $185.46\% \pm 80.71\%$; $p < 0.01$), and PPD clearly decreased (control PPR = 0.33 ± 0.06 ; CTZ PPR = 0.47 ± 0.07 ; paired-sample t-test $p < 0.0001$; Fig. 5.5 D, E). Notably, these findings differ from those obtained in CF-PC synapses, where receptor desensitization is not involved in short-term plasticity (Dittman and Regehr, 1998). Taken together, this data suggests that short-term plasticity in CF-NG2 synapses involves contributions from both pre- and postsynaptic sides.

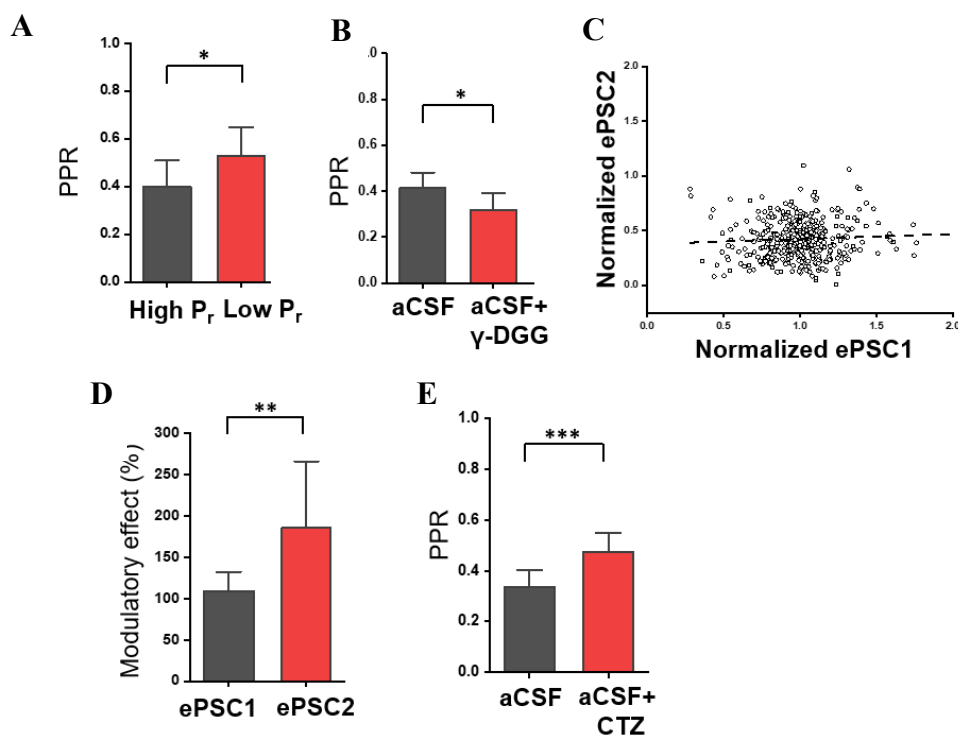


Fig. 5.5. Short-term plasticity mechanisms in cerebellar CF-NG2 synapses. **A)** PPR at different release probabilities (high P_r : 2 mM Ca^{2+} : N=6, n=18; low P_r : 1 mM Ca^{2+} : N=4, n=9; two-sample t-test), suggesting the importance of presynaptic Ca^{2+} in regulating PPD. **B)** Application of γ -DGG (1 mM), blocks more the second pulse than the first, reducing the PPR (N=6, n=11; γ -DGG: N=6, n=11, two-sample t-test) and suggesting that a lower concentration of glutamate is released on the second pulse. **C)** Regression analysis excludes vesicle depletion. Both ePSC1 and ePSC2 amplitudes of all cells were normalized to the median value of EPSC1 and pooled and a linear fit was performed. The dashed line represents linear regression (intercept: 0.37 ± 0.05 ; slope: 0.04 ± 0.05 ; $p = 0.37$; N=7, n=16). **D)** Modulatory effect of CTZ (50 μ M) on AMPA ePSCs evoked in NG2 glia after stimulation of CFs. The modulatory effect was calculated through the ratio of the median peak amplitudes after and before CTZ application (N=3, n=7; paired-sample t-test). **E)** CTZ significantly increases the PPR in cerebellar NG2 glia (paired-sample t-test; N=4, n=8). *: $p < 0.05$, **: $p < 0.01$, ***: $p < 0.001$.

5.2 Impact of NG2 glia AMPARs on neuronal signalling and behaviour

While in the previous chapter we compared NG2 glia AMPARs in the hippocampus and cerebellum, the role that these cells have in the considered regions and how they contribute to normal neuronal functioning is still not understood. For this reason, our laboratory, in collaboration with Prof. Kirchhoff group (Center for Integrative Physiology and Molecular Medicine, University of Saarland, Homburg, Germany), established a new inducible mouse line, here termed GluAko, in which adult NG2 glia lacks AMPAR subunits GluA1-4 (see chapter 4.1.3). In the first part of the next section, a functional characterization of NG2 glia in the cerebellum of GluAko mice will be made. Interestingly, previous data obtained through fEPSP recordings shows a reduction in LTP in CA1 pyramidal neurons following Schaffer collateral stimulation in GluAko mice (Nehal Gebril and Stefan Hardt, not published). Subsequently, I assessed LTP in cerebellar PCs. Additionally, I have performed patch-clamp recordings from cerebellar PCs to check whether neuronal firing and miniature PSCs properties are also affected in GluAko mice. Moreover, I investigated the impact of CP-AMPARs expressed by NG2 glia on neuronal signalling. Finally, we have conducted behavioural tests in control and GluAko mice to correlate neuronal dysfunctions in GluAko mice with behavioural abnormalities.

5.2.1 Inducible deletion of AMPARs in NG2 glia entails loss of receptor currents in the cerebellum

AMPA-mediated currents in inducible control and GluAko mouse lines were measured in the cerebellum from three weeks after tamoxifen injection. NG2 glia was recorded in whole-cell patch-clamp while CFs were stimulated to activate AMPARs (chapter 4.3.7.1), in the presence of picrotoxin (100 μ M). AMPAR-mediated responses in GluAko mice were either completely absent or severely reduced in 20 out of 27 NG2 glial cells (control: median= -157.7 pA, quartiles= -76.5 - -180.8 pA; GluAko: median= -22.4 pA, quartiles= -18.1 - -27.2 pA; GluAWT: median= -68.5 pA, quartiles= -60.6 - -242.6 pA; $p < 0.01$; Fig. 5.6 A, B). A small percentage of cells ($n=7$) was showing ePSCs in the same range as in control mice and they were thus termed GluAWT.

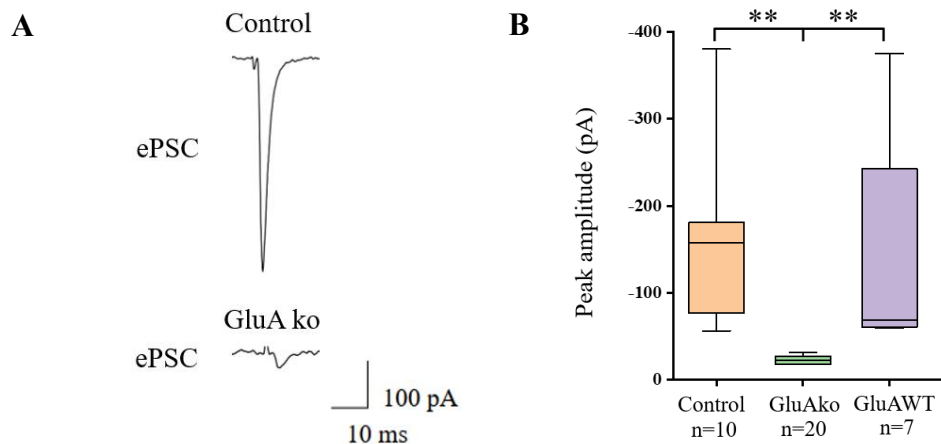


Fig. 5.6. Loss of AMPAR-mediated inward currents in the cerebellum of GluAko mice. **A)** Sample ePSCs recorded in NG2 glia upon stimulation of climbing fibers in both control and GluAko mice. Only small or no ePSCs could be observed in GluAko cells. **B)** Peak amplitudes of ePSCs in the presence of picrotoxin (Control: N=5 n=10, GluAko: N=7 n=20, GluA3WT: N=4 n=7). Vh: -70mV; Mann-Whitney test. **: $p < 0.01$.

5.2.2 Long-term plasticity is impaired in the cerebellum of GluAko mice

While the notion that cerebellar NG2 glia is synaptically innervated by both CFs and PFs is well established, no evidence so far could point out whether these synapses are important for normal functioning of the cerebellar network. Therefore, postsynaptic LTP between PFs and PCs was studied in both control and GluAko mice. In previous works, this type of plasticity was induced with different stimulation frequencies, mostly using whole-cell patch clamp (Lev-Ram *et al.*, 2002; Smith and Otis, 2005; Bouvier *et al.*, 2016; Belmeguenai *et al.*, 2010). While this single-cell recording technique might give more reproducible results, the question whether NG2 glia influences the cerebellar neuronal network can be better tackled if recordings are made from multiple PCs simultaneously. For this reason, fEPSPs of cerebellar slices were made in an interface recording chamber (chapter 4.3.9). Stimulation and recording electrodes were placed as shown in Fig. 4.3 and adjusted to clearly identify all components of fEPSPs. These consisted of a large and fast presynaptic fiber volley (FV), due to PF activation, followed by a smaller and slower post-synaptic response from PCs. In some experiments NBQX (10 μ M) and TTX (0.5 μ M) were added to the bath to block AMPARs (which mediate the postsynaptic response) and Na⁺ channels (which contribute to the FV) respectively, to unequivocally identify the components of the fEPSPs (Fig. 5.7A). Moreover, TTX (0.5 μ M) was also washed-in at the end of the experiments for post-recording subtraction of the stimulus artefact. Multiple stimulation frequencies and durations were first tested to achieve the most stable LTP in PF-

PC synapses (i.e., with lowest variance) in our experimental conditions (Fig. 5.7 B, C). The best protocol consisted of 10 stimulation pulses given at 150 Hz every 3 sec for 5 min. Since some authors argue that induction of LTP in sagittal slices at high-frequencies could interfere with intracellular Ca^{2+} dynamics because of the vicinity between stimulation electrode and recorded cells (Bouvier *et al.*, 2016), it was tested whether low- and high-frequency stimulation protocols could give good results also in cerebellar transverse slices. While it was still possible to evoke fEPSPs with similar shape as in sagittal slices, LTP protocols failed to induce plasticity. One reason for this could be that the dendritic tree of PCs is cut in transverse slices, reducing excitatory inputs and impairing LTP in these recording conditions. Therefore, LTP was induced in sagittal cerebellar slices with stimulation at 150 Hz. As first step, an input-output curve (I-O curve) was always obtained in slices by giving low-frequency (0.6 Hz) stimulation pulses at increasing intensities (25, 50, 100, 150, 200, 300, 400 μA). The intensity which gave half of the maximal response was used for the rest of the experiment. Averaged I-O curves from control and GluAko mice showed similar values (Fig. 5.8A) suggesting similar neuronal excitability in the genotypes. After determining the pulse intensity to be used, baseline paired-pulse recordings (10 min) were made at a frequency of 0.6 Hz.

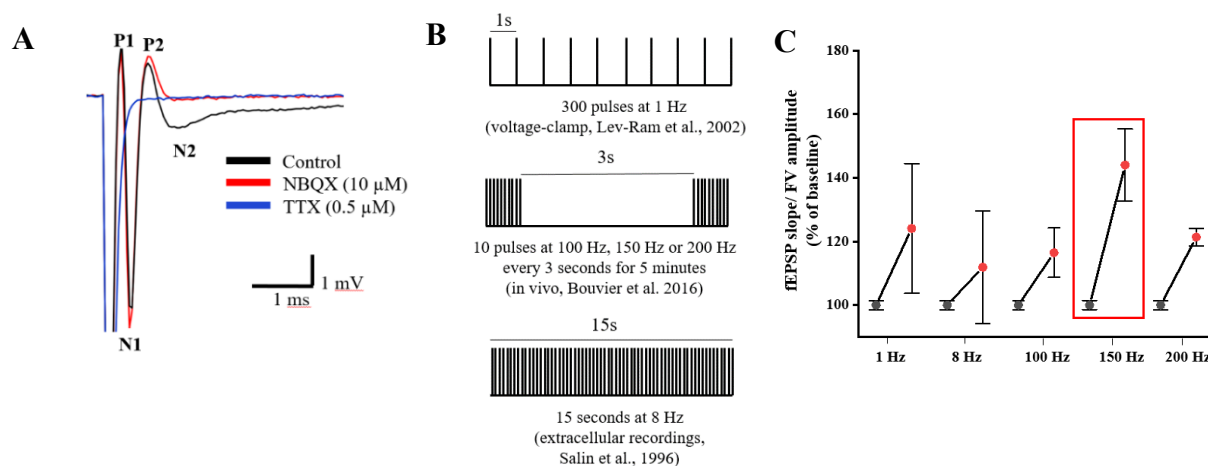


Fig. 5.7. Experimental protocol for recording fEPSPs in cerebellar slices. **A)** Sample fEPSP generated upon stimulation of parallel fibers. Stimulation in aCSF (control line) shows the stimulation artefact followed by positive (P) and negative (N) peaks. The curve from P1-N1-P2 represents the FV, from P2-N2 is the postsynaptic response. NBQX application abolishes P2-N2 peak, while TTX cancels out the FV. **B)** Schematic representation of the stimulation protocols used to test LTP. In parenthesis is the experimental method given in the literature. **C)** Plot showing results from different stimulation protocols in cerebellar sagittal slices. 150 Hz stimulation protocol gave the strongest potentiation (1 Hz: $124.11\% \pm 20.38\%$, $n=5$, $N=3$; 8 Hz: $111.91\% \pm 17.8\%$, $n=4$, $N=2$; 100 Hz: $116.47\% \pm 7.76\%$, $n=5$, $N=10$; 150 Hz: $144.03\% \pm 11.3\%$, $n=9$, $N=5$; 200 Hz: $121.36\% \pm 2.7\%$, $n=4$, $N=2$). Grey dot is the mean baseline value, red dot is the value after LTP induction.

Subsequently, slices were stimulated with the 150 Hz protocol mentioned above. Recordings continued at low-frequency stimulation for another 30 min. PTP (first 3 min) and LTP (last 5 min) were then assessed. Remarkably, LTP (last 5 min) was greatly reduced or absent in GluAko slices compared to controls while PTP was similar (1-3 min= control: $111.7 \pm 7.3\%$, GluAko: $98.2 \pm 5.2\%$; 25-30 min= control: $149.8 \pm 12.4\%$, GluAko: $95.8 \pm 4.4\%$; $p < 0.01$; Fig. 5.8 B-C). The paired-pulse ratio of the responses was also analysed before and after LTP induction but no differences were found between genotypes (Table 2).

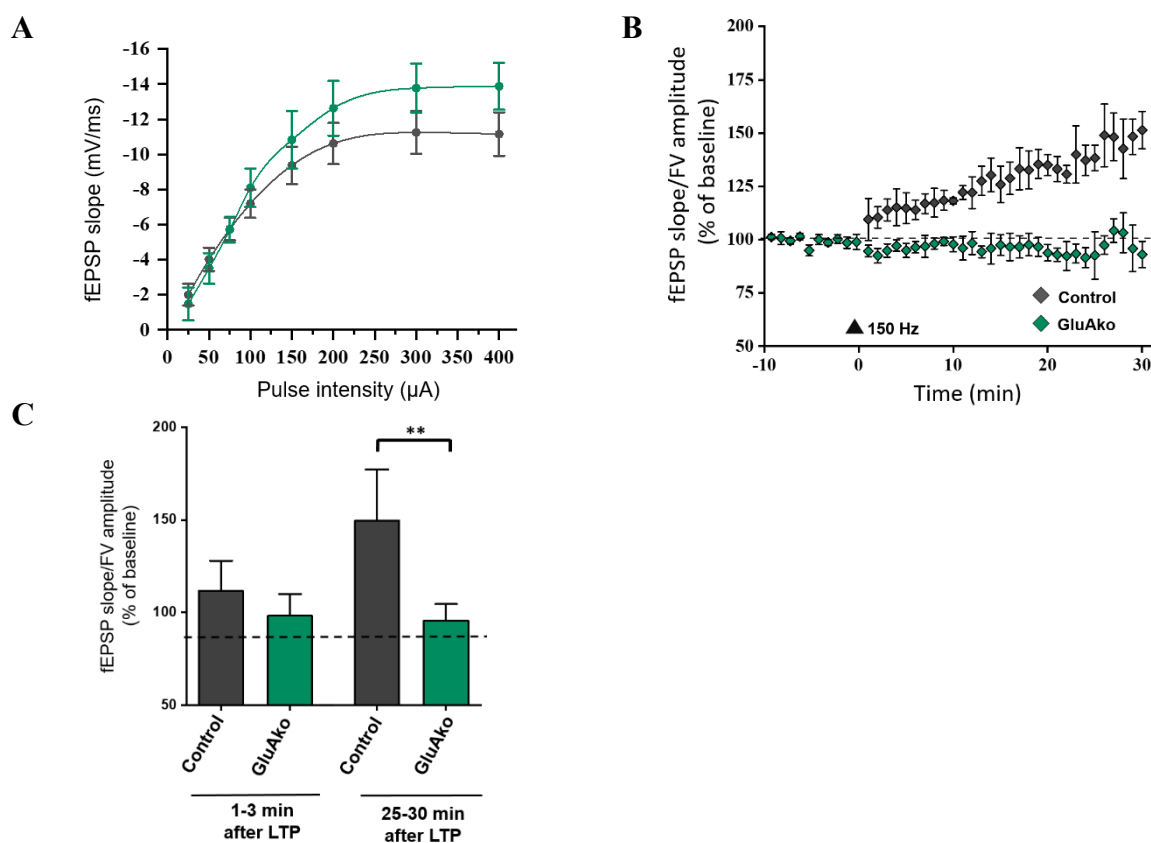


Fig. 5.8. LTP is impaired in the cerebellum of GluAko mice. **A**) Input-output curve of fEPSP slope at different pulse intensities. No differences were detected between control (grey) and GluAko (green) mice (tested with repeated measures ANOVA and post-hoc Tukey Test). **B**) Time-course of fEPSPs in cerebellar slices of control and GluAko mice. LTP was induced with a 150 Hz stimulation protocol. Time bin of 1 min. **C**) Average fEPSP slope/FV ratio in control and GluAko slices 1-3 min and 25-30 min after LTP induction. Differences were significant towards the end of recordings (Two-sample t-test). Control and GluAko: $N=5$, $n=13$. **: $p < 0.01$.

These results suggest that NG2 glia AMPARs are important mediators of normal neuronal processing in the cerebellum.

PPR		Control	GluAko	Control in 7,8-DHF	GluAko in 7,8 DHF
Baseline	Cerebellum	1.11 ± 0.03	1.11 ± 0.04	1.30 ± 0.2	1.12 ± 0.06
	Hippocampus	1.40 ± 0.1	1.38 ± 0.1	1.46 ± 0.1	1.44 ± 0.1
1-3 min	Cerebellum	1.10 ± 0.04	1.13 ± 0.04	1.08 ± 0.1	1.06 ± 0.03
	Hippocampus	1.22 ± 0.1	1.28 ± 0.1	1.19 ± 0.06	1.17 ± 0.1
25-30 min	Cerebellum	1.05 ± 0.04	1.11 ± 0.04	1.10 ± 0.2	1.09 ± 0.05
	Hippocampus	1.36 ± 0.05	1.32 ± 0.1	1.32 ± 0.1	1.35 ± 0.1

Table 2. PPR of fEPSPs of control and GluAko mice. PPR at different time points (baseline before LTP induction, 1-3 min and 25-30 min after LTP induction) shows no differences between genotypes in the hippocampus or cerebellum. Mean ± SD.

5.2.2.1 LTP can be rescued by a TrkB agonist

Data presented in chapter 5.2.2 shows that cerebellar NG2 glia can influence LTP in cerebellar PCs. This data goes in parallel with the one gathered by Stefan Hardt and PhD candidate Nehal Gebril in the hippocampus of GluAko mice, where LTP between SCs and pyramidal neurons is also reduced (1-3 min: control= 201.77 ± 12.6%, GluAko= 136.41 ± 6.6%, $p < 0.0001$; 25-30 min: control= 174.43 ± 8.9, GluAko in aCSF= 128.9 ± 6.8%; control: N= 16, n=34; $p < 0.0001$; not published). One intriguing hypothesis explaining how NG2 glial cells can interfere with neuronal processing is that they can regulate extracellular levels of neurotrophins like BDNF (chapter 1.6). To test this hypothesis, cerebellar and hippocampal slices from GluAko mice were perfused with aCSF containing 7,8-dihydroxyflavone (7,8-DHF, 1 μ M). This molecule is an agonist of TrkB receptors and it mimics BDNF actions, inducing receptor auto-phosphorylation and dimerization and the activation of downstream signalling cascades normally activated by BDNF (Du and Hill, 2015). Recordings from slices started 30 min after incubation with this molecule. Excitingly, in the hippocampus, application of 7,8 DHF completely rescued plasticity in GluAko slices both in the first 3 min after LTP induction and after 25 min (1-3 min: GluAko in 7,8-DHF= 226 ± 9.9, $p < 0.0001$; 25-30 min: GluAko in 7,8-DHF= 169.6 ± 12.6%, $p < 0.01$; data collected together with Nehal Gebril; Fig. 5.9A, B). In the cerebellum, LTP was also rescued in the last 5 min of recording (GluAko in 7,8-DHF: 131.2 ± 17 %, $p < 0.05$; Fig. 5.9C, D). In both areas, 7,8-DHF did not interfere with the PPR of the responses (see table 2). These results show that BDNF levels are downregulated in GluAko mice, but increased activation of TrkB receptors with 7,8-DHF can rescue the impaired plasticity.

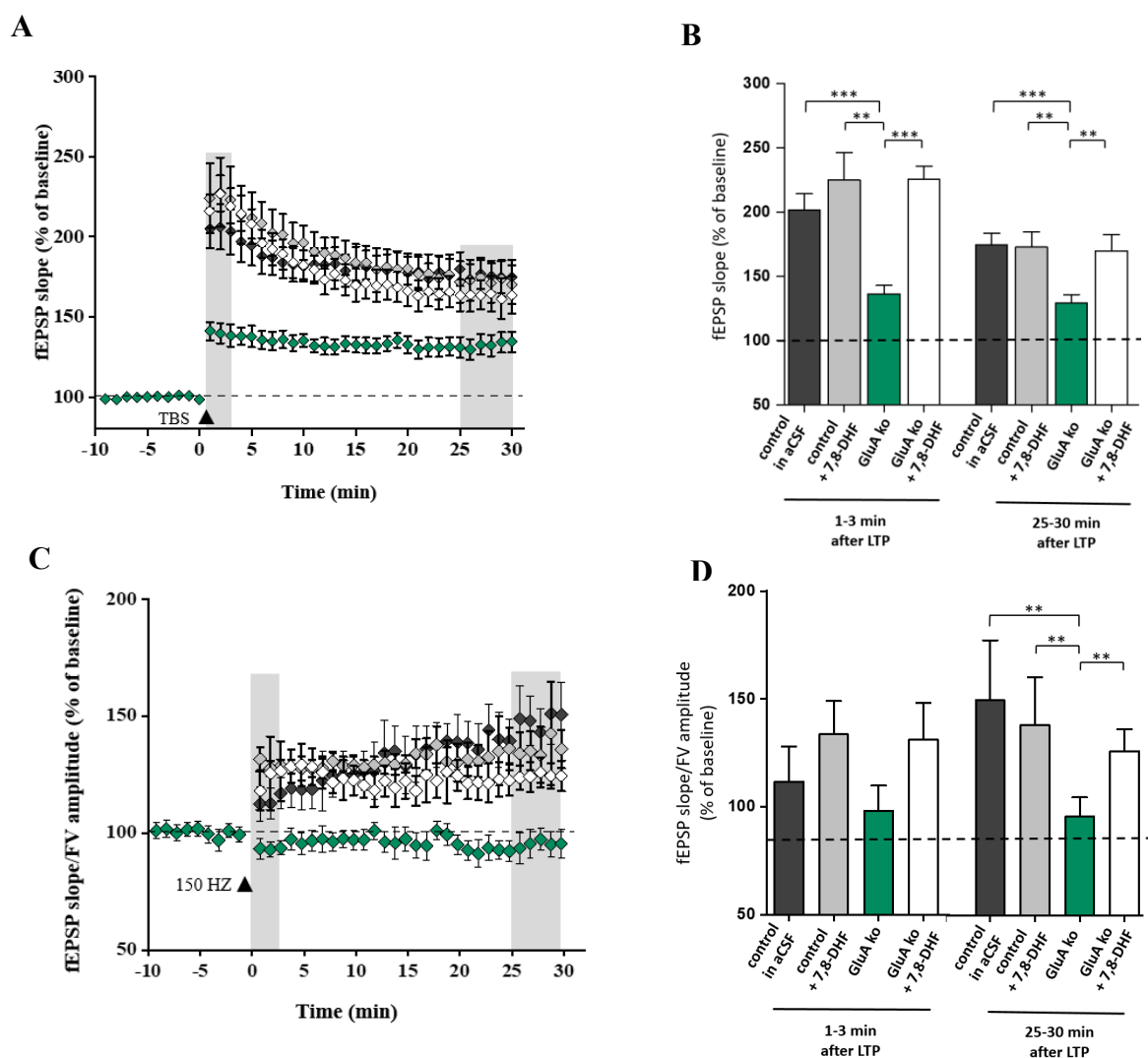


Fig. 5.9. Application of a TrkB agonist in GluAko mice rescues LTP in hippocampus and cerebellum. **A)** Time course of normalized fEPSP slopes of control and GluAko hippocampal slices perfused with aCSF or 7,8-DHF. TBS: Theta burst stimulation. **B)** Analysis of fEPSP slopes in the hippocampus 1-3 min and 25-30 min after TBS. LTP was lower in hippocampal slices of GluAko mice. Application of 7,8-DHF restored LTP. Control in aCSF: N= 16, n=34; control in 7,8-DHF: N=6, n=15; GluAko: N=15, n=32; GluAko in 7,8-DHF: N=8, n=20. **C)** Time-course of normalized fEPSP slope/FV amplitude ratio in the cerebellum before and after 150 Hz stimulation to induce LTP between PFs and PCs. **D)** Normalized fEPSP slope/FV amplitude ratios revealed decreased LTP in GluAko cerebellar slices during the last 5 min of recording ($p=0.01$), which was rescued by 7,8-DHF (1 μ M); control: N=5, n=13; control in 7,8-DHF: N=5, n=13; GluAko: N=5, n=13; GluAko in 7,8-DHF: N=4, n=11. Data was tested with two-sample t-tests. Mean \pm SEM; ** $p < .001$, *** $p < .0001$.

5.2.3 Purkinje neurons show altered AP firing in GluAko mice

Cerebellar LTP, studied in chapter 5.2.2, originates from the input of both PFs and CFs to PCs (D'Angelo, 2014). To verify possible changes in PC physiology, patch-clamp recordings were performed in both control and GluAko mice. Since PCs are very heterogeneous, they were subdivided into three groups according to their firing state: tonic firing (48% in control, 51% in GluAko), bursting (17% in control, 11.4% in GluAko) and silent (23% in control, 37% in GluAko). Only tonic firing PCs were considered for the analysis. No differences in passive membrane properties (V_m , R_m or C_m) were detected between genotypes (Table 3). Since PC firing properties were shown to be dependent on the expression of Zebrin II in some cerebellar lobules (see chapter 1.1.3), cells were first separated in Z+ and Z- groups according to their position in the lobule and to post-recording single-cell RT-PCR analyses of Zebrin mRNA (section 4.5.3). For a more detailed assessment, EAAT4 mRNA (expressed mainly in Z+ PCs; Zhou *et al.*, 2014) and mGluR1b mRNA (expressed in Z- PCs; Mateos *et al.*, 2001) were also quantified. Interestingly, data shows no difference in simple spike firing properties and AP waveform between Z+ and Z- PCs from lobule VI of control mice, contrarily to what has been previously described for other lobules (Zhou *et al.*, 2014; Viet *et al.*, 2022).

	V_m (mV)	R_m (M Ω)	C_m (pF)
Control	-57 ± 6.4	87 ± 44.5	401 ± 128
GluAko	-56 ± 6.4	91 ± 52.7	429 ± 134

Table 3. Passive membrane properties of PCs from control and GluAko mice. No significant differences were found in the above parameters (two-sample t-tests). Control: N=8, n=21; GluAko: N=8, n=26. Mean \pm SD.

Notably, when pooling together Z+ and Z- PCs, firing rate was significantly decreased in GluAko slices compared to controls (control: 76.22 ± 27.2 Hz; GluAko: 51.42 ± 11 Hz; $p < 0.05$; Fig. 5.10B). No other differences could be seen in AP shape or kinetics (Table 4). Next, excitatory transmission to PCs was assessed through mPSC recordings (section 4.3.8). In this case, no difference in mPSC frequency (control: median= 1.23 Hz, quartiles= 0.74 - 1.88 Hz; GluAko: median= 1.46 Hz, quartiles= 1.28 - 2.22; $p > 0.05$; Fig. 5.10 F) or amplitude (control: -12.13 ± 2.22 pA; GluAko: -13.44 ± 2.3 pA; $p > 0.05$; Fig. 5.10 E) was detected.

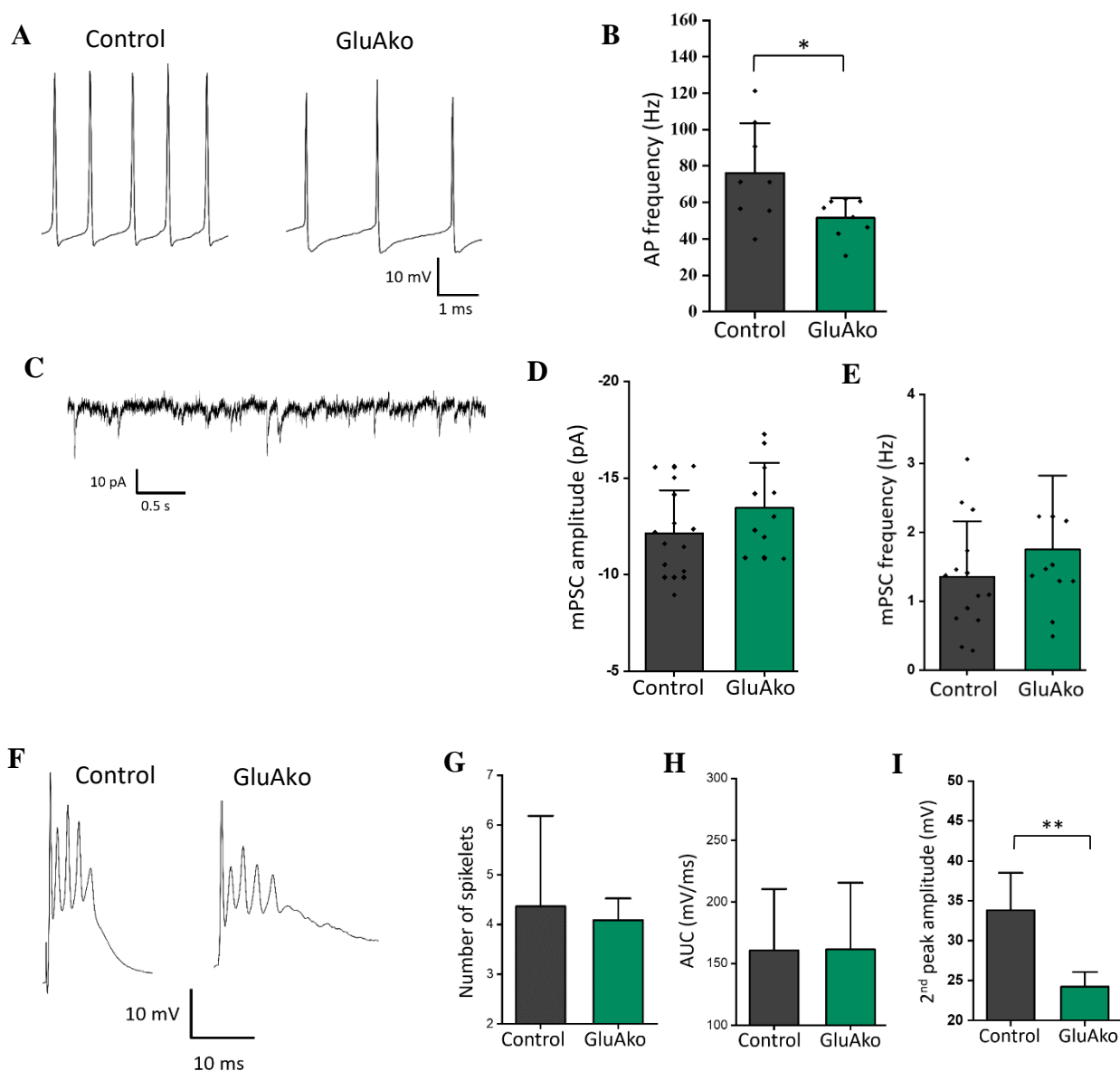


Fig. 5.10. Properties of PCs in control and GluAko slices. **A**) AP firing from PCs from control (left) and GluAko slices (right). **B**) AP frequency is significantly reduced in GluAko mice (two sample t-test). Control: N=8, n=21; GluAko: N=8, n=26. **C**) mPSCs sample trace from control slices recorded in the presence of TTX and picrotoxin. **D, E**) mPSC peak amplitude and frequency do not change in control and GluAko slices (peak amplitude: two-sample t-test; frequency: Mann-Whitney test). Control: N=14, n=30; GluAko: N=11, n=20; **F**) Sample trace of complex spikes generated in PCs upon CFs stimulation in both control and GluAko slices. **G, H, I**) Main parameters to quantify complex spike differences. While there is no change in the number of spikelets and area under the curve (AUC), the amplitude of the second peak is reduced in GluAko mice (two-sample t-test; control: N=5, n=9; GluAko: N=5, n=10). Mean \pm SD. *: $p < 0.05$; ** $p < .001$.

	Control N=8 n=21	GluAko N=8 n=26
Peak amplitude (mV)	45.75 ± 3.5	50.93 ± 5
Upstroke (mV)	36.6 ± 3.7	39.3 ± 4.1
Threshold (mV)	43.5 ± 3	43 ± 3.6
Half-width (ms)	0.34 ± 0.03	0.35 ± 0.02
Rise time (ms)	0.25 ± 0.05	0.27 ± 0.03
Decay time (ms)	0.40 ± 0.01	0.38 ± 0.03
CV_{ISI}	0.26 ± 0.1	0.25 ± 0.1
AHP (mV)	-11 ± 2.6	-9.5 ± 2

Table 4. AP properties and kinetics in control and GluAko slices. No significant differences were found in the above parameters (two-sample t-tests). Control: N=8, n=21; GluAko: N=8, n=26. Mean ± SD.

While simple spike firing of PCs is due to the input from PFs, inputs from CFs give rise to complex spikes (CS, chapter 1.1.2). Thus, CF functionality was assessed by evoking complex spikes in PCs in current-clamp mode upon CF stimulation in the GL. As the properties of CSs are dependent on the firing state of PCs (Servais *et al.*, 2004), only complex spikes from tonic firing PCs were analysed. No differences were found in the number of spikelets (control: 4.36 ± 1.2 ; GluAko: 4.09 ± 0.29 ; $p > 0.05$; Fig. 5.10 H) or area under the curve (control: $160.68 \text{ mV/ms} \pm 33.2 \text{ mV/ms}$; GluAko: $161.50 \text{ mV/ms} \pm 36 \text{ mV/ms}$; $p > 0.05$; Fig. 5.10 I) between genotypes. The amplitudes of the first three spikes in CSs were also analysed. In this case, amplitude of the second peak was significantly reduced in GluAko mice (control: $33.81 \text{ mV} \pm 4.7$, N=5, n=9; GluAko: 24.22 ± 1.8 ; $p < 0.01$ Fig. 5.11 J), while amplitude of the first (control: $40.3 \text{ mV} \pm 4 \text{ mV}$; GluAko: $39.7 \text{ mV} \pm 2.54 \text{ mV}$; $p > 0.05$) and third spike (control: $30.34 \pm 4.3 \text{ mV}$; GluAko: 28.6 ± 2.9 ; $p > 0.05$) remained unchanged. This shows that in GluAko mice both PF and CF inputs to PCs are altered, possibly contributing to impaired PC output and reduced LTP.

5.2.4 Behavioural tests

As shown in previous chapters, GluAko mice present impairments in LTP in both hippocampus and cerebellum. Since this type of plasticity is important for normal functioning of both hippocampus and cerebellum, memory and motor abilities of mice were tested in a series of behavioural tasks. These experiments were done together with Dr. Gerald Seifert and PhD candidates Nehal Gebril and Michela Palmisano. Before starting these tasks, mice were habituated to the new environment (a sawdust-covered 44x44 cm² arena) for 5 min per day in three consecutive days. During the first day of habituation, mouse movements were recorded to assess the locomotor activity in the open-field. Here, controls were similar to GluAko mice for immobility time (201 ± 18.42 s vs 194.78 ± 25.96 s; $p > 0.05$; Fig. 5.11A), distance travelled (50957.64 ± 7871.5 cm vs 50282.42 ± 8079.7 cm; $p > 0.05$; Fig. 5.11B) and speed (170.64 ± 25.6 cm/s vs 169.43 ± 26.3 cm/s; $p > 0.05$; Fig. 5.11C).

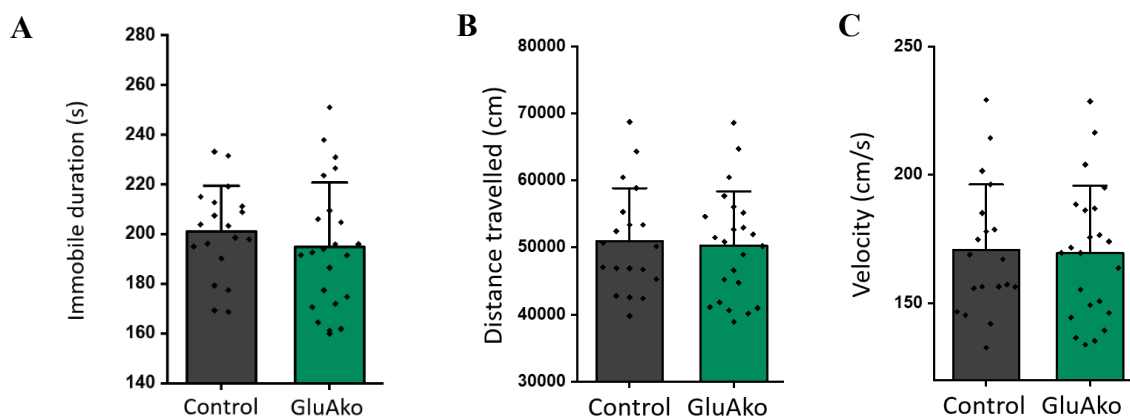


Fig. 5.11. Open-field test shows no differences in locomotor activity. A, B, C) Mice were free to move in a 44x44 cm arena for 5 min. No differences were found in duration of immobility (A), distance travelled (B) and speed (C) between control and GluAko mice. Mean \pm SD. Two-sample t-tests were performed between genotypes as no difference between sexes was detected after two-way ANOVA. Control: N=18; GluAko: N=22.

5.2.4.1 NOLR test

Hippocampus-dependent spatial memory has been assessed through the NOLR test (Vogel-Ciernia and Wood, 2014). As described in chapter 4.4.1, in the first trial of the test (6 min), mice were presented with three different objects, one of which was moved to a new location in trial 2 (3 min).

Time of exploration on the novel location did not differ between genotypes (control: $39.11 \pm 17.2\%$; GluAko: $47.37 \pm 17.8\%$; $p > 0.05$; Fig. 5.12A) nor did the preference for the novel location (control: $2.26 \pm 25.6\%$; GluAko: $4.25 \pm 29.1\%$; $p > 0.05$; Fig. 5.12B). Neither group spent more time in the new compared to the old location (one-sample t-test: $p > 0.05$ for both genotypes). Interestingly, distance travelled (control: median= 2587.35 cm, quartiles= 2504.4 - 3019.57 cm; GluAko: median= 2354.52, quartiles= 2034.6 – 2694.3 cm; $p < 0.05$) and velocity (control: median= 7.45 cm/s, quartiles= 6.9 - 8.5 cm/s; GluAko: median= 6.54 cm/s, quartiles= 5.6 – 7.7 cm/s; $p < 0.05$) was significantly lower in GluAko mice.

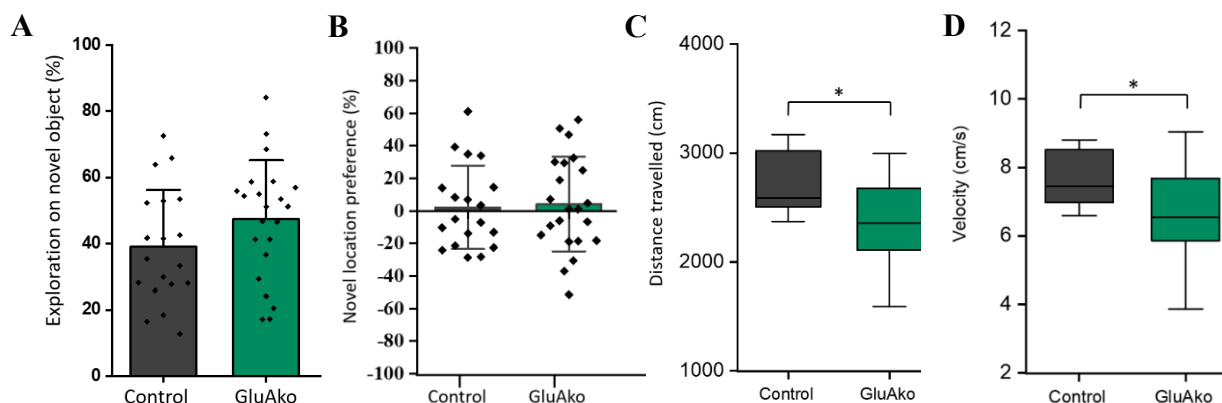


Fig. 5.12. No defects in spatial memory are present in GluAko mice according to the NOLR test.

A) Exploration time for each object was calculated as in chapter 4.4.1. No differences were detected with two-sample t-test $p > 0.05$. **B)** Preference for the novel location did not differ between genotypes (two-sample t-test $p > 0.05$). In both groups, mean was not different from zero as calculated with one-sample t-test $p > 0.05$. **C, D)** Motility and velocity differed significantly between groups (Mann-Whitney test). Control: N=18; GluAko: N=22. No difference between sexes was detected with two-way ANOVA. *: $p < 0.05$.

5.2.4.2 Partner recognition test

Social memory, also dependent on the hippocampus (Bilkei-Gorzo *et al.*, 2014), was assessed through the PRT (chapter 4.4.2). On each of the four days, mice were presented with a partner and an empty cage (object) in trial 1 and the same familiar partner together with a new one in trial 2. On the first day, inter-trial interval was 1hr. Here, both genotypes performed well in the sociability task during trial 1, passing more time interacting with the partner rather than with the object (control: mouse vs object interaction: $p < 0.0001$; GluAko: mouse vs object interaction: $p < 0.0001$; two-way ANOVA with Bonferroni post-hoc test; Fig. 5.13A). However, mice performed similarly in trial 2 ($5.88 \pm 18.4\%$ vs $10.18 \pm 31.2\%$; $p > 0.05$; Fig. 5.13B) spending the same amount of time with familiar and unfamiliar mice (one-sample t-test, $p > 0.05$). On the 2nd, 3rd and 4th day, mice did not seem to have a preference for either the object or the partner in trial 1. However, in trial 2 both genotypes spent more time with the unfamiliar

partner (Fig. 5.13 C-E). These results show that GluAko mice do not present deficits in social memory. On the other hand, like in the NOLR test, overall motility (3611.53 ± 634 cm vs 2480.3 ± 481 cm; $p < 0.0001$; Fig. 5.13F) and velocity (11.08 ± 1.3 cm/s vs 8.17 ± 1.1 cm/s; $p < 0.0001$; Fig. 5.13G) were strongly reduced in GluAko mice.

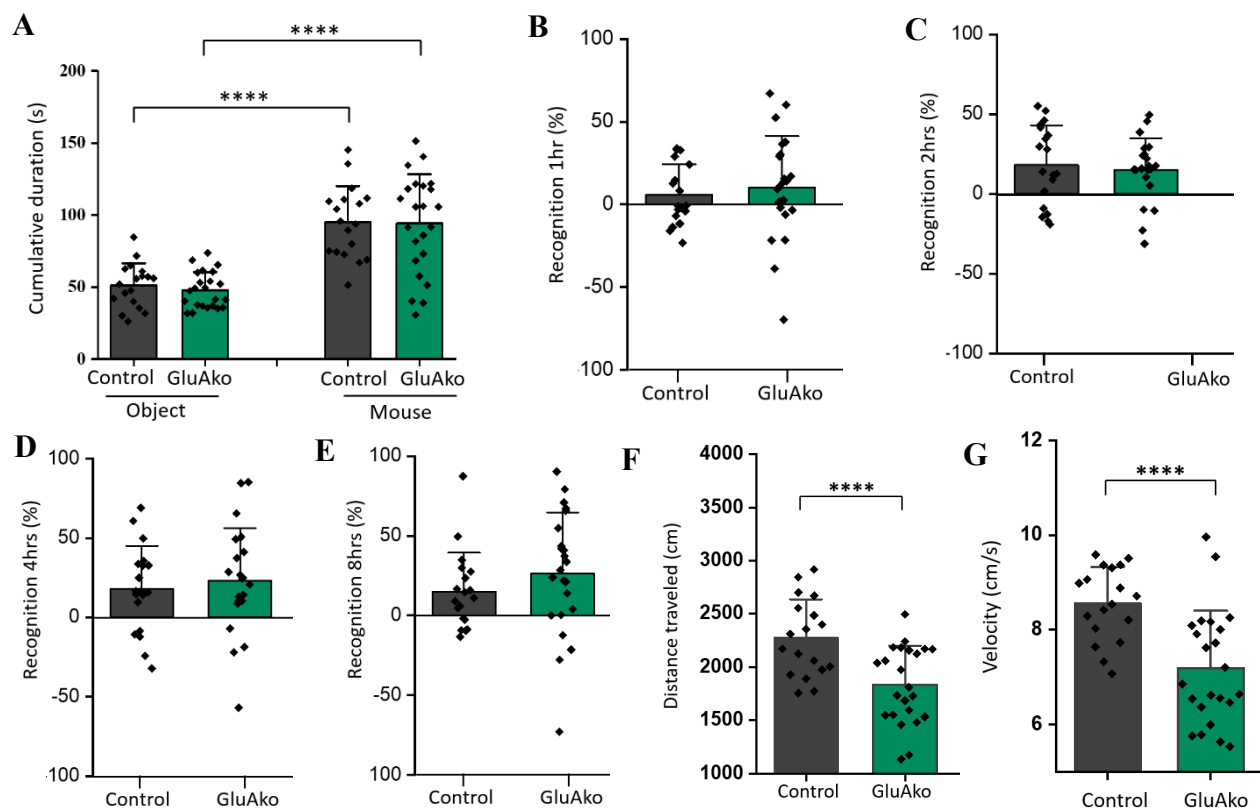


Fig. 5.13. Social memory is not impaired in GluAko mice as assessed by the PRT. **A)** Sociability task on day 1. Cumulative duration is measured as the total time mice spent with mouse or object. **B)** Recognition of the unfamiliar partner in trial 2 after an intertrial interval of 1 hr. Neither group spent more time with the unfamiliar partner. **C, D, E)** Recognition of the unfamiliar partner in trial 2 with inter-trial intervals of 2, 4 and 8 hrs respectively. In all cases, both mouse groups spent more time with the unfamiliar partner in a similar way (mean > 0, one-sample t-test). **F, G)** Locomotor activity of control and GluAko mice was different. Control: N=18; GluAko: N=22. Mean \pm SD. Data was tested with two-sample t-tests as no difference between sexes was detected after two-way ANOVA. ****: $p < 0.0001$.

5.2.4.3 Y-maze test

Short-term spatial memory, or working memory, was measured with the Y-maze test (see chapter 4.4.3). Here mice spent 10 min inside the maze, free to move from one arm to the other. Animals visiting always a new arm completed a spontaneous alternation. Control and GluAko mice displayed similar values of alternation ($43.48 \pm 7.8\%$ vs $40.76 \pm 9.1\%$; $p > 0.05$; Fig. 5.14 A) reflecting equivalent short-term memory functionality. Nevertheless, locomotor activity, measured either as total number of arm entries (control: 85.89 ± 12.7 ; GluAko: 55.17 ± 14.31 ; $p < 0.0001$; Fig. 5.14B), distance travelled (control: 142005 ± 17741 cm; GluAko: 103393 ± 20800 cm; $p < 0.0001$; Fig. 5.14C) or velocity (control: 236.68 ± 29.6 cm/s; GluAko: 174.94 ± 37.5 cm/s; $p < 0.0001$; Fig. 5.14D), was severely impaired in GluAko mice.

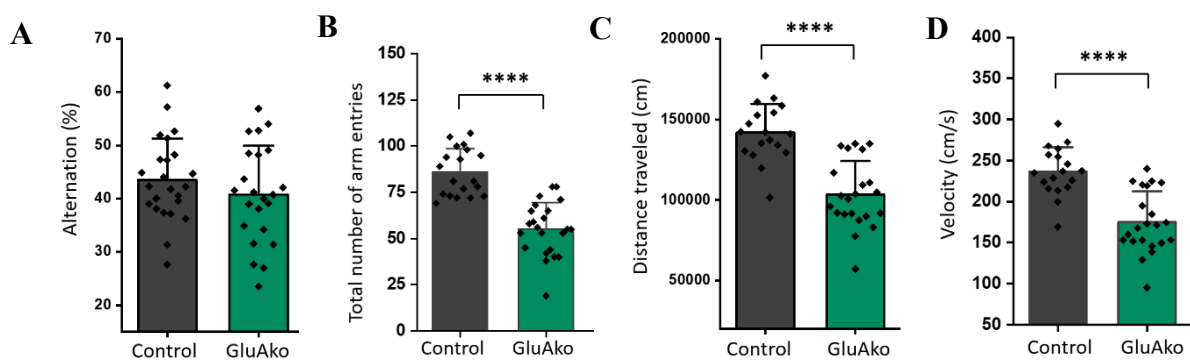


Fig. 5.14. Locomotion but not working memory is impaired in GluAko mice during Y-maze test. **A)** Spontaneous alternation, underlying short-term memory, is not different in GluAko mice. **B)** Total number of arm entries, a measure of locomotion in the Y-maze, is strongly reduced in GluAko mice, as it is motility **(C)** and velocity **(D)**. Control: N=18; GluAko: N=22. Mean \pm SD. Data was tested with two-sample t-tests as no difference between sexes was detected after two-way ANOVA. ****: $p < 0.0001$.

5.2.4.4 Beam-walking test

The beam test measures motor coordination and balance, which are functions related to the cerebellum. After 1 day of training, mice had to walk on rods of three different diameters (28mm, 14 mm and 8mm) until reaching a safe house. Trials on each rod were repeated three times and averaged. On the 28 mm rod, GluAko mice were significantly slower than controls (control: median= 5.17 s, quartiles= 3.9 s - 7.2 s; GluAko: median= 9.1 s, quartiles= 7.6 s - 13.5 s; two-sample t-test, $p < 0.001$; Fig. 5.15A). Here, number of hind limb slips was low and similar between control and GluAko (0.32 ± 0.02 vs 0.11 ± 0.08 ; $p > 0.05$). Similarly, for the 14 mm rod GluAko mice were slower (control: median= 11.09 s, quartiles= 6.5 s - 12.6 s; GluAko: median= 17.19 s, quartiles= 7.1 s - 22.3 s; Mann-Whitney test, $p < 0.05$; Fig. 5.15 B). Also here,

number of slips was comparable (1.2 ± 0.22 vs 1.06 ± 0.25 ; $p > 0.05$). Mice performed similarly on the smaller rod (control: median = 37.29 s, quartiles = 33.9 s - 44.3 s; GluAko: median = 38.04 s, quartiles = 29.7 s - 49.1 s; two-sample t-test, $p > 0.05$; Fig. 5.15 C). In this case, number of slips could not be measured as mice were crawling upside down through the rod.

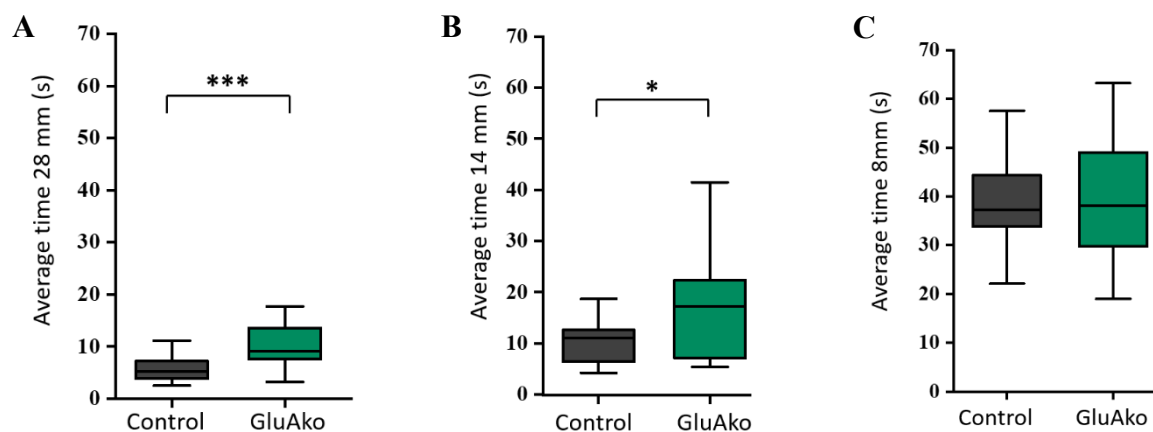


Fig. 5.15. GluAko mice move slower during the beam-walking test. **A)** Average time to cross the 28 mm beam was longer for GluAko mice (two-sample t-test). **B)** Also, on the 14 mm beam, GluAko mice were slower (Mann-Whitney test). **C)** No differences could be detected on the smaller 8 mm beam (two-sample t-test). Control: N=18; GluAko: N=22. Data was tested with either two-sample t-tests or Mann-Whitney test as no difference between sexes was detected after two-way ANOVA. ***: $p < 0.001$; *: $p < 0.05$.

5.2.5 NG2 glia CP-AMPARs regulate neuronal signalling in hippocampus and cerebellum

As shown in previous chapters, the loss of all four AMPAR subunits in NG2 glia influences neuronal transmission and behaviour. Nevertheless, whether all subunits are responsible for these changes is unclear. Data shown in sections 5.1.1 and 5.1.2 demonstrated that adult NG2 glia expresses CP-AMPARs in both hippocampus and cerebellum and that these receptors have an important role in modulating the efficiency of neuron-NG2 glia synapses. Thus, we explicitly addressed the question whether CP-AMPARs are necessary for neuronal processing by using another mouse line expressing only GluA3 subunits in NG2 glia (GluA3WT), because here only homomeric, GluA2-lacking, Ca^{2+} -permeable AMPARs are expressed. This hypothesis was confirmed by recording NG2 glia in both hippocampus and cerebellum by using an intracellular solution containing Nasp_m (100 μM) in the patch pipette (Fig. 5.16A, C). AMPAR current was isolated by co-applying a mix of blockers (quinine, 200 μM ; BaCl_2 , 100 μM ; TTX, 0.5 μM ; picrotoxin, 100 μM).

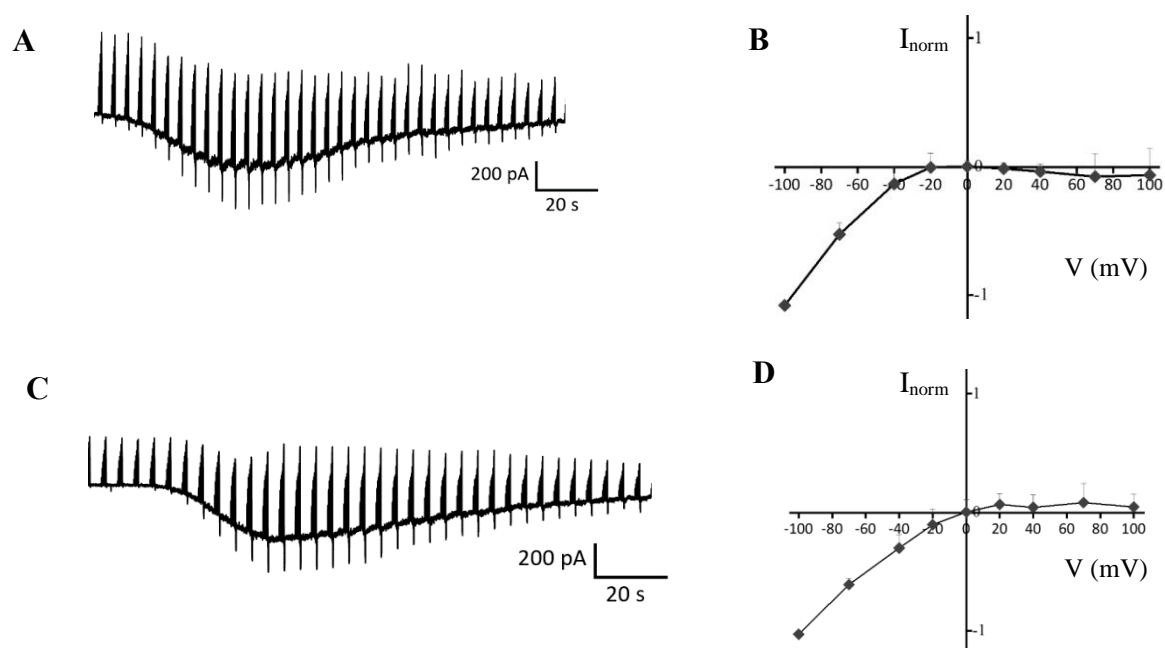


Fig. 5.16. Block of CP-AMPAR-mediated currents in hippocampal and cerebellar GluA3WT slices. **A, C)** Voltage step protocol (-70, -40, -20, 0, 20, 40, 70, 100, -100 mV; duration 100 ms, interval 100 ms, every 4.5 s) applied to NG2 glial cells from hippocampus (A) and cerebellum (C). The pipette solution contained Nasp_m (100 μM) and the extracellular solution blockers of K^+ and Na^+ channels. **B, D)** IV curves of kainate-induced responses in hippocampal (B) and cerebellar (D) NG2 glia from GluA3WT slices. Currents before and during agonist application were subtracted at corresponding voltages. Responses were then normalized to the maximum inward current and averaged (I_{norm} ; hippocampus: n=9; cerebellum: n=8; Mean \pm SD).

AMPA activation through kainate application (250 μ M) revealed a complete block of outward currents, confirming that NG2 glia from GluA3WT mice expresses solely CP-AMPA receptors (rectification index: hippocampus = 0.02 ± 0.02 , cerebellum = 0.03 ± 0.03 ; Fig. 5.16 B, D). Next, fEPSPs were recorded from hippocampal and cerebellar slices of GluA3WT mice. (1-3 min = control: $111.7 \pm 7.3\%$, GluA3WT: $98.2 \pm 11.6\%$; 25-30 min = control: $149.8 \pm 12.4\%$, GluA3WT: $136.26 \pm 5.2\%$; $p > 0.05$; Fig. 5.17 D). This data shows the relevant role of CP-AMPA receptors expressed by NG2 glia for proper functioning of these cells and of the neuronal network.

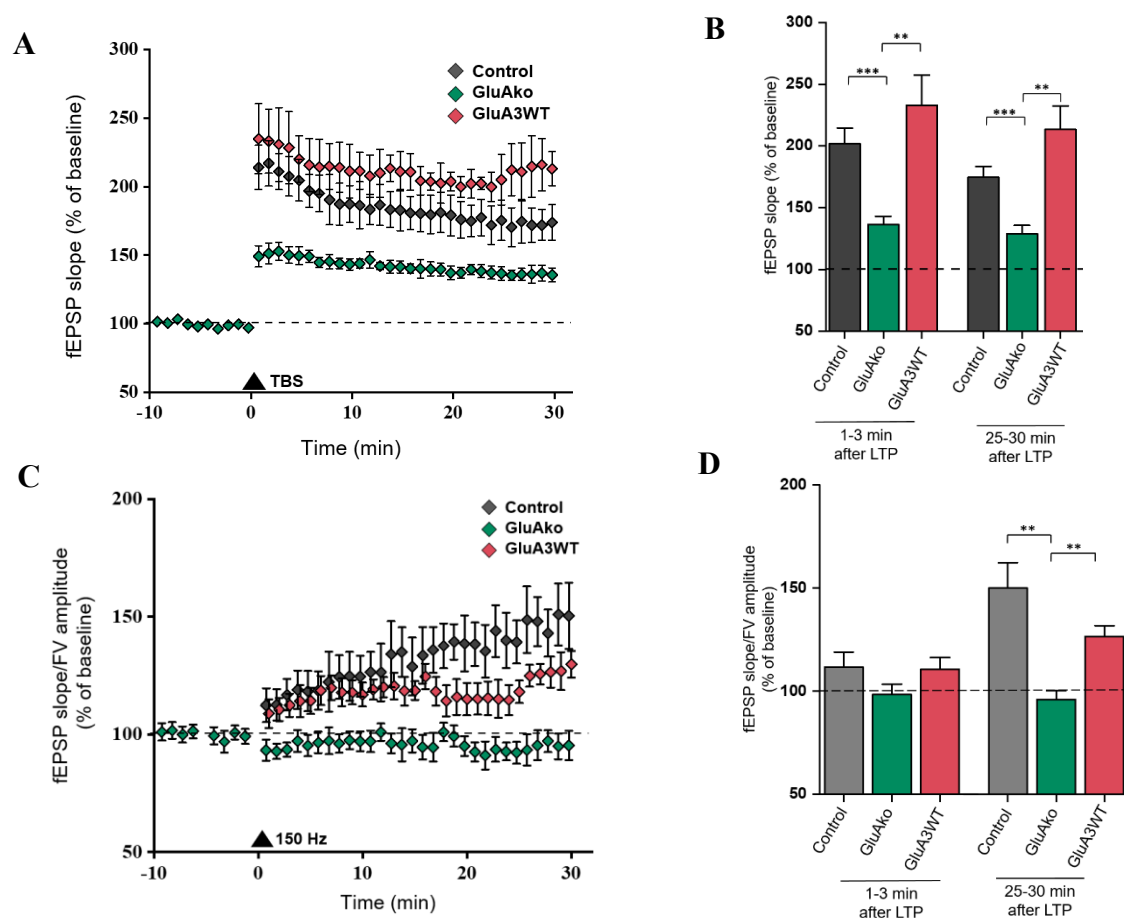


Fig. 5.17. fEPSP recordings from hippocampal and cerebellar GluA3WT slices. **A, C**) LTP time course in hippocampal slices upon induction of plasticity by TBS (hippocampus) or 150 Hz stimulation (cerebellum). Mean \pm SEM. **B, D**) Bar plot of fEPSP slopes showing that both PTP (1-3 min) and LTP (25-30 min) are similar in the hippocampus (**B**; control: N=4 n=9; GluAko: N=7 n=19; GluA3WT: N=4 n=9) and cerebellum (**D**; control: N=5 n=13; GluAko: N=5 n=13; GluA3WT: N=7 n=16) of GluA3WT mice compared to control mice. Data was tested with two-sample t-test. **: $p < 0.01$; ***: $p < 0.001$.

5.3 Deletion of Kir 4.1 channels in NG2 glia

Kir 4.1 channels represent the most important K^+ conductance in NG2 glia (see Seifert and Steinhäuser, 2018). A thorough characterization of a mouse line lacking Kir 4.1 channels in NG2 glia (Kir 4.1 ko, chapter 4.1.5) was recently published (Timmermann *et al.*, 2023). Here, our group has shown that Kir 4.1 ko mice present altered memory abilities, impaired hippocampal CA3-CA1 PTP and LTP, increased myelination and longer depolarizations during miniature postsynaptic potential recordings. I contributed to this work by investigating, through mPSC recordings, how in Kir 4.1 ko mice glutamatergic synaptic transmission to NG2 glia is altered and whether the impaired PTP and LTP could be rescued by a TrkB agonist. Moreover, I performed further experiments in the cerebellum to test whether also in this region NG2 glia dysfunctions lead to impaired neuronal signalling.

5.3.1 Miniature PSCs decay is prolonged in Kir 4.1 ko mice

Impairments in synaptic transmission to NG2 glia or in the properties of NG2 glia postsynaptic receptors were tested through mPSC recordings in control and Kir 4.1 ko slices. During recordings in the hippocampus, TTX was added to the bath and only events faster than 15ms (glutamatergic) were analysed. In this case, mPSC amplitudes remained unchanged between genotypes (control: -13.7 ± 5.7 pA; Kir 4.1 ko: -13.5 ± 3.6 pA; two-sample t-test, $p > 0.05$; Fig. 5.18 B), while the decay of currents was significantly prolonged (2.38 ± 1.62 ms vs 5.67 ± 3.31 ms; two-sample t-test $p < 0.05$; Fig. 5.18 C). Similarly, in the cerebellum mPSCs showed longer decays of mPSCs recorded in the presence of picrotoxin and TTX (control: median= 1.15 ms, quartiles 1.1 - 2 ms; Kir 4.1 ko: median= 2.03 ms, quartiles= 2.03 - 2.37 ms; $p < 0.05$; Fig. 5.18 F), while amplitudes (control: -8.17 ± 3.2 pA; Kir 4.1 ko: -12.24 ± 4.7 pA; Fig. 5.18 E) and rise times (control: median= 0.38 ms, quartiles= 0.38 - 0.76 ms; Kir 4.1 ko: median= 0.41 ms, quartiles= 0.27 - 0.52 ms; Fig. 5.18 G) were not different.

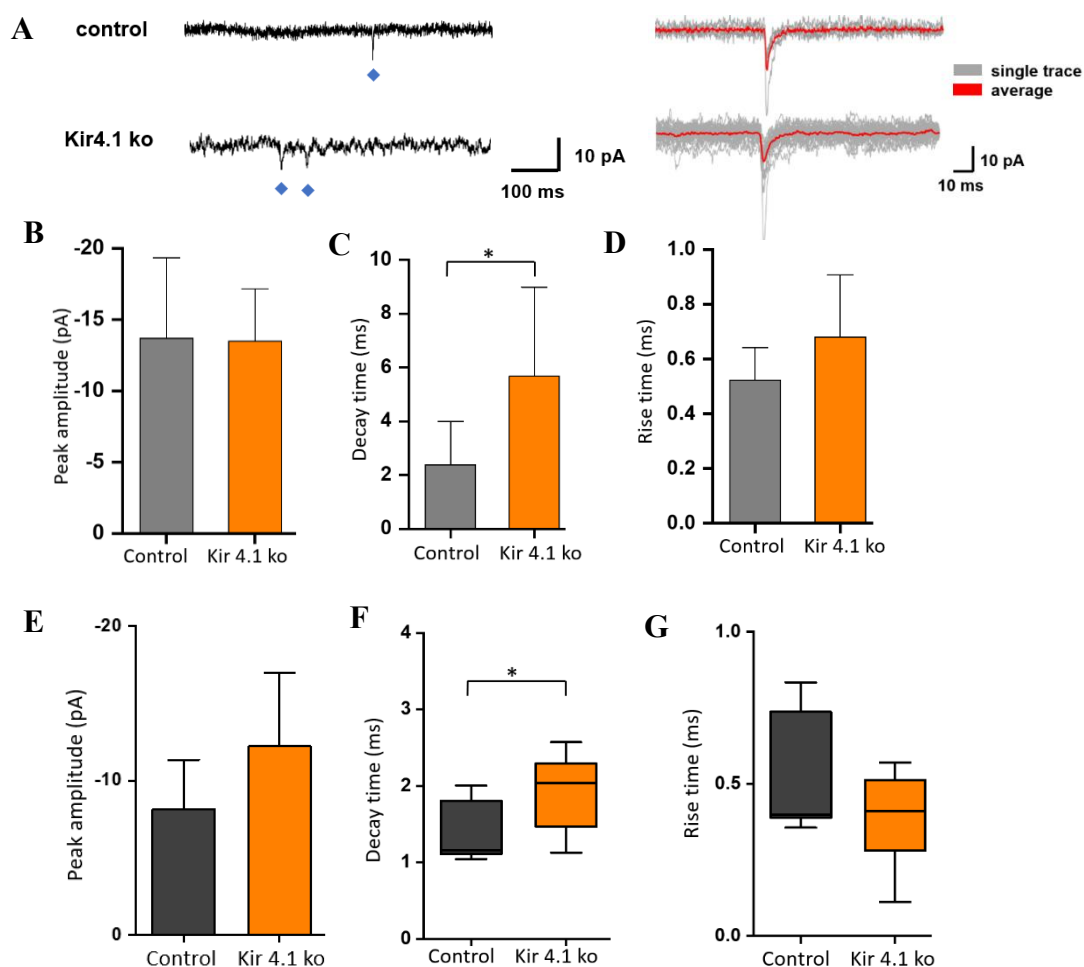


Fig. 5.18. mPSC recordings from hippocampal and cerebellar Kir 4.1 ko slices. **A)** Left: Sample traces of mPSCs from hippocampal NG2 glia of control and Kir 4.1 ko mice. Blue diamonds indicate individual events. Right: Corresponding superimposed single (gray) and average mPSC traces (red; average of 6 and 20 events, respectively). **B, C, D)** Properties of mPSCs recorded from control and Kir 4.1 ko cells in the hippocampus. TTX ($0.5 \mu\text{M}$) is present in the bath. Control: $N=3$, $n=7$; Kir 4.1 ko: $N=3$, $n=7$. Timmermann *et al.*, 2023. **E, F, G)** Peak amplitude and kinetics of mPSCs recorded in cerebellar NG2 glia. TTX ($0.5 \mu\text{M}$) and picrotoxin ($100 \mu\text{M}$) were both present in the bath; control: $N=4$, $n=6$; Kir 4.1 ko: $N=5$, $n=12$. Holding potential in control and Kir 4.1 ko cells: -80 and -60 mV, respectively. Peak amplitudes of Kir. 4.1 were corrected to -70 mV assuming a linear I/V curve between -80 and -60 mV. Two-sample t-tests or Mann-Whitney tests were used. * $p < 0.05$.

5.3.2 Reduced PTP and LTP in Kir 4.1 ko mice can be rescued by 7,8-DHF

To check whether increased excitability of NG2 glia in Kir 4.1 ko mice influences neuronal plasticity, fEPSPs were recorded in both hippocampus and cerebellum (chapter 4.3.9). As shown in Timmermann *et al.* (2023), TBS-induced PTP and LTP are strongly reduced in hippocampal slices from Kir 4.1 ko mice. To understand how dysfunctional NG2 glia can modulate these forms of plasticity, one of the main LTP pathways, the BDNF-TrkB pathway, was targeted through application of the TrkB agonist 7,8-DHF (1 μ M). Increasing TrkB activation completely rescued PTP and LTP in the hippocampus of Kir 4.1 ko mice (1–3 min: 163.11 ± 8.15 % vs 206.97 ± 16.44 %, $p < 0.05$; 25–30 min: 144.02 ± 3.98 % vs 179.36 ± 7.37 %, $p < 0.001$; Fig. 5.19 B), suggesting that NG2 glia can regulate BDNF levels.

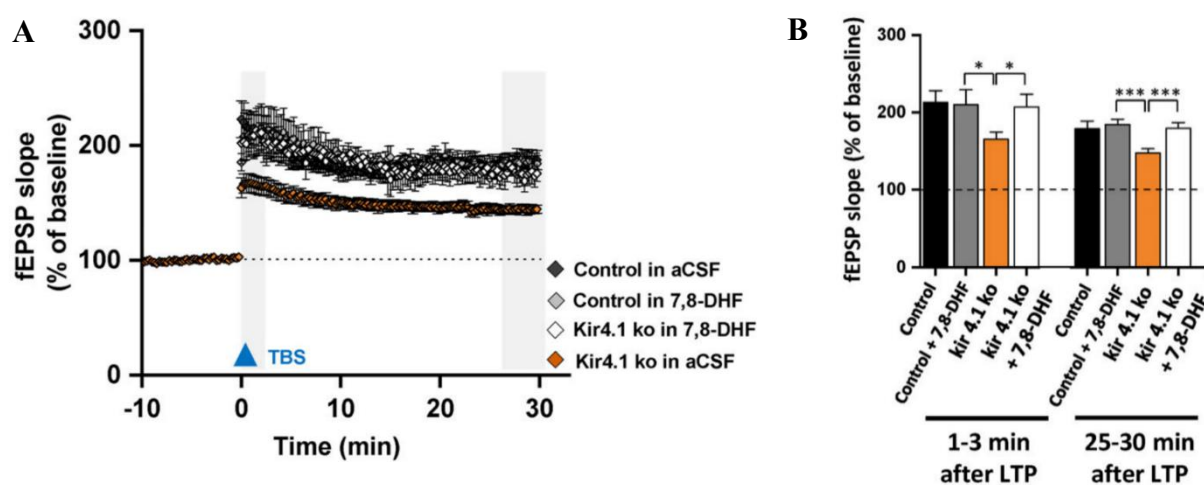


Fig. 5.19. Rescue of PTP and LTP by 7,8-DHF in hippocampal Kir 4.1 ko slices. **A)** Time-course of normalized fEPSP slopes of control and Kir 4.1 ko slices perfused with aCSF or 7,8-DHF (1 μ M in aCSF). **B)** Analysis of the fEPSP slopes at two time points (1–3 min after TBS and 25–30 min after TBS). Statistical significance was assessed with two-sample t-test. At both time points, potentiation was reduced in Kir 4.1 ko slices in aCSF ($n=39$, $N=15$) compared to Kir 4.1 ko slices perfused with 7,8-DHF ($N=4$, $n=10$) or to 7,8-DHF-treated controls (1–3 min: 209.80 ± 19.50 %, $p < 0.05$; 25–30 min: 184.37 ± 6.90 %; $N=4$, $n=9$). Differences between controls in aCSF and 7,8-DHF were not significant. Two-sample t-tests were used. Mean \pm SEM. *: $p < 0.05$; ****: $p < 0.001$. Adapted from Timmermann *et al.*, 2023.

Plasticity was then tested in the cerebellum of Kir 4.1 ko mice, using high-frequency stimulation to induce LTP between PFs and PCs. Here, like in the hippocampus, LTP was greatly reduced (25-30 min: control: 149.8 ± 12.4 %; Kir 4.1 ko: 89.36 ± 4.7 %, $p < 0.01$), while no difference was detected for PTP (1-3 min: control: 111.7 ± 7.3 %; Kir 4.1 ko: $101.79\% \pm 6.8$ %; $p > 0.05$; Fig. 5.20 B). These experiments suggest that cerebellar NG2 glia plays a relevant role in neuronal network functioning.

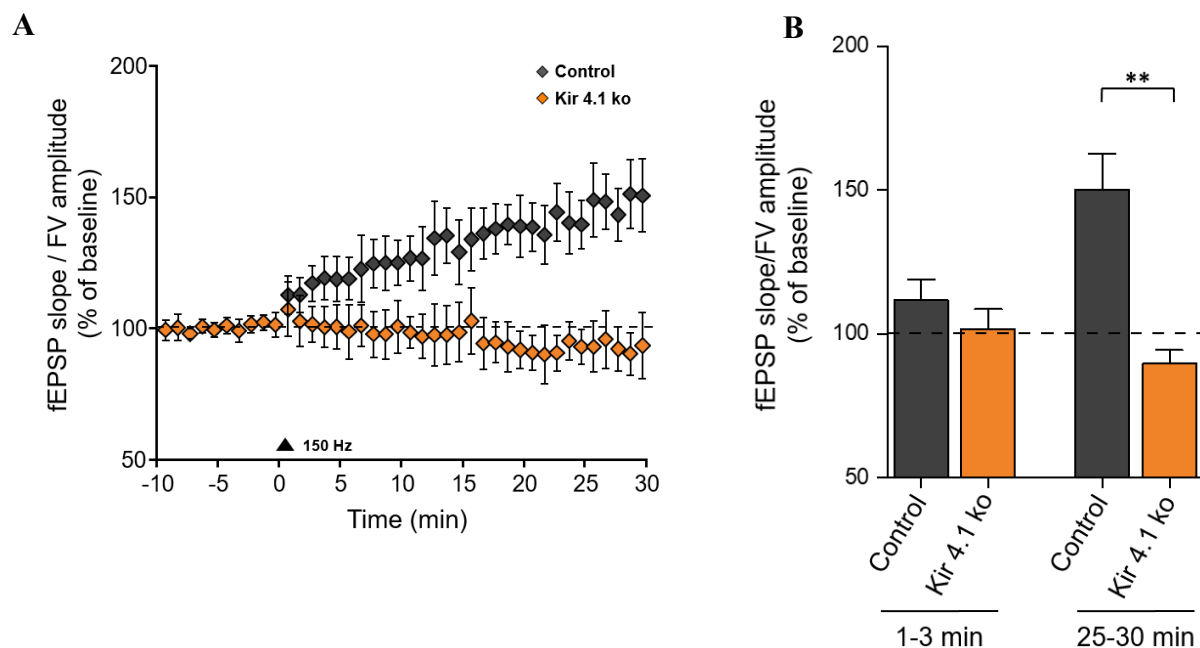


Fig. 5.20. LTP is reduced in cerebellar slices of Kir 4.1 ko mice. **A)** Plasticity time course in the cerebellum of Kir 4.1 ko mice and control. Plasticity is induced by stimulation at 150 Hz. **B)** Mean fEPSP slopes show impaired LTP 25-30 min after plasticity induction. Control: N=5, n=13, Kir 4.1 ko: N=6, n=12. Two sample t-test. Mean \pm SEM. **: $p < 0.01$.

5.4 Developmental regulation of GABA_A receptors in NG2 glia

While in previous sections I have described aspects of AMPAR transmission to NG2 glia, this chapter will unravel some of the properties of interneuron-NG2 glia synapses in the hippocampus during development. As previously described (chapter 1.4.2), NG2 glial cells receive GABAergic transmission, which leads to a depolarization of the cell. In the barrel cortex, a drastic developmental change in interneuron-NG2 glia synapse structure leads to a great reduction of synaptic GABA_AR activation, favouring an extrasynaptic mode of transmission (Vélez-Fort *et al.*, 2010). Current work from our group aims to study the developmental change of hippocampal interneuron-NG2 synapses. Here, Linda Patt showed how GABAergic spontaneous post-synaptic currents and mPSC frequency is reduced during development, hinting at a decreased innervation of NG2 glia. Moreover, our group revealed an increased sensitivity of tonic currents to $\alpha 5$ -subunit blocker, suggesting a higher expression of extrasynaptic receptors and a lower expression of $\gamma 2$, a subunit present in synaptic GABA_ARs. In addition, I performed experiments to unravel whether GABAergic transmission to NG2 glia is mainly extrasynaptic in adult mice. The data is being prepared for publication (Patt *et al.*, 2023).

5.4.1 Increased kinetics of ePSCs and developmental switch to a spillover mechanism

GABAergic PSCs were evoked in NG2 glia by placing the stimulation electrode around 30 μm distance from the recording one (near-field stimulation). Data was collected from interneurons located in CA1 stratum radiatum of the hippocampus in both juvenile (p7-12) and adult (p50-70) NG2-YFP mice (chapter 4.1.1). As previously shown by Linda Patt, the kinetics of events, recorded in the presence of 10 μM NBQX, 5 μM CGP-55845 and 50 μM D-AP5, changed in adult mice (rise time p10: 1.28 ms, N=8, n=17; p60: 4.74 ms, N=7, n=11; $p < 0.001$; decay time p10: 40.56 ms, N=8, n=23; p60: 57.36 ms, N=7, n=21; $p < 0.01$), indicating an activation of extrasynaptic receptors in these cells. If in NG2 glia from adult mice a pure GABA spillover mechanism is responsible for the activation of $\alpha 5$ -containing GABA_ARs, block of GATs should result in a prolongation of ePSC decay (Vélez-Fort *et al.*, 2010). To test this hypothesis, I applied GAT1 (NNC-711, 10 μM) and GAT3 (SNAP-5114, 100 μM) blockers during ePSC recordings. As predicted, neither blocker had a significant effect in NG2 glia from juvenile mice (control: 30.52 ± 8.72 ms; NNC-711: 32.22 ± 10.66 ms; $p < 0.05$; control: 33.95 ± 21.63 ms; SNAP-5114: 31.35 ± 14.41 ms; paired-sample t-test $p > 0.05$; Fig. 5.21B, D). However, in adult mice the decay time of NG2 glia ePSCs was significantly prolonged (control: 78.42 ± 31.14

ms; NNC-711: 190.96 ± 60.32 ms; $p < 0.001$; control: 56.83 ± 19.45 ms; SNAP-5114: 83.18 ± 30 ms; paired-sample t-test $p < 0.01$; Fig. 5.21 B, D). The effect of NNC-711 was significantly stronger than the one of SNAP-5114. These results confirm that GABAergic transmission to NG2 glia is mainly extrasynaptic in the hippocampus of adult mice.

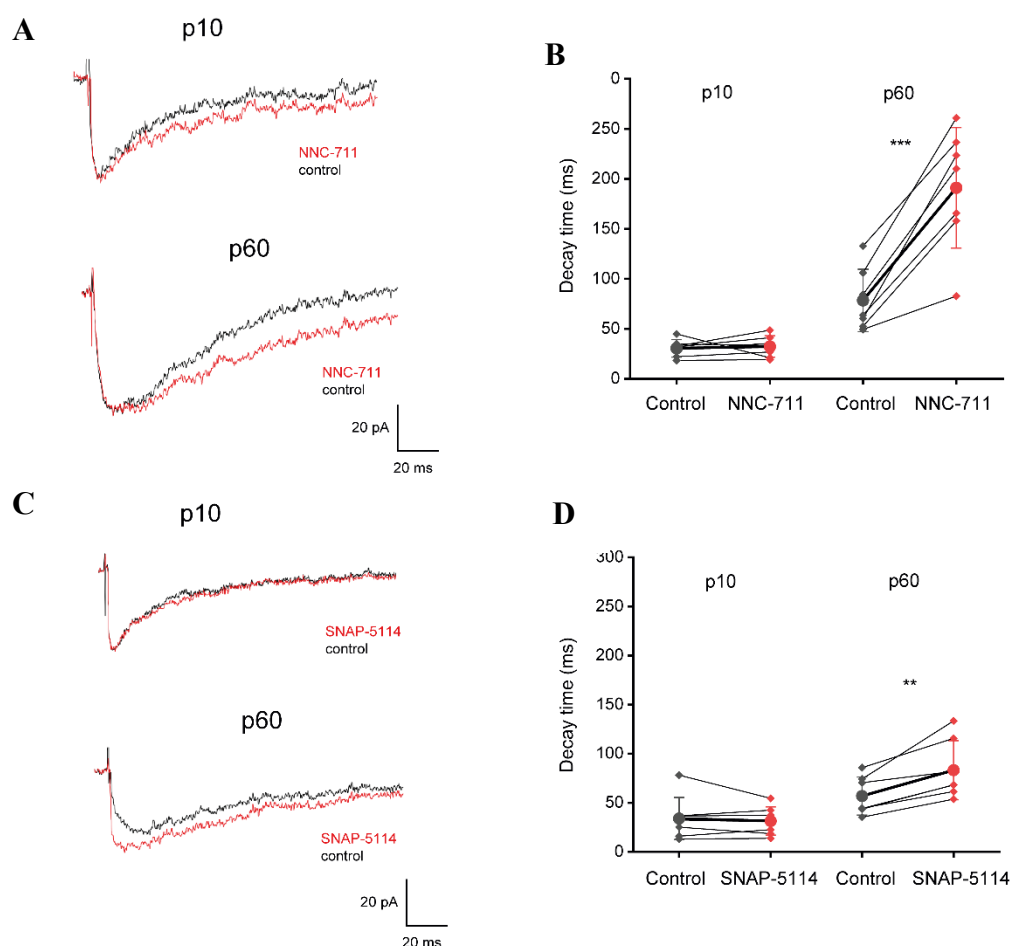


Fig. 5.21. GABA uptake blockers prolong ePSC decay only in adult NG2 glia. **A, C)** Original recordings of ePSCs in NG2 glia at p10 and p60 before (black trace) and after application (red) of NNC-711 (**A**, 10 μ M) and SNAP-5114 (**C**, 100 μ M). Bath solution contained 10 μ M NBQX, 50 μ M D-APV and 5 μ M CGP55845. **B, D)** Plots comparing changes in decay time constant (mono-exponential fit) after application of NNC-711 (**B**) and SNAP-5114 (**D**). NNC-711: p10: N=5, n=7, p60: N=4, n=7; SNAP-5114: p10: N=4, n=7, p60: N=3, n=7. Paired t-tests; ** $p < 0.01$, *** $p < 0.001$. Patt *et al.* 2023, in preparation.

6 Discussion

NG2 glia exhibits a unique ability to establish functional connections with both glutamatergic and GABAergic neurons, setting it apart from other types of non-neuronal cells (Bergles *et al.*, 2000; Lin and Bergles, 2004; Jabs *et al.*, 2005). The communication between neurons and NG2 glia has been extensively studied in the white matter, where the majority of NG2 glia differentiates into oligodendrocytes (Kukley *et al.*, 2007; Ziskin *et al.*, 2007). However, in the grey matter, most of these cells retain their NG2 phenotype throughout adulthood (Dimou *et al.*, 2008). The physiological impact of these cells and their synaptic input remains mysterious. Interestingly, grey matter NG2 glia express transcripts associated with neurons, astroglia and oligodendroglia, raising questions about their identity and lineage (Belachew *et al.*, 2003; Nishiyama *et al.*, 2009). Recent findings suggest that NG2 glia exhibit heterogeneous intrinsic properties (see Dimou and Simons, 2017; Hill and Nishiyama, 2014). In this study, NG2 glia heterogeneity in either different developmental stages or different grey matter regions was explored. Additionally, by taking advantage of knockout mouse lines for either AMPARs or Kir 4.1 channels expressed by NG2 glia, this work tried to tackle crucial unanswered questions regarding the role of neuron-NG2 synapses in the grey matter and their potential influence on neuronal communication.

6.1 CP-AMPARs in developing hippocampal NG2 glia

AMPARs expressed by NG2 glia contribute to the morphological development of these cells while promoting their proliferation and differentiation (Fannon, Tarmier and Fulton, 2015; Chen *et al.*, 2018). NG2 glia AMPARs synaptic activity increases in the first three postnatal weeks and it is synchronized to those of surrounding interneurons sharing the same presynaptic input (Mangin *et al.*, 2008). Previous studies also showed that NG2 glia in new-born mice express CP-AMPARs (Seifert *et al.*, 2003) which increases intracellular Ca^{2+} levels, contributing to neuron-NG2 synapse plasticity (Ge *et al.*, 2006). During hippocampal development, AMPARs in NG2 glia undergo a change in the associated auxiliary subunits and in their Ca^{2+} -permeability (Hardt *et al.*, 2021). As described in chapter 5.1.1, application of intracellular spermine exerts a partial block of kainate-activated AMPARs in juvenile NG2 glia, which increases at adult stages. Nevertheless, the prevalence of CP-AMPARs might be masked by the action of TARP- $\gamma 2$, which can reduce spermine potency by reshaping the selectivity filter (Brown, McGuire and Bowie, 2017; Coombs *et al.*, 2023). This problem was overcome by replacing spermine with Nasp in the intracellular solution, leading to a complete block of outward currents which remains unaltered also in the presence of auxiliary subunits (Coombs

et al., 2023). Accordingly, intracellular block of CP-AMPARs was stronger in adult mice confirming a developmental upregulation of these receptors. In contrast with these results, extracellular CP-AMPAR blockers, namely Naspnm and IEM-1460, had a similar efficiency in reducing evoked synaptic currents in juvenile and adult NG2 glia. These results are also in discordance with the finding that Naspnm and IEM-1460 extracellular block increases with age in acute isolated cells (Hardt *et al.*, 2021). Nonetheless, since polyamine extracellular block of synaptic currents has slow kinetics and it is use-dependent (Twomey *et al.*, 2018), its efficiency relies on the activation of AMPARs and this can explain the discrepancies with isolated cells and with intracellular polyamines. Moreover, in isolated cells processes are sheared off, suggesting that CP-AMPARs are more present in the soma rather than in the processes. Overall, the results from these experiments show a developmental increase of CP-AMPAR expression in hippocampal NG2 glia. This is in line with studies showing that CP-AMPARs promote proliferation of NG2 glia while Ca^{2+} -impermeable receptors activate in response to differentiation cues (Chen *et al.*, 2018).

6.2 High synaptic efficiency of CF-NG2 synapses is mediated by CP-AMPARs and multivesicular release

CFs in the cerebellum innervate NG2 glia, making hundreds of synaptic contacts (Lin *et al.*, 2005). This strong innervation results in large PSCs, ranging from 60 to 900 pA. In the hippocampus, glutamatergic innervation of NG2 glia is much lower, leading to 10-fold smaller ePSCs (Bergles *et al.*, 2000; Jabs *et al.*, 2005). Aside from the stronger innervation, other concurrent mechanisms could explain the highest responsiveness of cerebellar NG2 glia, for example a different composition of AMPARs and their auxiliary subunits or a larger transient of glutamate activating the receptors. The former hypothesis was partially confirmed by the higher expression of TARP γ 2, a subunit needed for membrane localization of CP-AMPARs in NG2 glia (Zonouzi *et al.*, 2011). As shown in chapter 5.1.2, functional analyses proved a stronger expression of CP-AMPARs in NG2 glia, which contributed to a higher synaptic efficiency. Indeed, extracellular block of CF-mediated PSCs by Naspnm and IEM-1460 was much stronger than in the hippocampus. The results were also confirmed by applying Naspnm intracellularly which, as discussed in chapter 6.1, proved a higher prevalence of CP-AMPARs in cerebellar NG2 glia independently of TARP expression. Differences in neuronal AMPAR composition have been found throughout many brain regions and seem to be developmentally regulated and dependent on the cell and synapse type (Lalanne *et al.*, 2016), other than from the cell's developmental origin (Matta *et al.*, 2013). While more studies are needed to

understand the reasons and the mechanisms underlying these regional differences, CP-AMPARs, with their rapid current kinetics and higher single-channel conductance (Swanson, Kamboj and Cull-Candy, 1997), could give NG2 glia the ability to sense and respond efficiently to the strong inputs coming from CFs.

As previously shown, CFs produce high P_r synapses with PCs in which a high amount of glutamate is released through multivesicular release (Wadiche and Jahr, 2001). A first hint that the same mechanism is valid also for CF-NG2 synapses comes from the longer decay time of ePSCs compared to SC-NG2 synapses, which could be due to a larger glutamate transient. However, possible differences in the composition of AMPARs and their assembly with auxiliary subunits could also lead to different receptor kinetics between the two synapses. Nevertheless, a lower γ -DGG block in the cerebellum compared to the hippocampus means a larger glutamate transient generated in the former region. This could potentially activate extrasynaptic AMPARs, which prolong the decay of ePSCs even though this hypothesis should be confirmed by further experiments (i.e., by testing the desensitization rate of synaptic AMPARs). As at CF-PC synapses, reducing P_r increased γ -DGG-mediated block of ePSCs, suggesting that the high P_r of CF-NG2 synapses leads to multivesicular release which in turn produces a large glutamate transient. We have confirmed multivesicular release at CF-NG2 synapses by performing experiments at low P_r . Indeed, in these conditions, multivesicular release is less likely to happen and glutamate transients are lower, as confirmed by a stronger efficiency of γ -DGG block. Other P_r -dependent mechanisms which increase glutamate concentration can take place, like spillover and accumulating of glutamate coming from neighbouring synapses. Indeed, the high number of closely spaced synaptic contacts between CFs and NG2 glia, together with the absence of lamellar processes of Bergmann glia to enwrap these synapses and to rapidly clear the neurotransmitter (Lin *et al.*, 2005), could very well contribute to an accumulation of glutamate in the cleft and longer ePSC decays. However, this hypothesis was discarded as blocking transporters did not increase the glutamate concentration in the cleft. Taken together, experiments described in chapter 5.1.2 and 5.1.3 draw a clear picture of the differences in glutamatergic transmission to NG2 glia in hippocampus and cerebellum: a higher proportion of CP-AMPARs and larger glutamate transients due to multivesicular release, together with the extensive innervation from CFs, drastically increase the efficiency of cerebellar synapses.

6.3 Short-term plasticity at CF-NG2 synapses

The high P_r of CF-NG2 synapses causes a marked PPD. In CF-PC synapses, mechanisms for this kind of short-term plasticity have been shown to be only presynaptic (Dittman and Regehr, 1998; Hashimoto and Kano, 1998) and mainly due to decreased neurotransmitter release in response to vesicle depletion. The depletion model can easily explain PPD at many synapses (Liley and North, 1953; Betz, 1970; Zucker and Regehr, 2002). According to this model, the readily releasable pool of vesicles in the presynaptic terminal is limited and, when many vesicles fuse in response to a first stimulus, fewer vesicles will be available for release upon the second one. Can the depletion model also explain PPD in CF-NG2 synapses? As shown in chapter 5.1.4, the decrease in PPD after reducing extracellular $[Ca^{2+}]$ suggests that presynaptic Ca^{2+} -dependent mechanisms, like depletion, can have a role. Moreover, application of the competitive antagonist γ -DGG reduced PPR. While this can be explained by a lower concentration of glutamate after the 2nd stimulus, it is not possible to rule out AMPAR saturation (Rabl, Cadetti and Thoreson, 2006). Vesicle depletion was directly tested through regression analyses, which showed no correlation in the amplitudes of the first and second ePSC. These results hint to release-independent, presynaptic mechanisms for PPD in CF-NG2 synapses, like seen in other regions of the CNS (Chen *et al.*, 2004; Kraushaar and Jonas, 2000; Thomson and Bannister, 1999; see also Regehr, 2012). However, the precise mechanisms should be investigated with further experiments. On the other hand, application of CTZ significantly increases PPR. This molecule is an allosteric modulator of AMPARs, which eliminates rapid desensitization, enhances the ePSC amplitude and slows down the decay of AMPA-mediated PSCs (Yamada and Tang, 1993). CTZ is also known to have a number of effects on the presynaptic terminal: indeed, this molecule can interfere with the P_r , either by inactivating presynaptic Ca^{2+} channels or inhibiting presynaptic K^+ currents (Ishikawa and Takahashi, 2001). The suppression of K^+ currents can slow down the repolarizing phase of action potentials, thereby increasing Ca^{2+} influx through voltage-dependent Ca^{2+} channels. This leads to an increase in P_r and subsequently in PPD. To overcome these side effects, CTZ was applied in lower concentrations (50 μ M), which have negligible consequences on the presynaptic terminal (Xu-Friedman and Regehr, 2003; Yang and Xu-Friedman, 2008). Therefore, the effect of CTZ on PPD hints at AMPAR desensitization as a postsynaptic mechanism regulating short-term plasticity at CF-NG2 synapses. Notably, in previous studies on CF-PC synapses, CTZ had no effect on PPD (Dittman and Regehr, 1998; Hashimoto and Kano, 1998). It is possible that the evident structural differences between CF-PC synapses and CF-NG2 synapses and the absence of Bergmann glia isolation play a crucial role in these differences (see Xu-Friedman

and Regehr, 2004). Thus, while NG2 glia and PCs share the same presynaptic fibers, different structural and molecular properties of the two synapses lead to postsynaptic modifications of the inputs so that distinct information can be conveyed.

6.4 AMPAR deletion in NG2 glia impairs neuronal plasticity and PC firing

The impact of AMPAR signaling on NG2 glia and whether these cells can influence back neuronal networks remain the most intriguing yet unanswered questions in the field. Divergent evidences propose different roles for NG2 glia AMPARs in modulating the proliferation/differentiation balance of these cells in the white matter. In one study, mice with double- and triple-AMPAR knockout in germline NG2 glia possess normal NG2 glia proliferation rate but a reduction in oligodendrocyte differentiation and subsequent myelination, which is independent from the Ca^{2+} -permeability of AMPARs (Kougioumtzidou *et al.*, 2017). Other *in vivo* studies suggest instead that AMPAR manipulation later in development leads to altered proliferation/differentiation balance in NG2 glia, dependent on CP-AMPARs (Chen *et al.*, 2018). A further study shows that higher GluA2 levels do not change oligodendrocyte numbers but increase NG2 glia proliferation (Khawaja *et al.*, 2021). In the present work, mice lacking all four subunits of AMPARs in NG2 glia were used to determine the impact of these receptors on neuronal signaling and behaviour. Functional analyses shown in chapter 5.2.1 revealed a complete loss of AMPAR currents in 75% of cells tested in the cerebellum, while previous data showed similar results in the hippocampus (unpublished observation). This high knockout efficiency allowed for further functional studies. Previous results from our group revealed impaired TBS-induced LTP in the hippocampus of GluAko mice. As shown in chapter 5.2.2, LTP between PFs and PCs was greatly impaired also in the GluAko cerebellum. The high-frequency stimulation protocol used for these experiments induced a form of LTP which involved the postsynaptic side (Bouvier *et al.*, 2016). This is confirmed by the unchanged PPR upon LTP induction, suggesting that presynaptic fibers are not affected. Moreover, no differences were seen in neuronal excitability. A fascinating theory to explain LTP deficiencies in GluAko mice involves the ability of NG2 glia to release neurotrophic factors in response to neuronal stimulation (see chapter 1.6). One of the main neurotrophins involved in LTP is BDNF. Indeed, in the hippocampus, BDNF positively modulates LTP (Chen, Harata and Tsien, 2004) and in BDNF knockout mice, a reduction in LTP induced by tetanic stimulation was observed (Korte *et al.*, 1995). In the cerebellum, TrkB receptors are located on both granule cells and PCs and BDNF is highly expressed in the matured cerebellar cortex (Wetmore *et al.*, 1990; Kawamoto *et al.*, 1996). Application of a TrkB receptor agonist showed that increasing

TrkB activation could rescue LTP in both regions, linking impaired AMPAR signaling in NG2 glia to a reduced expression of BDNF. While evidences of BDNF expression and release from NG2 glia is limited (Tanaka *et al.*, 2009; Prasad *et al.*, 2017), these cells express TrkB receptors whose activation has been linked to activity-dependent myelination and proper cognitive performance (Geraghty *et al.*, 2019). On the other hand, it is also possible that NG2 glia releases other neurotrophic factors which in turn could induce BDNF release from other cell types, like astrocytes (Holt *et al.*, 2019) or microglia (Coull *et al.*, 2005; Parkhurst *et al.*, 2013; see Zhang *et al.*, 2022). In both hippocampus and cerebellum, NG2 glia is known to have completely overlapping domains with astrocytes and Bergmann glia, suggesting a close interaction of these cell types (Wigley *et al.*, 2007; Wigley and Butt, 2009) which could be key for the maintenance and modulation of neuronal networks. However, further studies are needed to verify whether these interactions are impaired in GluAko mice and whether other soluble factors released from NG2 glia are essential for neuronal LTP.

As described in detail in chapter 1.5.3, LTP between PFs and PCs requires synchronous and precise inputs from both PFs and CFs. If synapses with one or the other glutamatergic fiber are altered, this can result in an impaired LTP and eventually an altered output from PCs, as observed in other studies (Servais *et al.*, 2007; Hoxha *et al.*, 2018; Grasselli *et al.*, 2020). Notably, experiments in chapter 5.2.3 depict a similar scenario: in GluAko mice, simple spike firing frequency as well as complex spike waveform are altered suggesting altered synaptic transmission. Simple spike firing results from PF inputs, inhibitory inputs and the intrinsic activity of PCs (see De Zeeuw *et al.*, 2011). A complex spike instead originates directly from CF activation. Its components include a first AP and a series of smaller high-frequency spikelets all originating from the axon (Davie, Clark and Häusser, 2008). In GluAko mice, the amplitude of the first spikelet is reduced. The amplitude of each individual spikelet plays a crucial role as it dictates the probability of propagation towards deep cerebellar nuclei (Monsivais *et al.*, 2005). A previous study linked simple spike firing impairments in PCs to alterations of p75 receptor signaling (Tian *et al.*, 2014) while another work suggests that slowed AP firing in PCs could be rescued by applying 7,8-DHF to a mouse model of ataxia (Cook *et al.*, 2021). Accordingly, if in GluAko mice BDNF levels are reduced like shown during fEPSP recordings, application of the TrkB agonist could rescue the impaired PC activity. Further experiments will be performed to explore this hypothesis.

6.5 GluAko mice exhibit a reduction in locomotor activity

In chapter 5.2.5, it was checked whether deficits in LTP in GluAko mice could translate into behavioural dysfunctions. In the memory tasks, GluAko mice performed similar to controls, showing similar declarative, social and working memory. However, as a constant during these tests, GluAko mice showed a drastically decreased locomotor activity, concerning both distance traveled and speed. These deficits were confirmed in the beam-walking test, where GluAko mice were slower in crossing the rod but no difference in hindlimb slipping, therefore in their coordination, was detected. These results are quite enigmatic, considering that locomotor activity is unaffected during the open-field test. While it is not possible to exclude motor deficits without further tests, this discrepancy could also hint to altered anxious or fear-related behaviour of mice when placed in an environment with different stimuli, a lack of motivation in performing the tasks or a faster habituation to the environment. Indeed, previous studies already relate reduced locomotion to anxious behaviour (McKinney *et al.*, 2008; Eudave, BeLow and Flandreau, 2018; Qin *et al.*, 2021). A more detailed assessment of the open-field test, in particular of thigmotaxis, which is the tendency of mice to remain close to the walls of the arena rather than exploring the central part, could give us more clues about possible anxiety-related behaviours (Simon, Dupuis and Costentin, 1994). Interestingly, impairments in NG2 glia physiology have already been directly associated to anxious or depressive-like states. Indeed, reducing FGF-2 expression of NG2 glia in the medial prefrontal cortex led to anxious phenotypes (Birey *et al.*, 2015). Moreover, modulation of inhibitory GABAergic transmission by photoactivated NG2 glia triggers anxiety-like behaviour in vivo (Zhang *et al.*, 2021). In most cases, the deficits are also associated with reduced myelination (Roy *et al.*, 2007; Chen *et al.*, 2015). Notably, preliminary results from our group on myelin basic protein (MBP) expression in GluAko mice confirm a decreased myelination compared to controls (unpublished observations), which could be related to lower expression of BDNF or other neurotrophins (Fletcher, Murray and Xiao, 2018). However, evidences of altered myelination have been seen also in mice lacking GABA_B receptors or Kir 4.1 channels in NG2 glia (Fang *et al.*, 2022; Timmermann *et al.*, 2023). Interestingly, these mouse models showed a different set of behavioural deficits, either in social or declarative memory with no effect on the locomotor activity suggesting that impaired myelination can have diverse effects depending on the brain regions that are most affected. While anxious-like behaviours are mostly associated with the amygdala, many studies also correlate these deficits to both hippocampal and cerebellar alterations (see Chin and Augustine, 2023; Ghasemi *et al.*, 2022). The cerebellum has extensive connections to many brain regions and an increasing number of evidences relate its functions

to cognitive or emotional states as well as to a large variety of psychiatric disorders (see Phillips *et al.*, 2015). Indeed, the cerebellum exhibits a topographic organization wherein each anatomical or functional area is responsible for controlling a distinct set of behaviours (Stoodley, Valera and Schmahmann, 2012). As example, lobule VI is linked to fear-related responses in Pavlovian fear-conditioned mice (Zhu *et al.*, 2007) while lobule VII to anxiety behaviours tested with the elevated-plus maze (Badura *et al.*, 2018). In any case, further studies would be necessary to describe GluAko mice behavioural phenotype with more precision, understanding whether the effects on locomotion seen in this work relate to differences in motor learning, anxious behaviour or motivational impairments.

6.6 CP-AMPA mediates LTP in hippocampus and cerebellum

As presented in this work, deletion of all four subunits of AMPARs in NG2 glia leads to functional and behavioural deficits. Whether all subunits are necessary for normal neuronal processing or if the expression of single subunits could rescue the phenotype remains an open question. In previous work, mice overexpressing GluA2 in NG2 glia showed suppressed Ca^{2+} responses, increased proliferation and post-injury oligodendrocyte regeneration (Khawaja *et al.*, 2021). As described in chapter 5.2.6, mice expressing only the GluA3 subunit of AMPARs in NG2 glia showed a complete block of outward currents by intracellular polyamines. Notably, these mice exhibit normal PTP and LTP in both hippocampus and cerebellum, demonstrating the relevance of this receptor subtype for signal processing in NG2 glia. Further studies will continue to examine this topic, exploring whether the sole presence of other AMPAR subunits (GluA1 or GluA4) leads to similar effects.

6.7 Kir 4.1 mice dysfunction in hippocampus and cerebellum

As mentioned in chapter 5.3, a recent work from our group investigated the relevance of glia-mediated signaling for neuronal processing and behaviour in a mouse model lacking Kir 4.1 channels in NG2 glia (Timmermann *et al.*, 2023). These mice present deficits in declarative memory, associated to hippocampal functioning, altered myelination and NG2 glia with depolarized membrane potentials. As shown in chapter 5.3.1, NG2 glia from Kir 4.1 ko mice exhibit higher excitability both in hippocampus and cerebellum, as testified from the longer decay of mEPSCs. Excitingly, the impaired LTP in the hippocampus could be rescued by 7,8-DHF, showing also in this case, like for GluAko mice, a reduced BDNF presence in this region (see chapter 6.4). In the cerebellum, LTP was also reduced and further studies should examine whether stimulation of the BDNF-TrkB pathway restores the plasticity. This work suggests that the deletion of Kir 4.1 leads to a more depolarized resting membrane potential in NG2 glia,

which may facilitate the activation of voltage-gated calcium channels in NG2 glia and lead to an altered transcription of factors, which modify the behaviour of the surrounding neural network.

6.8 GABA_AR signalling switches to a spillover-mediated transmission in adult NG2 glia

Data presented in chapter 5.4.1 contributes to evidences from our group (Patt *et al.*, 2023, in preparation) of a change during development of GABAergic transmission between hippocampal interneurons and NG2 glia. Indeed, block of GABA transporters led to an increase in decay of ePSCs only in the adult. This suggests that neuronal communication to NG2 cells in the hippocampus is mediated by a pure spillover mechanism. This extrasynaptic mode of transmission has been documented in several synapses of the neocortex and cerebellum (Rossi and Hamann, 1998; Szapiro and Barbour, 2007; Oláh *et al.*, 2009). However, a parallel hypothesis is that, in juvenile mice, the process of synapse formation is still incomplete and release sites might not be correctly clustered. As shown in previous work, this could result in higher synapse independency, faster decay kinetics and, importantly, in insensitivity to GABA uptake blockers (Overstreet and Westbrook, 2003). Thus, GATs activity might still have to reach its full potential in juvenile mice and GABA clearance might occur mainly by diffusion. This could also explain the lack of effect of GAT blockers in juvenile mice. However, other analyses from our group prove a decreased innervation of adult NG2 glia and a different molecular composition of GABA receptors, validating the hypothesis of extrasynaptic GABA transmission to NG2 glia in the adult. As last note, blocking GAT1 resulted in a stronger prolongation of decays than blocking GAT3. While both transporters are able to limit the diffusion of GABA and to maintain both the synaptic and extrasynaptic neurotransmitter levels constant (Kersanté *et al.*, 2013), GAT1 is more expressed and it is located on the membrane of presynaptic neurons, closer to the synaptic cleft than GAT3, located on astrocytes (Frahm and Draguhn, 2001; Brunskine *et al.* 2022).

7 Perspectives

This work showed that glutamatergic transmission to NG2 glia has a critical role in regulating neuronal plasticity and mouse behaviour. The expression of CP-AMPARs in adult NG2 glia can favour Ca^{2+} entry and lead to the transcription of neurotrophic factors like BDNF or FGF-2 and their secretion in the extracellular space, where they can potentially influence neuronal and glial network activity. Molecular and transcriptomic analyses could be employed to detect which neurotrophic factors can be released by NG2 glia in the hippocampus and cerebellum. Further analyses could be done to assess whether the expression of any of these factors is affected in GluAko mice or if it is dependent on CP-AMPARs. It will also be essential to perform molecular and immunohistochemical analyses to determine whether proliferation or differentiation of NG2 glia, together with myelination levels, are altered in GluAko or in GluA3WT mice. Indeed, impairments in neuronal plasticity, observed in GluAko mice, could lead to deficits in activity-dependent myelination and to subsequent behavioural alterations. Modifications to myelin structure could also be analysed through expansion microscopy. This technique could also be used to resolve at the subcellular level the relation between NG2 glia processes and myelin sheaths. Moreover, while behavioural tests hint at deficits in locomotion in GluAko mice, further motor tasks, like the rotarod test, or fear-related tasks can help to pinpoint the underlying cause of these dysfunctions.

8 Summary

Grey matter NG2 glia constitute a heterogeneous glial population whose functions remain incompletely understood. Their ability to make synapses with neurons is unique among glial cells, but the purpose of these connections is not clear. NG2 glia can sense both glutamatergic and GABAergic inputs thanks to the expression of AMPARs and GABARs. In the hippocampus, SCs activate AMPARs in NG2 glia, giving rise to small post-synaptic currents. Cerebellar CFs also form synapses with NG2 glia, producing much larger PSCs. The main aim of this work was to assess mechanisms underlying these regional differences and to better understand the role of NG2 glia AMPARs in influencing the activity of neuronal networks and eventually behaviour. Moreover, the developmental regulation of glutamatergic and GABAergic neuron-glia synapses has been studied.

Patch-clamp analyses allowed for determining regional and developmental differences of AMPARs expressed by NG2 glia while fEPSP recordings performed in a mouse line with inducible deletion of AMPARs subunits GluA1-4 in NG2 glia (GluAko) permitted to assess possible impairments in long-term plasticity. Moreover, memory and motor abilities of GluAko mice were evaluated with a series of behavioural tests.

Results revealed an increased expression of CP-AMPARs in adult hippocampal NG2 glia. On the other hand, GABAergic transmission was mainly extrasynaptic in later developmental stages.

As for regional differences between hippocampal and cerebellar NG2 glia, previous RT-PCR data suggested selective expression of the auxiliary AMPAR subunit TARP- γ 2 in cerebellar NG2 glia, which is required for translocation of CP-AMPARs to the plasma membrane. Comparing excitatory ePSCs in NG2 glia of both regions while applying intra- and extracellular CP-AMPAR antagonists revealed a higher expression of those receptors in the cerebellum. Moreover, application of a competitive AMPAR antagonist (γ -DGG) during ePSC recordings demonstrated that a larger glutamate transient is sensed by cerebellar NG2 glia, due to multivesicular release from CFs. This data shows that NG2 glia in the cerebellum can make more efficient synapses compared to the hippocampal counterpart, thanks to a higher expression of CP-AMPARs and a larger glutamate concentration in the cleft. Additional analyses on PPD of cerebellar CF-NG2 synapses uncovered that this form of plasticity depends on both presynaptic and postsynaptic mechanisms. fEPSP recordings in slices from GluAko mice unravelled impaired long-term potentiation in both hippocampus and cerebellum, which could be rescued pharmacologically by applying a TrkB receptor agonist, hinting at a crucial role of

NG2 glia in regulating BDNF levels. These results are confirmed also in Kir 4.1 ko mice, suggesting that alterations to NG2 glia physiology lead to lower neurotrophin levels and altered LTP. Notably, LTP in hippocampus and cerebellum was similar to controls in a mouse model expressing only the GluA3 subunit of AMPARs in NG2 glia, revealing a major role for CP-AMPARs in modulating neuronal activity. Further experiments showed that PCs in GluAko cerebellar slices receive impaired input from PFs and CFs which leads to reduced firing frequency. Moreover, GluAko mice displayed a reduced locomotor activity in most of the tasks, which indicates the presence of motor deficits or anxious behaviour. Overall, this study significantly contributes to our understanding of the role of NG2 glia, filling in numerous gaps and providing crucial insights into the essential functions performed by these cells in the grey matter.

9 References

- Abraham, W.C. *et al.* (2002) ‘Induction and Experience-Dependent Consolidation of Stable Long-Term Potentiation Lasting Months in the Hippocampus’, *The Journal of Neuroscience*, 22(21), pp. 9626–9634. Available at: <https://doi.org/10.1523/JNEUROSCI.22-21-09626.2002>.
- Ahmed, M.S. and Siegelbaum, S.A. (2009) ‘Recruitment of N-Type Ca²⁺ Channels during LTP Enhances Low Release Efficacy of Hippocampal CA1 Perforant Path Synapses’, *Neuron*, 63(3), pp. 372–385. Available at: <https://doi.org/10.1016/j.neuron.2009.07.013>.
- Ahn, A.H. *et al.* (1994) ‘The cloning of zebrin II reveals its identity with aldolase C’, *Development (Cambridge, England)*, 120(8), pp. 2081–2090. Available at: <https://doi.org/10.1242/dev.120.8.2081>.
- Akiyoshi, R. *et al.* (2018) ‘Microglia Enhance Synapse Activity to Promote Local Network Synchronization’, *Eneuro*, 5(5), p. UNSP e0088-18.2018. Available at: <https://doi.org/10.1523/ENEURO.0088-18.2018>.
- Albus, J.S. (1971) ‘A theory of cerebellar function’, *Mathematical Biosciences*, 10(1), pp. 25–61. Available at: [https://doi.org/10.1016/0025-5564\(71\)90051-4](https://doi.org/10.1016/0025-5564(71)90051-4).
- Álvarez-Aznar, A. *et al.* (2020) ‘Tamoxifen-independent recombination of reporter genes limits lineage tracing and mosaic analysis using CreERT2 lines’, *Transgenic Research*, 29(1), pp. 53–68. Available at: <https://doi.org/10.1007/s11248-019-00177-8>.
- Amaral, D.G. and Cowan, W.M. (1980) ‘Subcortical afferents to the hippocampal formation in the monkey’, *Journal of Comparative Neurology*, 189(4), pp. 573–591. Available at: <https://doi.org/10.1002/cne.901890402>.
- Amaral, M.D. and Pozzo-Miller, L. (2012) ‘Intracellular Ca²⁺ Stores and Ca²⁺ Influx Are Both Required for BDNF to Rapidly Increase Quantal Vesicular Transmitter Release’, *Neural Plasticity*, 2012, p. e203536. Available at: <https://doi.org/10.1155/2012/203536>.
- Ango, F. *et al.* (2008) ‘Bergmann Glia and the Recognition Molecule CHL1 Organize GABAergic Axons and Direct Innervation of Purkinje Cell Dendrites’, *PLOS Biology*, 6(4), p. e103. Available at: <https://doi.org/10.1371/journal.pbio.0060103>.

- Auguste, Y.S.S. *et al.* (2022) ‘Oligodendrocyte precursor cells engulf synapses during circuit remodeling in mice’, *Nature Neuroscience*, 25(10), pp. 1273–1278. Available at: <https://doi.org/10.1038/s41593-022-01170-x>.
- Azevedo, F.A.C. *et al.* (2009) ‘Equal numbers of neuronal and nonneuronal cells make the human brain an isometrically scaled-up primate brain’, *The Journal of Comparative Neurology*, 513(5), pp. 532–541. Available at: <https://doi.org/10.1002/cne.21974>.
- Badura, A. *et al.* (2018) ‘Normal cognitive and social development require posterior cerebellar activity’, *eLife*, 7, p. e36401. Available at: <https://doi.org/10.7554/eLife.36401>.
- Barbour, B. *et al.* (1994) ‘Prolonged presence of glutamate during excitatory synaptic transmission to cerebellar Purkinje cells’, *Neuron*, 12(6), pp. 1331–1343. Available at: [https://doi.org/10.1016/0896-6273\(94\)90448-0](https://doi.org/10.1016/0896-6273(94)90448-0).
- Barde, Y. a., Edgar, D. and Thoenen, H. (1982) ‘Purification of a new neurotrophic factor from mammalian brain.’, *The EMBO Journal*, 1(5), pp. 549–553. Available at: <https://doi.org/10.1002/j.1460-2075.1982.tb01207.x>.
- von Bartheld, C.S., Bahney, J. and Herculano-Houzel, S. (2016) ‘The Search for True Numbers of Neurons and Glial Cells in the Human Brain: A Review of 150 Years of Cell Counting’, *The Journal of comparative neurology*, 524(18), pp. 3865–3895. Available at: <https://doi.org/10.1002/cne.24040>.
- Baumbauer, K.M. *et al.* (2009) ‘Timing in the Absence of Supraspinal Input II: Regularly Spaced Stimulation Induces a Lasting Alteration in Spinal Function That Depends on the NMDA Receptor, BDNF Release, and Protein Synthesis’, *Journal of Neuroscience*, 29(46), pp. 14383–14393. Available at: <https://doi.org/10.1523/JNEUROSCI.3583-09.2009>.
- Belachew, S. *et al.* (2003) ‘Postnatal NG2 proteoglycan–expressing progenitor cells are intrinsically multipotent and generate functional neurons’, *Journal of Cell Biology*, 161(1), pp. 169–186. Available at: <https://doi.org/10.1083/jcb.200210110>.
- Bellamy, T.C. and Ogden, D. (2006) ‘Long-term depression of neuron to glial signalling in rat cerebellar cortex’, *European Journal of Neuroscience*, 23(2), pp. 581–586. Available at: <https://doi.org/10.1111/j.1460-9568.2005.04588.x>.

- Bergerot, A. *et al.* (2013) ‘Persistent Posttetanic Depression at Cerebellar Parallel Fiber to Purkinje Cell Synapses’, *PLOS ONE*, 8(7), p. e70277. Available at: <https://doi.org/10.1371/journal.pone.0070277>.
- Bergles, D.E. *et al.* (2000) ‘Glutamatergic synapses on oligodendrocyte precursor cells in the hippocampus’, *Nature*, 405(6783), pp. 187–191. Available at: <https://doi.org/10.1038/35012083>.
- Bergles, D.E., Jabs, R. and Steinhäuser, C. (2010) ‘Neuron-glia synapses in the brain’, *Brain Research Reviews*, 63(1), pp. 130–137. Available at: <https://doi.org/10.1016/j.brainresrev.2009.12.003>.
- Betz, W.J. (1970) ‘Depression of transmitter release at the neuromuscular junction of the frog’, *The Journal of Physiology*, 206(3), pp. 629–644. Available at: <https://doi.org/10.1113/jphysiol.1970.sp009034>.
- Bilkei-Gorzo, A. *et al.* (2014) ‘Dynorphins regulate the strength of social memory’, *Neuropharmacology*, 77, pp. 406–413. Available at: <https://doi.org/10.1016/j.neuropharm.2013.10.023>.
- Binda, F., Pernaci, C. and Saxena, S. (2020) ‘Cerebellar Development and Circuit Maturation: A Common Framework for Spinocerebellar Ataxias’, *Frontiers in Neuroscience*, 14. Available at: <https://www.frontiersin.org/articles/10.3389/fnins.2020.00293>.
- Binder, D.K. and Steinhäuser, C. (2021) ‘Astrocytes and Epilepsy’, *Neurochemical Research*, 46(10), pp. 2687–2695. Available at: <https://doi.org/10.1007/s11064-021-03236-x>.
- Birey, F. *et al.* (2015) ‘Genetic and Stress-Induced Loss of NG2 Glia Triggers Emergence of Depressive-like Behaviors through Reduced Secretion of FGF2’, *Neuron*, 88(5), pp. 941–956. Available at: <https://doi.org/10.1016/j.neuron.2015.10.046>.
- Bliss, T.V.P. and Lømo, T. (1973) ‘Long-lasting potentiation of synaptic transmission in the dentate area of the anaesthetized rabbit following stimulation of the perforant path’, *The Journal of Physiology*, 232(2), pp. 331–356. Available at: <https://doi.org/10.1113/jphysiol.1973.sp010273>.

- Blitz, D.M., Foster, K.A. and Regehr, W.G. (2004) ‘Short-term synaptic plasticity: a comparison of two synapses’, *Nature Reviews Neuroscience*, 5(8), pp. 630–640. Available at: <https://doi.org/10.1038/nrn1475>.
- Bouvier, G. *et al.* (2016) ‘Burst-Dependent Bidirectional Plasticity in the Cerebellum Is Driven by Presynaptic NMDA Receptors’, *Cell Reports*, 15(1), pp. 104–116. Available at: <https://doi.org/10.1016/j.celrep.2016.03.004>.
- Bowie, D. and Mayer, M.L. (1995) ‘Inward rectification of both AMPA and kainate subtype glutamate receptors generated by polyamine-mediated ion channel block’, *Neuron*, 15(2), pp. 453–462. Available at: [https://doi.org/10.1016/0896-6273\(95\)90049-7](https://doi.org/10.1016/0896-6273(95)90049-7).
- Bramham, C.R. (2008) ‘Local protein synthesis, actin dynamics, and LTP consolidation’, *Current Opinion in Neurobiology*, 18(5), pp. 524–531. Available at: <https://doi.org/10.1016/j.conb.2008.09.013>.
- Brochu, G., Maler, L. and Hawkes, R. (1990) ‘Zebrin II: A polypeptide antigen expressed selectively by purkinje cells reveals compartments in rat and fish cerebellum’, *Journal of Comparative Neurology*, 291(4), pp. 538–552. Available at: <https://doi.org/10.1002/cne.902910405>.
- Bröer, S. and Brookes, N. (2001) ‘Transfer of glutamine between astrocytes and neurons’, *Journal of Neurochemistry*, 77(3), pp. 705–719. Available at: <https://doi.org/10.1046/j.1471-4159.2001.00322.x>.
- Brown, P.M.G.E., McGuire, H. and Bowie, D. (2017) ‘Stargazin and cornichon-3 relieve polyamine block of AMPA receptors by enhancing blocker permeation’, *Journal of General Physiology*, 150(1), pp. 67–82. Available at: <https://doi.org/10.1085/jgp.201711895>.
- Brunskine, C., Passlick, S. and Henneberger, C. (2022) ‘Structural Heterogeneity of the GABAergic Tripartite Synapse’, *Cells*, 11(19), p. 3150. Available at: <https://doi.org/10.3390/cells11193150>.
- Buckner, R.L. (2013) ‘The Cerebellum and Cognitive Function: 25 Years of Insight from Anatomy and Neuroimaging’, *Neuron*, 80(3), pp. 807–815. Available at: <https://doi.org/10.1016/j.neuron.2013.10.044>.

- Buffo, A. and Rossi, F. (2013) 'Origin, lineage and function of cerebellar glia', *Progress in Neurobiology*, 109, pp. 42–63. Available at: <https://doi.org/10.1016/j.pneurobio.2013.08.001>.
- Butt, A.M. *et al.* (2002) 'Synantocytes: New functions for novel NG2 expressing glia', *Journal of Neurocytology*, 31(6), p. 551 – 565. Available at: <https://doi.org/10.1023/A:1025751900356>.
- Camuso, S. *et al.* (2022) 'Pleiotropic effects of BDNF on the cerebellum and hippocampus: Implications for neurodevelopmental disorders', *Neurobiology of Disease*, 163, p. 105606. Available at: <https://doi.org/10.1016/j.nbd.2021.105606>.
- Cardoso, F.L. *et al.* (2015) 'Systemic inflammation in early neonatal mice induces transient and lasting neurodegenerative effects', *Journal of Neuroinflammation*, 12, p. 82. Available at: <https://doi.org/10.1186/s12974-015-0299-3>.
- Carter, A.R. *et al.* (2002) 'Brain-Derived Neurotrophic Factor Modulates Cerebellar Plasticity and Synaptic Ultrastructure', *The Journal of Neuroscience*, 22(4), pp. 1316–1327. Available at: <https://doi.org/10.1523/JNEUROSCI.22-04-01316.2002>.
- Cerminara, N.L. *et al.* (2015) 'Redefining the cerebellar cortex as an assembly of non-uniform Purkinje cell microcircuits', *Nature Reviews Neuroscience*, 16(2), pp. 79–93. Available at: <https://doi.org/10.1038/nrn3886>.
- Chen, C.H. *et al.* (2014) 'Short latency cerebellar modulation of the basal ganglia', *Nature Neuroscience*, 17(12), pp. 1767–1775. Available at: <https://doi.org/10.1038/nn.3868>.
- Chen, G., Harata, N.C. and Tsien, R.W. (2004) 'Paired-pulse depression of unitary quantal amplitude at single hippocampal synapses', *Proceedings of the National Academy of Sciences*, 101(4), pp. 1063–1068. Available at: <https://doi.org/10.1073/pnas.0307149101>.
- Chen, T.-J. *et al.* (2018) 'In Vivo Regulation of Oligodendrocyte Precursor Cell Proliferation and Differentiation by the AMPA-Receptor Subunit GluA2', *Cell Reports*, 25(4), pp. 852–861.e7. Available at: <https://doi.org/10.1016/j.celrep.2018.09.066>.
- Chen, X. *et al.* (2015) 'Impairment of Oligodendroglia Maturation Leads to Aberrantly Increased Cortical Glutamate and Anxiety-Like Behaviors in Juvenile Mice', *Frontiers in Cellular Neuroscience*, 9. Available at: <https://www.frontiersin.org/articles/10.3389/fncel.2015.00467>.

- Chin, P.W. and Augustine, G.J. (2023) ‘The cerebellum and anxiety’, *Frontiers in Cellular Neuroscience*, 17. Available at: <https://www.frontiersin.org/articles/10.3389/fncel.2023.1130505>.
- Cook, A.A. *et al.* (2021) *Restoration of BDNF-TrkB signaling rescues deficits in a mouse model of SCA6*. preprint. Neuroscience. Available at: <https://doi.org/10.1101/2021.02.21.432180>.
- Coombs, I.D. *et al.* (2023) ‘Enhanced functional detection of synaptic calcium-permeable AMPA receptors using intracellular NASPM’, *eLife*. Edited by L. Overstreet-Wadiche, 12, p. e66765. Available at: <https://doi.org/10.7554/eLife.66765>.
- Coull, J.A.M. *et al.* (2005) ‘BDNF from microglia causes the shift in neuronal anion gradient underlying neuropathic pain’, *Nature*, 438(7070), pp. 1017–1021. Available at: <https://doi.org/10.1038/nature04223>.
- Cull-Candy, S.G. and Farrant, M. (2021) ‘Ca²⁺-permeable AMPA receptors and their auxiliary subunits in synaptic plasticity and disease’, *The Journal of Physiology*, 599(10), pp. 2655–2671. Available at: <https://doi.org/10.1113/JP279029>.
- Dahmane, N. and Ruiz-i-Altaba, A. (1999) ‘Sonic hedgehog regulates the growth and patterning of the cerebellum’, *Development*, 126(14), pp. 3089–3100. Available at: <https://doi.org/10.1242/dev.126.14.3089>.
- D’Angelo, E. (2014) ‘The Organization of Plasticity in the Cerebellar Cortex: From Synapses to Control’, in *Progress in Brain Research*. Elsevier, pp. 31–58. Available at: <https://doi.org/10.1016/B978-0-444-63356-9.00002-9>.
- Datta, I. *et al.* (2018) ‘Location and Number of Astrocytes Determine Dopaminergic Neuron Survival and Function Under 6-OHDA Stress Mediated Through Differential BDNF Release’, *Molecular Neurobiology*, 55(7), pp. 5505–5525. Available at: <https://doi.org/10.1007/s12035-017-0767-0>.
- Davie, J.T., Clark, B.A. and Häusser, M. (2008) ‘The Origin of the Complex Spike in Cerebellar Purkinje Cells’, *Journal of Neuroscience*, 28(30), pp. 7599–7609. Available at: <https://doi.org/10.1523/JNEUROSCI.0559-08.2008>.

- Davies, C.H. and Collingridge, G.L. (1993) 'The physiological regulation of synaptic inhibition by GABAB autoreceptors in rat hippocampus', *The Journal of Physiology*, 472, pp. 245–265. Available at: <https://doi.org/10.1113/jphysiol.1993.sp019945>.
- Dawson, M.R.L. *et al.* (2003) 'NG2-expressing glial progenitor cells: an abundant and widespread population of cycling cells in the adult rat CNS', *Molecular and Cellular Neuroscience*, 24(2), pp. 476–488. Available at: [https://doi.org/10.1016/S1044-7431\(03\)00210-0](https://doi.org/10.1016/S1044-7431(03)00210-0).
- De Zeeuw, C.I. *et al.* (2011) 'Spatiotemporal firing patterns in the cerebellum', *Nature Reviews Neuroscience*, 12(6), pp. 327–344. Available at: <https://doi.org/10.1038/nrn3011>.
- Dean, C. *et al.* (2009) 'Synaptotagmin-IV modulates synaptic function and long-term potentiation by regulating BDNF release', *Nature Neuroscience*, 12(6), pp. 767–776. Available at: <https://doi.org/10.1038/nn.2315>.
- Derkach, V., Barria, A. and Soderling, T.R. (1999) 'Ca²⁺/calmodulin-kinase II enhances channel conductance of α -amino-3-hydroxy-5-methyl-4-isoxazolepropionate type glutamate receptors', *Proceedings of the National Academy of Sciences*, 96(6), pp. 3269–3274. Available at: <https://doi.org/10.1073/pnas.96.6.3269>.
- Di Benedetto, B. and Rupprecht, R. (2013) 'Targeting Glia Cells: Novel Perspectives for the Treatment of Neuropsychiatric Diseases', *Current Neuropharmacology*, 11(2), pp. 171–185. Available at: <https://doi.org/10.2174/1570159X11311020004>.
- Dimou, L. *et al.* (2008) 'Progeny of Olig2-Expressing Progenitors in the Gray and White Matter of the Adult Mouse Cerebral Cortex', *Journal of Neuroscience*, 28(41), pp. 10434–10442. Available at: <https://doi.org/10.1523/JNEUROSCI.2831-08.2008>.
- Dimou, L. and Gallo, V. (2015) 'NG2-glia and their functions in the central nervous system', *Glia*, 63(8), pp. 1429–1451. Available at: <https://doi.org/10.1002/glia.22859>.
- Dimou, L. and Simons, M. (2017) 'Diversity of oligodendrocytes and their progenitors', *Current Opinion in Neurobiology*, 47, pp. 73–79. Available at: <https://doi.org/10.1016/j.conb.2017.09.015>.
- Dittman, J.S. and Regehr, W.G. (1998) 'Calcium Dependence and Recovery Kinetics of Presynaptic Depression at the Climbing Fiber to Purkinje Cell Synapse', *Journal of*

Neuroscience, 18(16), pp. 6147–6162. Available at: <https://doi.org/10.1523/JNEUROSCI.18-16-06147.1998>.

Djalali, S. *et al.* (2005) ‘Effects of brain-derived neurotrophic factor (BDNF) on glial cells and serotonergic neurones during development’, *Journal of Neurochemistry*, 92(3), pp. 616–627. Available at: <https://doi.org/10.1111/j.1471-4159.2004.02911.x>.

Djukic, B. *et al.* (2007) ‘Conditional Knock-Out of Kir4.1 Leads to Glial Membrane Depolarization, Inhibition of Potassium and Glutamate Uptake, and Enhanced Short-Term Synaptic Potentiation’, *Journal of Neuroscience*, 27(42), pp. 11354–11365. Available at: <https://doi.org/10.1523/JNEUROSCI.0723-07.2007>.

Du, X. *et al.* (2021) ‘Differential Modulators of NG2-Glia Differentiation into Neurons and Glia and Their Crosstalk’, *Cellular and Molecular Neurobiology*, 41(1), pp. 1–15. Available at: <https://doi.org/10.1007/s10571-020-00843-0>.

Du, X. and Hill, R.A. (2015) ‘7,8-Dihydroxyflavone as a pro-neurotrophic treatment for neurodevelopmental disorders’, *Neurochemistry International*, 89, pp. 170–180. Available at: <https://doi.org/10.1016/j.neuint.2015.07.021>.

Du, Y. *et al.* (2022) ‘Microglia maintain the normal structure and function of the hippocampal astrocyte network’, *Glia*, 70(7), pp. 1359–1379. Available at: <https://doi.org/10.1002/glia.24179>.

Dudek, S.M. and Bear, M.F. (1992) ‘Homosynaptic long-term depression in area CA1 of hippocampus and effects of N-methyl-D-aspartate receptor blockade.’, *Proceedings of the National Academy of Sciences of the United States of America*, 89(10), pp. 4363–4367.

Dum, R.P. and Strick, P.L. (2003) ‘An Unfolded Map of the Cerebellar Dentate Nucleus and its Projections to the Cerebral Cortex’, *Journal of Neurophysiology*, 89(1), pp. 634–639. Available at: <https://doi.org/10.1152/jn.00626.2002>.

Eccles, J.C., Llinás, R. and Sasaki, K. (1966) ‘The excitatory synaptic action of climbing fibres on the Purkinje cells of the cerebellum’, *The Journal of Physiology*, 182(2), pp. 268–296. Available at: <https://doi.org/10.1113/jphysiol.1966.sp007824>.

- Egawa, K. *et al.* (2013) 'Cl⁻ homeodynamics in gap junction-coupled astrocytic networks on activation of GABAergic synapses', *The Journal of Physiology*, 591(16), pp. 3901–3917. Available at: <https://doi.org/10.1113/jphysiol.2013.257162>.
- Eudave, D.M., BeLow, M.N. and Flandreau, E.I. (2018) 'Effects of high fat or high sucrose diet on behavioral-response to social defeat stress in mice', *Neurobiology of Stress*, 9, pp. 1–8. Available at: <https://doi.org/10.1016/j.ynstr.2018.05.005>.
- Fang, L.-P. *et al.* (2022) 'Impaired bidirectional communication between interneurons and oligodendrocyte precursor cells affects social cognitive behavior', *Nature Communications*, 13(1), p. 1394. Available at: <https://doi.org/10.1038/s41467-022-29020-1>.
- Fannon, J., Tarmier, W. and Fulton, D. (2015) 'Neuronal activity and AMPA-type glutamate receptor activation regulates the morphological development of oligodendrocyte precursor cells', *Glia*, 63(6), pp. 1021–1035. Available at: <https://doi.org/10.1002/glia.22799>.
- Farrant, M. and Nusser, Z. (2005) 'Variations on an inhibitory theme: phasic and tonic activation of GABA_A receptors', *Nature Reviews Neuroscience*, 6(3), pp. 215–229. Available at: <https://doi.org/10.1038/nrn1625>.
- Feil, R. *et al.* (1997) 'Regulation of Cre Recombinase Activity by Mutated Estrogen Receptor Ligand-Binding Domains', *Biochemical and Biophysical Research Communications*, 237(3), pp. 752–757. Available at: <https://doi.org/10.1006/bbrc.1997.7124>.
- Ferbinteanu, J., Holsinger, R.M.D. and McDonald, R.J. (1999) 'Lesions of the medial or lateral perforant path have different effects on hippocampal contributions to place learning and on fear conditioning to context', *Behavioural Brain Research*, 101(1), pp. 65–84. Available at: [https://doi.org/10.1016/S0166-4328\(98\)00144-2](https://doi.org/10.1016/S0166-4328(98)00144-2).
- Finch, D.M., Nowlin, N.L. and Babb, T.L. (1983) 'Demonstration of axonal projections of neurons in the rat hippocampus and subiculum by intracellular injection of HRP', *Brain Research*, 271(2), pp. 201–216. Available at: [https://doi.org/10.1016/0006-8993\(83\)90283-4](https://doi.org/10.1016/0006-8993(83)90283-4).
- Fisher, S.A., Fischer, T.M. and Carew, T.J. (1997) 'Multiple overlapping processes underlying short-term synaptic enhancement', *Trends in Neurosciences*, 20(4), pp. 170–177. Available at: [https://doi.org/10.1016/S0166-2236\(96\)01001-6](https://doi.org/10.1016/S0166-2236(96)01001-6).

- Fletcher, J., Murray, S. and Xiao, J. (2018) 'Brain-Derived Neurotrophic Factor in Central Nervous System Myelination: A New Mechanism to Promote Myelin Plasticity and Repair', *International Journal of Molecular Sciences*, 19(12), p. 4131. Available at: <https://doi.org/10.3390/ijms19124131>.
- Forsythe, I.D. *et al.* (1998) 'Inactivation of Presynaptic Calcium Current Contributes to Synaptic Depression at a Fast Central Synapse', *Neuron*, 20(4), pp. 797–807. Available at: [https://doi.org/10.1016/S0896-6273\(00\)81017-X](https://doi.org/10.1016/S0896-6273(00)81017-X).
- Frahm, C. and Draguhn, A. (2001) 'GAD and GABA transporter (GAT-1) mRNA expression in the developing rat hippocampus', *Developmental Brain Research*, 132, pp. 1–13. Available at: [https://doi.org/10.1016/S0165-3806\(01\)00288-7](https://doi.org/10.1016/S0165-3806(01)00288-7).
- Gallo, V. and Deneen, B. (2014) 'Glial Development: The Crossroads of Regeneration and Repair in the CNS', *Neuron*, 83(2), pp. 283–308. Available at: <https://doi.org/10.1016/j.neuron.2014.06.010>.
- Gautier, H.O.B. *et al.* (2015) 'Neuronal activity regulates remyelination via glutamate signalling to oligodendrocyte progenitors', *Nature Communications*, 6(1), p. 8518. Available at: <https://doi.org/10.1038/ncomms9518>.
- Ge, W.-P. *et al.* (2006) 'Long-Term Potentiation of Neuron-Glia Synapses Mediated by Ca²⁺-Permeable AMPA Receptors', *Science*, 312(5779), pp. 1533–1537. Available at: <https://doi.org/10.1126/science.1124669>.
- Ge, Y. *et al.* (2010) 'Hippocampal long-term depression is required for the consolidation of spatial memory', *Proceedings of the National Academy of Sciences of the United States of America*, 107(38), pp. 16697–16702. Available at: <https://doi.org/10.1073/pnas.1008200107>.
- Geiger, J.R. *et al.* (1995) 'Relative abundance of subunit mRNAs determines gating and Ca²⁺ permeability of AMPA receptors in principal neurons and interneurons in rat CNS', *Neuron*, 15(1), pp. 193–204. Available at: [https://doi.org/10.1016/0896-6273\(95\)90076-4](https://doi.org/10.1016/0896-6273(95)90076-4).
- Geraghty, A.C. *et al.* (2019) 'Loss of adaptive myelination contributes to methotrexate chemotherapy-related cognitive impairment', *Neuron*, 103(2), pp. 250-265.e8. Available at: <https://doi.org/10.1016/j.neuron.2019.04.032>.

- Ghasemi, M. *et al.* (2022) ‘Anxiety and hippocampal neuronal activity: Relationship and potential mechanisms’, *Cognitive, Affective, & Behavioral Neuroscience*, 22(3), pp. 431–449. Available at: <https://doi.org/10.3758/s13415-021-00973-y>.
- Ghit, A. *et al.* (2021) ‘GABAA receptors: structure, function, pharmacology, and related disorders’, *Journal of Genetic Engineering & Biotechnology*, 19, p. 123. Available at: <https://doi.org/10.1186/s43141-021-00224-0>.
- Gibson, E.M. *et al.* (2014) ‘Neuronal Activity Promotes Oligodendrogenesis and Adaptive Myelination in the Mammalian Brain’, *Science (New York, N.Y.)*, 344(6183), p. 1252304. Available at: <https://doi.org/10.1126/science.1252304>.
- Gomes, C. *et al.* (2013) ‘Activation of microglial cells triggers a release of brain-derived neurotrophic factor (BDNF) inducing their proliferation in an adenosine A2A receptor-dependent manner: A2A receptor blockade prevents BDNF release and proliferation of microglia’, *Journal of Neuroinflammation*, 10(1), p. 780. Available at: <https://doi.org/10.1186/1742-2094-10-16>.
- Grasselli, G. *et al.* (2020) ‘SK2 channels in cerebellar Purkinje cells contribute to excitability modulation in motor-learning-specific memory traces’, *PLOS Biology*, 18(1), p. e3000596. Available at: <https://doi.org/10.1371/journal.pbio.3000596>.
- Grosche, J., Kettenmann, H. and Reichenbach, A. (2002) ‘Bergmann glial cells form distinct morphological structures to interact with cerebellar neurons’, *Journal of Neuroscience Research*, 68(2), pp. 138–149. Available at: <https://doi.org/10.1002/jnr.10197>.
- Guijarro, P. *et al.* (2006) ‘Netrin1 exerts a chemorepulsive effect on migrating cerebellar interneurons in a Dcc-independent way’, *Molecular and Cellular Neuroscience*, 33(4), pp. 389–400. Available at: <https://doi.org/10.1016/j.mcn.2006.08.010>.
- Hagiwara, S. and Takahashi, K. (1974) ‘The anomalous rectification and cation selectivity of the membrane of a starfish egg cell’, *The Journal of Membrane Biology*, 18(1), pp. 61–80. Available at: <https://doi.org/10.1007/BF01870103>.
- Han, V.Z., Grant, K. and Bell, C.C. (2000) ‘Reversible Associative Depression and Nonassociative Potentiation at a Parallel Fiber Synapse’, *Neuron*, 27(3), pp. 611–622. Available at: [https://doi.org/10.1016/S0896-6273\(00\)00070-2](https://doi.org/10.1016/S0896-6273(00)00070-2).

- Hansel, C. and Linden, D.J. (2000) 'Long-Term Depression of the Cerebellar Climbing Fiber–Purkinje Neuron Synapse', *Neuron*, 26(2), pp. 473–482. Available at: [https://doi.org/10.1016/S0896-6273\(00\)81179-4](https://doi.org/10.1016/S0896-6273(00)81179-4).
- Hardt, S. *et al.* (2021) 'Auxiliary Subunits Control Function and Subcellular Distribution of AMPA Receptor Complexes in NG2 Glia of the Developing Hippocampus', *Frontiers in Cellular Neuroscience*, 15. Available at: <https://www.frontiersin.org/articles/10.3389/fncel.2021.669717..>
- Hashimoto, K. and Kano, M. (1998) 'Presynaptic origin of paired-pulse depression at climbing fibre–Purkinje cell synapses in the rat cerebellum', *The Journal of Physiology*, 506(Pt 2), pp. 391–405. Available at: <https://doi.org/10.1111/j.1469-7793.1998.391bw.x>.
- Hashimoto, M. and Hibi, M. (2012) 'Development and evolution of cerebellar neural circuits', *Development, Growth & Differentiation*, 54(3), pp. 373–389. Available at: <https://doi.org/10.1111/j.1440-169X.2012.01348.x>.
- Häusser, M. and Clark, B.A. (1997) 'Tonic Synaptic Inhibition Modulates Neuronal Output Pattern and Spatiotemporal Synaptic Integration', *Neuron*, 19(3), pp. 665–678. Available at: [https://doi.org/10.1016/S0896-6273\(00\)80379-7](https://doi.org/10.1016/S0896-6273(00)80379-7).
- Herculano-Houzel, S. (2010) 'Coordinated scaling of cortical and cerebellar numbers of neurons', *Frontiers in Neuroanatomy*, 4. Available at: <https://www.frontiersin.org/articles/10.3389/fnana.2010.00012>.
- Herculano-Houzel, S., Mota, B. and Lent, R. (2006) 'Cellular scaling rules for rodent brains', *Proceedings of the National Academy of Sciences*, 103(32), pp. 12138–12143. Available at: <https://doi.org/10.1073/pnas.0604911103>.
- Herguedas, B., Krieger, J. and Greger, I.H. (2013) 'Receptor heteromeric assembly-how it works and why it matters: the case of ionotropic glutamate receptors', *Progress in Molecular Biology and Translational Science*, 117, pp. 361–386. Available at: <https://doi.org/10.1016/B978-0-12-386931-9.00013-1>.
- Hestrin, S. (1992) 'Activation and desensitization of glutamate-activated channels mediating fast excitatory synaptic currents in the visual cortex', *Neuron*, 9(5), pp. 991–999. Available at: [https://doi.org/10.1016/0896-6273\(92\)90250-H](https://doi.org/10.1016/0896-6273(92)90250-H).

- Hibino, H. *et al.* (2010) 'Inwardly Rectifying Potassium Channels: Their Structure, Function, and Physiological Roles', *Physiological Reviews*, 90(1), pp. 291–366. Available at: <https://doi.org/10.1152/physrev.00021.2009>.
- Higashi, K. *et al.* (2001) 'An inwardly rectifying K(+) channel, Kir4.1, expressed in astrocytes surrounds synapses and blood vessels in brain', *American Journal of Physiology. Cell Physiology*, 281(3), pp. C922-931. Available at: <https://doi.org/10.1152/ajpcell.2001.281.3.C922>.
- Hill, R.A. and Nishiyama, A. (2014) 'NG2 cells (polydendrocytes): Listeners to the neural network with diverse properties', *Glia*, 62(8), pp. 1195–1210. Available at: <https://doi.org/10.1002/glia.22664>.
- Holt, L.M. *et al.* (2019) 'Astrocyte morphogenesis is dependent on BDNF signaling via astrocytic TrkB.T1', *eLife*. Edited by C. Eroglu, D.Y. Stainier, and M. Freeman, 8, p. e44667. Available at: <https://doi.org/10.7554/eLife.44667>.
- Hoser, M. *et al.* (2007) 'Prolonged Glial Expression of Sox4 in the CNS Leads to Architectural Cerebellar Defects and Ataxia', *Journal of Neuroscience*, 27(20), pp. 5495–5505. Available at: <https://doi.org/10.1523/JNEUROSCI.1384-07.2007>.
- Hoxha, E. *et al.* (2018) 'Purkinje Cell Signaling Deficits in Animal Models of Ataxia', *Frontiers in Synaptic Neuroscience*, 10. Available at: <https://www.frontiersin.org/articles/10.3389/fnsyn.2018.00006>.
- Hughes, E.G. *et al.* (2018) 'Myelin remodeling through experience-dependent oligodendrogenesis in the adult somatosensory cortex', *Nature Neuroscience*, 21(5), pp. 696–706. Available at: <https://doi.org/10.1038/s41593-018-0121-5>.
- Iino, M. *et al.* (2001) 'Glial-synapse interaction through Ca²⁺-permeable AMPA receptors in Bergmann glia', *Science (New York, N.Y.)*, 292(5518), pp. 926–929. Available at: <https://doi.org/10.1126/science.1058827>.
- Incontro, S. *et al.* (2018) 'The CaMKII/NMDA receptor complex controls hippocampal synaptic transmission by kinase-dependent and independent mechanisms', *Nature Communications*, 9(1), p. 2069. Available at: <https://doi.org/10.1038/s41467-018-04439-7>.

- Insausti, R., Amaral, D.G. and Cowan, W.M. (1987) 'The entorhinal cortex of the monkey: II. Cortical afferents', *Journal of Comparative Neurology*, 264(3), pp. 356–395. Available at: <https://doi.org/10.1002/cne.902640306>.
- Ito, M. and Kano, M. (1982) 'Long-lasting depression of parallel fiber-Purkinje cell transmission induced by conjunctive stimulation of parallel fibers and climbing fibers in the cerebellar cortex', *Neuroscience Letters*, 33(3), pp. 253–258. Available at: [https://doi.org/10.1016/0304-3940\(82\)90380-9](https://doi.org/10.1016/0304-3940(82)90380-9).
- Jabs, R. *et al.* (2005) 'Synaptic transmission onto hippocampal glial cells with hGFAP promoter activity', *Journal of Cell Science*, 118(16), pp. 3791–3803. Available at: <https://doi.org/10.1242/jcs.02515>.
- Johnson, E.M., Craig, E.T. and Yeh, H.H. (2007) 'TrkB is necessary for pruning at the climbing fibre–Purkinje cell synapse in the developing murine cerebellum', *The Journal of Physiology*, 582(2), pp. 629–646. Available at: <https://doi.org/10.1113/jphysiol.2007.133561>.
- Jörntell, H. and Hansel, C. (2006) 'Synaptic Memories Upside Down: Bidirectional Plasticity at Cerebellar Parallel Fiber-Purkinje Cell Synapses', *Neuron*, 52(2), pp. 227–238. Available at: <https://doi.org/10.1016/j.neuron.2006.09.032>.
- Karram, K. *et al.* (2008) 'NG2-expressing cells in the nervous system revealed by the NG2-EYFP-knockin mouse', *genesis*, 46(12), pp. 743–757. Available at: <https://doi.org/10.1002/dvg.20440>.
- Katz, B. and Thesleff, S. (1957) 'A study of the “desensitization” produced by acetylcholine at the motor end-plate', *The Journal of Physiology*, 138(1), pp. 63–80. Available at: <https://doi.org/10.1113/jphysiol.1957.sp005838>.
- Kawamoto, Y. *et al.* (1996) 'Immunohistochemical localization of brain-derived neurotrophic factor in adult rat brain', *Neuroscience*, 74(4), pp. 1209–1226. Available at: [https://doi.org/10.1016/0306-4522\(96\)00245-X](https://doi.org/10.1016/0306-4522(96)00245-X).
- Keller, D., Erö, C. and Markram, H. (2018) 'Cell Densities in the Mouse Brain: A Systematic Review', *Frontiers in Neuroanatomy*, 12. Available at: <https://www.frontiersin.org/articles/10.3389/fnana.2018.00083>.

- Kersanté, F. *et al.* (2013) ‘A functional role for both γ -aminobutyric acid (GABA) transporter-1 and GABA transporter-3 in the modulation of extracellular GABA and GABAergic tonic conductances in the rat hippocampus’, *The Journal of Physiology*, 591(10), pp. 2429–2441. Available at: <https://doi.org/10.1113/jphysiol.2012.246298>.
- Kettenmann, H. and Verkhratsky, A. (2008) ‘Neuroglia: the 150 years after’, *Trends in Neurosciences*, 31(12), pp. 653–659. Available at: <https://doi.org/10.1016/j.tins.2008.09.003>.
- Khawaja, R.R. *et al.* (2021) ‘GluA2 overexpression in oligodendrocyte progenitors promotes postinjury oligodendrocyte regeneration’, *Cell Reports*, 35(7), p. 109147. Available at: <https://doi.org/10.1016/j.celrep.2021.109147>.
- Kofuji, P. and Newman, E.A. (2004) ‘Potassium buffering in the central nervous system’, *Neuroscience*, 129(4), pp. 1043–1054. Available at: <https://doi.org/10.1016/j.neuroscience.2004.06.008>.
- Korpi, E.R. and Sinkkonen, S.T. (2006) ‘GABA_A receptor subtypes as targets for neuropsychiatric drug development’, *Pharmacology & Therapeutics*, 109(1), pp. 12–32. Available at: <https://doi.org/10.1016/j.pharmthera.2005.05.009>.
- Korte, M. *et al.* (1995) ‘Hippocampal long-term potentiation is impaired in mice lacking brain-derived neurotrophic factor.’, *Proceedings of the National Academy of Sciences of the United States of America*, 92(19), pp. 8856–8860.
- Kougioumtzidou, E. *et al.* (2017) ‘Signalling through AMPA receptors on oligodendrocyte precursors promotes myelination by enhancing oligodendrocyte survival’, *eLife*. Edited by C.A. Mason, 6, p. e28080. Available at: <https://doi.org/10.7554/eLife.28080>.
- Kraushaar, U. and Jonas, P. (2000) ‘Efficacy and Stability of Quantal GABA Release at a Hippocampal Interneuron–Principal Neuron Synapse’, *Journal of Neuroscience*, 20(15), pp. 5594–5607. Available at: <https://doi.org/10.1523/JNEUROSCI.20-15-05594.2000>.
- Krettek, J.E. and Price, J.L. (1977) ‘Projections from the amygdaloid complex and adjacent olfactory structures to the entorhinal cortex and to the subiculum in the rat and cat’, *Journal of Comparative Neurology*, 172(4), pp. 723–752. Available at: <https://doi.org/10.1002/cne.901720409>.

- Kristensen, A.S. *et al.* (2011) ‘Mechanism of Ca²⁺/calmodulin-dependent kinase II regulation of AMPA receptor gating’, *Nature Neuroscience*, 14(6), pp. 727–735. Available at: <https://doi.org/10.1038/nn.2804>.
- Kukley, M., Capetillo-Zarate, E. and Dietrich, D. (2007) ‘Vesicular glutamate release from axons in white matter’, *Nature Neuroscience*, 10(3), pp. 311–320. Available at: <https://doi.org/10.1038/nn1850>.
- Kullmann, J.A. *et al.* (2012) ‘Profilin1 is required for glial cell adhesion and radial migration of cerebellar granule neurons’, *EMBO reports*, 13(1), pp. 75–82. Available at: <https://doi.org/10.1038/embor.2011.211>.
- Lalanne, T. *et al.* (2016) ‘Synapse-specific expression of calcium-permeable AMPA receptors in neocortical layer 5’, *The Journal of Physiology*, 594(4), pp. 837–861. Available at: <https://doi.org/10.1113/JP271394>.
- Lanore, F. and Silver, R.A. (2016) ‘Extracting quantal properties of transmission at central synapses’, *Neuromethods*, 113, pp. 193–211. Available at: https://doi.org/10.1007/978-1-4939-3411-9_10.
- Leal, G., Bramham, C.R. and Duarte, C.B. (2017) ‘BDNF and Hippocampal Synaptic Plasticity’, in *Vitamins and Hormones*. Elsevier, pp. 153–195. Available at: <https://doi.org/10.1016/bs.vh.2016.10.004>.
- Lee, J., Kim, S.W. and Kim, K.-T. (2022) ‘Region-Specific Characteristics of Astrocytes and Microglia: A Possible Involvement in Aging and Diseases’, *Cells*, 11(12), p. 1902. Available at: <https://doi.org/10.3390/cells11121902>.
- Levi-Montalcini, R. (1987) ‘The Nerve Growth Factor 35 Years Later’, *Science*, 237(4819), pp. 1154–1162. Available at: <https://doi.org/10.1126/science.3306916>.
- Levine, J. (2016) ‘The reactions and role of NG2 glia in spinal cord injury’, *Brain Research*, 1638, pp. 199–208. Available at: <https://doi.org/10.1016/j.brainres.2015.07.026>.
- Lev-Ram, V. *et al.* (2002) ‘A new form of cerebellar long-term potentiation is postsynaptic and depends on nitric oxide but not cAMP’, *Proceedings of the National Academy of Sciences*, 99(12), pp. 8389–8393. Available at: <https://doi.org/10.1073/pnas.122206399>.

- Lewin, G.R. and Barde, Y.-A. (no date) 'Physiology of the Neurotrophins'.
- Liley, A.W. and North, K. a. K. (1953) 'An electrical investigation of effects of repetitive stimulation on mammalian neuromuscular junction', *Journal of Neurophysiology*, 16(5), pp. 509–527. Available at: <https://doi.org/10.1152/jn.1953.16.5.509>.
- Lin, S. *et al.* (2005) 'Climbing Fiber Innervation of NG2-Expressing Glia in the Mammalian Cerebellum', *Neuron*, 46(5), pp. 773–785. Available at: <https://doi.org/10.1016/j.neuron.2005.04.025>.
- Lin, S. and Bergles, D.E. (2004) 'Synaptic signaling between GABAergic interneurons and oligodendrocyte precursor cells in the hippocampus', *Nature Neuroscience*, 7(1), pp. 24–32. Available at: <https://doi.org/10.1038/nn1162>.
- Liu, S.J. and Zukin, R.S. (2007) 'Ca²⁺-permeable AMPA receptors in synaptic plasticity and neuronal death', *Trends in Neurosciences*, 30(3), pp. 126–134. Available at: <https://doi.org/10.1016/j.tins.2007.01.006>.
- Liu, Y. and Aguzzi, A. (2020) 'NG2 glia are required for maintaining microglia homeostatic state', *Glia*, 68(2), pp. 345–355. Available at: <https://doi.org/10.1002/glia.23721>.
- Lordkipanidze, T. and Dunaevsky, A. (2005) 'Purkinje cell dendrites grow in alignment with Bergmann glia', *Glia*, 51(3), pp. 229–234. Available at: <https://doi.org/10.1002/glia.20200>.
- Lorente De Nó, R. (1934) 'Studies on the structure of the cerebral cortex. II. Continuation of the study of the ammonic system', *Journal für Psychologie und Neurologie*, 46, pp. 113–177.
- Macdonald, R.L., Kang, J.-Q. and Gallagher, M.J. (2010) 'Mutations in GABAA receptor subunits associated with genetic epilepsies', *The Journal of Physiology*, 588(11), pp. 1861–1869. Available at: <https://doi.org/10.1113/jphysiol.2010.186999>.
- MacDougall, M.J. and Fine, A. (2014) 'The expression of long-term potentiation: reconciling the preists and the postivists', *Philosophical Transactions of the Royal Society B: Biological Sciences*, 369(1633), p. 20130135. Available at: <https://doi.org/10.1098/rstb.2013.0135>.
- Malenka, R.C. (2003) 'Synaptic Plasticity and AMPA Receptor Trafficking', *Annals of the New York Academy of Sciences*, 1003(1), pp. 1–11. Available at: <https://doi.org/10.1196/annals.1300.001>.

- Mangin, J.-M. *et al.* (2008) ‘Satellite NG2 Progenitor Cells Share Common Glutamatergic Inputs with Associated Interneurons in the Mouse Dentate Gyrus’, *The Journal of Neuroscience*, 28(30), pp. 7610–7623. Available at: <https://doi.org/10.1523/JNEUROSCI.1355-08.2008>.
- Mangin, J.-M. *et al.* (2012) ‘Experience-dependent regulation of NG2 progenitors in the developing barrel cortex’, *Nature Neuroscience*, 15(9), pp. 1192–1194. Available at: <https://doi.org/10.1038/nn.3190>.
- Marín-Teva, J.L. *et al.* (2004) ‘Microglia Promote the Death of Developing Purkinje Cells’, *Neuron*, 41(4), pp. 535–547. Available at: [https://doi.org/10.1016/S0896-6273\(04\)00069-8](https://doi.org/10.1016/S0896-6273(04)00069-8).
- Marr, D. (1969) ‘A theory of cerebellar cortex’, *The Journal of Physiology*, 202(2), pp. 437–470. Available at: <https://doi.org/10.1113/jphysiol.1969.sp008820>.
- Mateos, J.M. *et al.* (no date) ‘Parasagittal compartmentalization of the metabotropic glutamate receptor mGluR1b in the cerebellar cortex’.
- Mathis, C., Collin, L. and Borrelli, E. (2003) ‘Oligodendrocyte ablation impairs cerebellum development’, *Development*, 130(19), pp. 4709–4718. Available at: <https://doi.org/10.1242/dev.00675>.
- Matusue, Y. *et al.* (2014) ‘Distribution of Corticosteroid Receptors in Mature Oligodendrocytes and Oligodendrocyte Progenitors of the Adult Mouse Brain’, *Journal of Histochemistry & Cytochemistry*, 62(3), pp. 211–226. Available at: <https://doi.org/10.1369/0022155413517700>.
- Matta, J.A. *et al.* (2013) ‘Developmental origin dictates interneuron AMPA and NMDA receptor subunit composition and plasticity’, *Nature Neuroscience*, 16(8), pp. 1032–1041. Available at: <https://doi.org/10.1038/nn.3459>.
- McKinney, B.C. *et al.* (2008) ‘Decreased locomotor activity in mice expressing tTA under control of the CaMKII α promoter’, *Genes, Brain and Behavior*, 7(2), pp. 203–213. Available at: <https://doi.org/10.1111/j.1601-183X.2007.00339.x>.
- Minichiello, L. *et al.* (2002) ‘Mechanism of TrkB-Mediated Hippocampal Long-Term Potentiation’, *Neuron*, 36(1), pp. 121–137. Available at: [https://doi.org/10.1016/S0896-6273\(02\)00942-X](https://doi.org/10.1016/S0896-6273(02)00942-X).

- Monsivais, P. *et al.* (2005) ‘Determinants of Action Potential Propagation in Cerebellar Purkinje Cell Axons’, *Journal of Neuroscience*, 25(2), pp. 464–472. Available at: <https://doi.org/10.1523/JNEUROSCI.3871-04.2005>.
- Moyon, S. *et al.* (2015) ‘Demyelination Causes Adult CNS Progenitors to Revert to an Immature State and Express Immune Cues That Support Their Migration’, *Journal of Neuroscience*, 35(1), pp. 4–20. Available at: <https://doi.org/10.1523/JNEUROSCI.0849-14.2015>.
- Müller, J. *et al.* (2009) ‘The principal neurons of the medial nucleus of the trapezoid body and NG2+ glial cells receive coordinated excitatory synaptic input’, *The Journal of General Physiology*, 134(2), pp. 115–127. Available at: <https://doi.org/10.1085/jgp.200910194>.
- Muñoz-Cuevas, J., Vara, H. and Colino, A. (2004) ‘Characterization of release-independent short-term depression in the juvenile rat hippocampus’, *The Journal of Physiology*, 558(Pt 2), pp. 527–548. Available at: <https://doi.org/10.1113/jphysiol.2004.062133>.
- Munyeshyaka, M. and Fields, R.D. (2022) ‘Oligodendroglia are emerging players in several forms of learning and memory’, *Communications Biology*, 5(1), pp. 1–12. Available at: <https://doi.org/10.1038/s42003-022-04116-y>.
- Neher, E. and Sakmann, B. (1976) ‘Single-channel currents recorded from membrane of denervated frog muscle fibres’, *Nature*, 260(5554), pp. 799–802. Available at: <https://doi.org/10.1038/260799a0>.
- Neusch, C. *et al.* (2001) ‘Kir4.1 Potassium Channel Subunit Is Crucial for Oligodendrocyte Development and In Vivo Myelination’, *Journal of Neuroscience*, 21(15), pp. 5429–5438. Available at: <https://doi.org/10.1523/JNEUROSCI.21-15-05429.2001>.
- Neusch, C. *et al.* (2006) ‘Lack of the Kir4.1 Channel Subunit Abolishes K⁺ Buffering Properties of Astrocytes in the Ventral Respiratory Group: Impact on Extracellular K⁺ Regulation’, *Journal of Neurophysiology*, 95(3), pp. 1843–1852. Available at: <https://doi.org/10.1152/jn.00996.2005>.
- Newman, E.A. (1993) ‘Inward-rectifying potassium channels in retinal glial (Muller) cells’, *Journal of Neuroscience*, 13(8), pp. 3333–3345. Available at: <https://doi.org/10.1523/JNEUROSCI.13-08-03333.1993>.

- Nguyen-Minh, V.T., Tran-Anh, K. and Sugihara, I. (2020) ‘Heterogeneity of intrinsic excitability in Purkinje cells linked with longitudinal zebrin zones in the mouse cerebellum’, *bioRxiv*, p. 2020.06.22.164830. Available at: <https://doi.org/10.1101/2020.06.22.164830>.
- Nishiyama, A. *et al.* (2009) ‘Polydendrocytes (NG2 cells): multifunctional cells with lineage plasticity’, *Nature Reviews Neuroscience*, 10(1), pp. 9–22. Available at: <https://doi.org/10.1038/nrn2495>.
- Ohno, Y., Kinboshi, M. and Shimizu, S. (2018) ‘Inwardly Rectifying Potassium Channel Kir4.1 as a Novel Modulator of BDNF Expression in Astrocytes’, *International Journal of Molecular Sciences*, 19(11), p. 3313. Available at: <https://doi.org/10.3390/ijms19113313>.
- Oláh, S. *et al.* (2009) ‘Regulation of cortical microcircuits by unitary GABA-mediated volume transmission’, *Nature*, 461(7268), pp. 1278–1281. Available at: <https://doi.org/10.1038/nature08503>.
- Olsen, R.W. and Sieghart, W. (2008) ‘International Union of Pharmacology. LXX. Subtypes of γ -Aminobutyric AcidA Receptors: Classification on the Basis of Subunit Composition, Pharmacology, and Function. Update’, *Pharmacological Reviews*, 60(3), pp. 243–260. Available at: <https://doi.org/10.1124/pr.108.00505>.
- Overstreet, L.S. and Westbrook, G.L. (2003) ‘Synapse Density Regulates Independence at Unitary Inhibitory Synapses’, *Journal of Neuroscience*, 23(7), pp. 2618–2626. Available at: <https://doi.org/10.1523/JNEUROSCI.23-07-02618.2003>.
- Pang, P.T. *et al.* (2004) ‘Cleavage of proBDNF by tPA/Plasmin Is Essential for Long-Term Hippocampal Plasticity’, *Science*, 306(5695), pp. 487–491. Available at: <https://doi.org/10.1126/science.1100135>.
- Paolicelli, R.C. *et al.* (2011) ‘Synaptic Pruning by Microglia Is Necessary for Normal Brain Development’, *Science*, 333(6048), pp. 1456–1458. Available at: <https://doi.org/10.1126/science.1202529>.
- Park, H. and Poo, M. (2013) ‘Neurotrophin regulation of neural circuit development and function’, *Nature Reviews Neuroscience*, 14(1), pp. 7–23. Available at: <https://doi.org/10.1038/nrn3379>.

- Parkhurst, C.N. *et al.* (2013) ‘Microglia promote learning-dependent synapse formation through BDNF’, *Cell*, 155(7), pp. 1596–1609. Available at: <https://doi.org/10.1016/j.cell.2013.11.030>.
- Parolisi, R. and Boda, E. (2018) ‘NG2 Glia: Novel Roles beyond Re-/Myelination’, *Neuroglia*, 1(1), pp. 151–175. Available at: <https://doi.org/10.3390/neuroglia1010011>.
- Perea, G. and Araque, A. (2010) ‘GLIA modulates synaptic transmission’, *Brain Research Reviews*, 63(1), pp. 93–102. Available at: <https://doi.org/10.1016/j.brainresrev.2009.10.005>.
- Perin, M.S. *et al.* (1990) ‘Phospholipid binding by a synaptic vesicle protein homologous to the regulatory region of protein kinase C’, *Nature*, 345(6272), pp. 260–263. Available at: <https://doi.org/10.1038/345260a0>.
- Passlick, S. *et al.* (2013) ‘Expression of the γ 2-Subunit Distinguishes Synaptic and Extrasynaptic GABAA Receptors in NG2 Cells of the Hippocampus’, *Journal of Neuroscience*, 33(29), pp. 12030–12040. Available at: <https://doi.org/10.1523/JNEUROSCI.5562-12.2013>.
- Linda Patt, Dario Tascio, Catia Domingos, Aline Timmermann, Ronald Jabs, Christian Henneberger, Christian Steinhäuser and Gerald Seifert. Impact of developmental changes of GABAA receptors on interneuron-NG2 glia transmission in the hippocampus. **In preparation.**
- Phillips, J.R. *et al.* (2015) ‘The Cerebellum and Psychiatric Disorders’, *Frontiers in Public Health*, 3, p. 66. Available at: <https://doi.org/10.3389/fpubh.2015.00066>.
- Popova, E. (2014) ‘Ionotropic GABA Receptors and Distal Retinal ON and OFF Responses’, *Scientifica*, 2014, p. e149187. Available at: <https://doi.org/10.1155/2014/149187>.
- Prasad, A. *et al.* (2017) ‘Static Magnetic Field Stimulation Enhances Oligodendrocyte Differentiation and Secretion of Neurotrophic Factors’, *Scientific Reports*, 7(1), p. 6743. Available at: <https://doi.org/10.1038/s41598-017-06331-8>.
- Qin, N.-X. *et al.* (2021) ‘Anxiety and depression-like behaviours are more frequent in aged male mice conceived by ART compared with natural conception’, *Reproduction*, 162(6), pp. 437–448. Available at: <https://doi.org/10.1530/REP-21-0175>.

- Quirk, G.J. *et al.* (1992) ‘The positional firing properties of medial entorhinal neurons: description and comparison with hippocampal place cells’, *Journal of Neuroscience*, 12(5), pp. 1945–1963. Available at: <https://doi.org/10.1523/JNEUROSCI.12-05-01945.1992>.
- Rabl, K., Cadetti, L. and Thoreson, W.B. (2006) ‘Paired-Pulse Depression at Photoreceptor Synapses’, *Journal of Neuroscience*, 26(9), pp. 2555–2563. Available at: <https://doi.org/10.1523/JNEUROSCI.3667-05.2006>.
- Raman, I.M. and Trussell, L.O. (1995) ‘The mechanism of alpha-amino-3-hydroxy-5-methyl-4-isoxazolepropionate receptor desensitization after removal of glutamate.’, *Biophysical Journal*, 68(1), pp. 137–146.
- Regehr, W.G. (2012) ‘Short-term presynaptic plasticity’, *Cold Spring Harbor Perspectives in Biology*, 4(7), p. a005702. Available at: <https://doi.org/10.1101/cshperspect.a005702>.
- Reichenbach, A., Derouiche, A. and Kirchhoff, F. (2010) ‘Morphology and dynamics of perisynaptic glia’, *Brain Research Reviews*, 63(1), pp. 11–25. Available at: <https://doi.org/10.1016/j.brainresrev.2010.02.003>.
- Richardson, W.D. *et al.* (2011) ‘NG2-glia as Multipotent Neural Stem Cells: Fact or Fantasy?’, *Neuron*, 70(4), pp. 661–673. Available at: <https://doi.org/10.1016/j.neuron.2011.05.013>.
- Rivera, C. *et al.* (1999) ‘The K⁺/Cl⁻ co-transporter KCC2 renders GABA hyperpolarizing during neuronal maturation’, *Nature*, 397(6716), pp. 251–255. Available at: <https://doi.org/10.1038/16697>.
- Roostaei, T. *et al.* (2014) ‘The Human Cerebellum: A Review of Physiologic Neuroanatomy’, *Neurologic Clinics*, 32(4), pp. 859–869. Available at: <https://doi.org/10.1016/j.ncl.2014.07.013>.
- Rossi, D.J. and Hamann, M. (1998) ‘Spillover-mediated transmission at inhibitory synapses promoted by high affinity alpha6 subunit GABA(A) receptors and glomerular geometry’, *Neuron*, 20(4), pp. 783–795. Available at: [https://doi.org/10.1016/s0896-6273\(00\)81016-8](https://doi.org/10.1016/s0896-6273(00)81016-8).
- Rossi, F., Gianola, S. and Corvetti, L. (2006) ‘The strange case of Purkinje axon regeneration and plasticity’, *The Cerebellum*, 5(2), pp. 174–182. Available at: <https://doi.org/10.1080/14734220600786444>.

-
- Rossi, F., Gianola, S. and Corvetto, L. (2007) 'Regulation of intrinsic neuronal properties for axon growth and regeneration', *Progress in Neurobiology*, 81(1), pp. 1–28. Available at: <https://doi.org/10.1016/j.pneurobio.2006.12.001>.
- Roy, K. *et al.* (2007) 'Loss of erbB signaling in oligodendrocytes alters myelin and dopaminergic function, a potential mechanism for neuropsychiatric disorders', *Proceedings of the National Academy of Sciences*, 104(19), pp. 8131–8136. Available at: <https://doi.org/10.1073/pnas.0702157104>.
- Ryan, T.A. and Smith, S.J. (1995) 'Vesicle pool mobilization during action potential firing at hippocampal synapses', *Neuron*, 14(5), pp. 983–989. Available at: [https://doi.org/10.1016/0896-6273\(95\)90336-4](https://doi.org/10.1016/0896-6273(95)90336-4).
- Saab, A.S. *et al.* (2012) 'Bergmann Glial AMPA Receptors Are Required for Fine Motor Coordination', *Science*, 337(6095), pp. 749–753. Available at: <https://doi.org/10.1126/science.1221140>.
- Salin, P.A., Malenka, R.C. and Nicoll, R.A. (1996) 'Cyclic AMP mediates a presynaptic form of LTP at cerebellar parallel fiber synapses', *Neuron*, 16(4), pp. 797–803. Available at: [https://doi.org/10.1016/s0896-6273\(00\)80099-9](https://doi.org/10.1016/s0896-6273(00)80099-9).
- Sancho, L., Contreras, M. and Allen, N.J. (2021) 'Glia as sculptors of synaptic plasticity', *Neuroscience Research*, 167, pp. 17–29. Available at: <https://doi.org/10.1016/j.neures.2020.11.005>.
- Sasaki, T. *et al.* (2012) 'Application of an optogenetic byway for perturbing neuronal activity via glial photostimulation', *Proceedings of the National Academy of Sciences*, 109(50), pp. 20720–20725. Available at: <https://doi.org/10.1073/pnas.1213458109>.
- Scanziani, M. *et al.* (1997) 'Use-dependent increases in glutamate concentration activate presynaptic metabotropic glutamate receptors', *Nature*, 385(6617), pp. 630–634. Available at: <https://doi.org/10.1038/385630a0>.
- Schafer, D.P. *et al.* (2012) 'Microglia Sculpt Postnatal Neural Circuits in an Activity and Complement-Dependent Manner', *Neuron*, 74(4), pp. 691–705. Available at: <https://doi.org/10.1016/j.neuron.2012.03.026>.

- Schultz, C. and Engelhardt, M. (2014) ‘Anatomy of the Hippocampal Formation’, *The Hippocampus in Clinical Neuroscience*, 34, pp. 6–17. Available at: <https://doi.org/10.1159/000360925>.
- Segal, R.A., Takahashi, H. and McKay, R.D.G. (1992) ‘Changes in neurotrophin responsiveness during the development of cerebellar granule neurons’, *Neuron*, 9(6), pp. 1041–1052. Available at: [https://doi.org/10.1016/0896-6273\(92\)90064-K](https://doi.org/10.1016/0896-6273(92)90064-K).
- Segev, A., Garcia-Oscos, F. and Kourrich, S. (2016) ‘Whole-cell Patch-clamp Recordings in Brain Slices’, *Journal of Visualized Experiments: JoVE* [Preprint], (112). Available at: <https://doi.org/10.3791/54024>.
- Seifert, G. *et al.* (2003) ‘Changes in splice variant expression and subunit assembly of AMPA receptors during maturation of hippocampal astrocytes’, *Molecular and Cellular Neuroscience*, 22(2), pp. 248–258. Available at: [https://doi.org/10.1016/S1044-7431\(03\)00039-3](https://doi.org/10.1016/S1044-7431(03)00039-3).
- Seifert, G. and Steinhäuser, C. (1995) ‘Glial cells in the mouse hippocampus express AMPA receptors with an intermediate Ca²⁺ permeability’, *The European Journal of Neuroscience*, 7(9), pp. 1872–1881. Available at: <https://doi.org/10.1111/j.1460-9568.1995.tb00708.x>.
- Seifert, G. and Steinhäuser, C. (2018) ‘Heterogeneity and function of hippocampal macroglia’, *Cell and Tissue Research*, 373(3), pp. 653–670. Available at: <https://doi.org/10.1007/s00441-017-2746-1>.
- Sekerli, M. *et al.* (2004) ‘Estimating action potential thresholds from neuronal time-series: new metrics and evaluation of methodologies’, *IEEE Transactions on Biomedical Engineering*, 51(9), pp. 1665–1672. Available at: <https://doi.org/10.1109/TBME.2004.827531>.
- Servais, L. *et al.* (2004) ‘Effect of simple spike firing mode on complex spike firing rate and waveform in cerebellar Purkinje cells in non-anesthetized mice’, *Neuroscience Letters*, 367(2), pp. 171–176. Available at: <https://doi.org/10.1016/j.neulet.2004.05.109>.
- Servais, L. *et al.* (2007) ‘Purkinje cell dysfunction and alteration of long-term synaptic plasticity in fetal alcohol syndrome’, *Proceedings of the National Academy of Sciences*, 104(23), pp. 9858–9863. Available at: <https://doi.org/10.1073/pnas.0607037104>.

- Serwanski, D.R., Jukkola, P. and Nishiyama, A. (2017) 'Heterogeneity of astrocyte and NG2 cell insertion at the node of ranvier', *Journal of Comparative Neurology*, 525(3), pp. 535–552. Available at: <https://doi.org/10.1002/cne.24083>.
- Shields, S.D. *et al.* (2012) 'A channelopathy contributes to cerebellar dysfunction in a model of multiple sclerosis', *Annals of Neurology*, 71(2), pp. 186–194. Available at: <https://doi.org/10.1002/ana.22665>.
- Sigel, E. and Luscher, B.P. (no date) 'A Closer Look at the High Affinity Benzodiazepine Binding Site on GABAA Receptors', *Current Topics in Medicinal Chemistry*, 11(2), pp. 241–246.
- Sillitoe, R.V. *et al.* (2005) 'Conservation of the architecture of the anterior lobe vermis of the cerebellum across mammalian species', *Progress in Brain Research*, 148, pp. 283–297. Available at: [https://doi.org/10.1016/S0079-6123\(04\)48022-4](https://doi.org/10.1016/S0079-6123(04)48022-4).
- Simon, P., Dupuis, R. and Costentin, J. (1994) 'Thigmotaxis as an index of anxiety in mice. Influence of dopaminergic transmissions', *Behavioural Brain Research*, 61(1), pp. 59–64. Available at: [https://doi.org/10.1016/0166-4328\(94\)90008-6](https://doi.org/10.1016/0166-4328(94)90008-6).
- Smeets, C.J.L.M. and Verbeek, D.S. (2016) 'Climbing fibers in spinocerebellar ataxia: A mechanism for the loss of motor control', *Neurobiology of Disease*, 88, pp. 96–106. Available at: <https://doi.org/10.1016/j.nbd.2016.01.009>.
- Smith, S.L. and Otis, T.S. (2005) 'Pattern-dependent, simultaneous plasticity differentially transforms the input-output relationship of a feedforward circuit', *Proceedings of the National Academy of Sciences*, 102(41), pp. 14901–14906. Available at: <https://doi.org/10.1073/pnas.0505028102>.
- Song, F. *et al.* (2018) 'Kir4.1 channels in NG2-glia play a role in development, potassium signaling, and ischemia-related myelin loss', *Communications Biology*, 1, p. 80. Available at: <https://doi.org/10.1038/s42003-018-0083-x>.
- Soto, D. *et al.* (2007) 'Stargazin attenuates intracellular polyamine block of calcium-permeable AMPA receptors', *Nature Neuroscience*, 10(10), pp. 1260–1267. Available at: <https://doi.org/10.1038/nn1966>.

- Špaček, J. (1985) 'Three-dimensional analysis of dendritic spines', *Anatomy and Embryology*, 171(2), pp. 245–252. Available at: <https://doi.org/10.1007/BF00341419>.
- Stallcup, W.B. and Beasley, L. (1987) 'Bipotential glial precursor cells of the optic nerve express the NG2 proteoglycan', *The Journal of Neuroscience: The Official Journal of the Society for Neuroscience*, 7(9), pp. 2737–2744. Available at: <https://doi.org/10.1523/JNEUROSCI.07-09-02737.1987>.
- Steinhäuser, C., Jabs, R. and Kettenmann, H. (1994) 'Properties of GABA and glutamate responses in identified glial cells of the mouse hippocampal slice', *Hippocampus*, 4(1), pp. 19–35. Available at: <https://doi.org/10.1002/hipo.450040105>.
- Steinhäuser, C. *et al.* (1992) 'Heterogeneity in the Membrane Current Pattern of Identified Glial Cells in the Hippocampal Slice', *European Journal of Neuroscience*, 4(6), pp. 472–484. Available at: <https://doi.org/10.1111/j.1460-9568.1992.tb00897.x>.
- Stern-Bach, Y. *et al.* (1998) 'A Point Mutation in the Glutamate Binding Site Blocks Desensitization of AMPA Receptors', *Neuron*, 21(4), pp. 907–918. Available at: [https://doi.org/10.1016/S0896-6273\(00\)80605-4](https://doi.org/10.1016/S0896-6273(00)80605-4).
- Stevens, B. *et al.* (2007) 'The Classical Complement Cascade Mediates CNS Synapse Elimination', *Cell*, 131(6), pp. 1164–1178. Available at: <https://doi.org/10.1016/j.cell.2007.10.036>.
- Stoodley, C.J., Valera, E.M. and Schmahmann, J.D. (2012) 'Functional topography of the cerebellum for motor and cognitive tasks: an fMRI study', *NeuroImage*, 59(2), pp. 1560–1570. Available at: <https://doi.org/10.1016/j.neuroimage.2011.08.065>.
- van Strien, N.M., Cappaert, N.L.M. and Witter, M.P. (2009) 'The anatomy of memory: an interactive overview of the parahippocampal–hippocampal network', *Nature Reviews Neuroscience*, 10(4), pp. 272–282. Available at: <https://doi.org/10.1038/nrn2614>.
- Sturrock, R.R. (1980) 'Myelination of the Mouse Corpus Callosum', *Neuropathology and Applied Neurobiology*, 6(6), pp. 415–420. Available at: <https://doi.org/10.1111/j.1365-2990.1980.tb00219.x>.
- Swanson, G.T., Kamboj, S.K. and Cull-Candy, S.G. (1997) 'Single-Channel Properties of Recombinant AMPA Receptors Depend on RNA Editing, Splice Variation, and Subunit

-
- Composition', *Journal of Neuroscience*, 17(1), pp. 58–69. Available at: <https://doi.org/10.1523/JNEUROSCI.17-01-00058.1997>.
- Szapiro, G. and Barbour, B. (2007) 'Multiple climbing fibers signal to molecular layer interneurons exclusively via glutamate spillover', *Nature Neuroscience*, 10(6), pp. 735–742. Available at: <https://doi.org/10.1038/nn1907>.
- Takei, N. *et al.* (2004) 'Brain-Derived Neurotrophic Factor Induces Mammalian Target of Rapamycin-Dependent Local Activation of Translation Machinery and Protein Synthesis in Neuronal Dendrites', *Journal of Neuroscience*, 24(44), pp. 9760–9769. Available at: <https://doi.org/10.1523/JNEUROSCI.1427-04.2004>.
- Tanaka, Y. *et al.* (2009) 'Excitatory GABAergic Activation of Cortical Dividing Glial Cells', *Cerebral Cortex*, 19(9), pp. 2181–2195. Available at: <https://doi.org/10.1093/cercor/bhn238>.
- Tao, X. *et al.* (1998) 'Ca²⁺ Influx Regulates BDNF Transcription by a CREB Family Transcription Factor-Dependent Mechanism', *Neuron*, 20(4), pp. 709–726. Available at: [https://doi.org/10.1016/S0896-6273\(00\)81010-7](https://doi.org/10.1016/S0896-6273(00)81010-7).
- Temido-Ferreira, M. *et al.* (2019) 'Novel Players in the Aging Synapse: Impact on Cognition', *Journal of Caffeine and Adenosine Research*, 9(3), pp. 104–127. Available at: <https://doi.org/10.1089/caff.2019.0013>.
- Teng, H.K. *et al.* (2005) 'ProBDNF induces neuronal apoptosis via activation of a receptor complex of p75NTR and sortilin', *The Journal of Neuroscience: The Official Journal of the Society for Neuroscience*, 25(22), pp. 5455–5463. Available at: <https://doi.org/10.1523/JNEUROSCI.5123-04.2005>.
- Thomson, A.M. and Bannister, A.P. (1999) 'Release-independent depression at pyramidal inputs onto specific cell targets: dual recordings in slices of rat cortex', *The Journal of Physiology*, 519(1), pp. 57–70. Available at: <https://doi.org/10.1111/j.1469-7793.1999.00570.x>.
- Thomzig, A. *et al.* (2001) 'Kir6.1 is the principal pore-forming subunit of astrocyte but not neuronal plasma membrane K-ATP channels', *Molecular and Cellular Neurosciences*, 18(6), pp. 671–690. Available at: <https://doi.org/10.1006/mcne.2001.1048>.

- Tian, J. *et al.* (2014) ‘p75 Regulates Purkinje Cell Firing by Modulating SK Channel Activity through Rac1 *’, *Journal of Biological Chemistry*, 289(45), pp. 31458–31472. Available at: <https://doi.org/10.1074/jbc.M114.589937>.
- Timmermann, A. *et al.* (2023) ‘Dysfunction of NG2 glial cells affects neuronal plasticity and behavior’, *Glia*, 71(6), pp. 1481–1501. Available at: <https://doi.org/10.1002/glia.24352>.
- Titley, H.K. and Hansel, C. (2016) ‘Asymmetries in Cerebellar Plasticity and Motor Learning’, *The Cerebellum*, 15(2), pp. 87–92. Available at: <https://doi.org/10.1007/s12311-014-0635-7>.
- Todd, A.C. *et al.* (2017) ‘SNAT3-mediated glutamine transport in perisynaptic astrocytes in situ is regulated by intracellular sodium’, *Glia*, 65(6), pp. 900–916. Available at: <https://doi.org/10.1002/glia.23133>.
- Tomita, S. *et al.* (2005) ‘Stargazin modulates AMPA receptor gating and trafficking by distinct domains’, *Nature*, 435(7045), pp. 1052–1058. Available at: <https://doi.org/10.1038/nature03624>.
- Tong, X. *et al.* (2009) ‘Ca²⁺ signaling evoked by activation of Na⁺ channels and Na⁺/Ca²⁺ exchangers is required for GABA-induced NG2 cell migration’, *Journal of Cell Biology*, 186(1), pp. 113–128. Available at: <https://doi.org/10.1083/jcb.200811071>.
- Torres, A. *et al.* (2012) ‘Extracellular Ca²⁺ Acts as a Mediator of Communication from Neurons to Glia’, *Science Signaling*, 5(208), pp. ra8–ra8. Available at: <https://doi.org/10.1126/scisignal.2002160>.
- Treccani, G. *et al.* (2021) ‘Early life adversity targets the transcriptional signature of hippocampal NG2⁺ glia and affects voltage gated sodium (Nav) channels properties’, *Neurobiology of Stress*, 15, p. 100338. Available at: <https://doi.org/10.1016/j.ynstr.2021.100338>.
- Twomey, E.C. *et al.* (2018) ‘Mechanisms of Channel Block in Calcium-Permeable AMPA Receptors’, *Neuron*, 99(5), pp. 956-968.e4. Available at: <https://doi.org/10.1016/j.neuron.2018.07.027>.
- Ullian, E.M., Christopherson, K.S. and Barres, B.A. (2004) ‘Role for glia in synaptogenesis’, *Glia*, 47(3), pp. 209–216. Available at: <https://doi.org/10.1002/glia.20082>.

- V, L.-R. *et al.* (2002) ‘A new form of cerebellar long-term potentiation is postsynaptic and depends on nitric oxide but not cAMP’, *Proceedings of the National Academy of Sciences of the United States of America*, 99(12). Available at: <https://doi.org/10.1073/pnas.122206399>.
- Valny, M. *et al.* (2018) ‘A single-cell analysis reveals multiple roles of oligodendroglial lineage cells during post-ischemic regeneration’, *GLIA*, 66(5), pp. 1068–1081. Available at: <https://doi.org/10.1002/glia.23301>.
- Vélez-Fort, M. *et al.* (2010) ‘Postnatal Switch from Synaptic to Extrasynaptic Transmission between Interneurons and NG2 Cells’, *The Journal of Neuroscience*, 30(20), pp. 6921–6929. Available at: <https://doi.org/10.1523/JNEUROSCI.0238-10.2010>.
- Ventura, R. and Harris, K.M. (1999) ‘Three-dimensional relationships between hippocampal synapses and astrocytes’, *The Journal of Neuroscience: The Official Journal of the Society for Neuroscience*, 19(16), pp. 6897–6906. Available at: <https://doi.org/10.1523/JNEUROSCI.19-16-06897.1999>.
- Verkhatsky, A. and Nedergaard, M. (2018) ‘Physiology of Astroglia’, *Physiological Reviews*, 98(1), pp. 239–389. Available at: <https://doi.org/10.1152/physrev.00042.2016>.
- Viet, N.-M. *et al.* (2022) ‘Heterogeneity of intrinsic plasticity in cerebellar Purkinje cells linked with cortical molecular zones’, *iScience*, 25(1), p. 103705. Available at: <https://doi.org/10.1016/j.isci.2021.103705>.
- Viganò, F. and Dimou, L. (2016) ‘The heterogeneous nature of NG2-glia’, *Brain Research*, 1638, pp. 129–137. Available at: <https://doi.org/10.1016/j.brainres.2015.09.012>.
- Vogel-Ciernia, A. and Wood, M.A. (2014) ‘Examining Object Location and Object Recognition Memory in Mice’, *Current protocols in neuroscience / editorial board, Jacqueline N. Crawley ... [et al.]*, 69, p. 8.31.1-8.31.17. Available at: <https://doi.org/10.1002/0471142301.ns0831s69>.
- VonDran, M.W. *et al.* (2011) ‘Levels of BDNF Impact Oligodendrocyte Lineage Cells following a Cuprizone Lesion’, *The Journal of Neuroscience*, 31(40), pp. 14182–14190. Available at: <https://doi.org/10.1523/JNEUROSCI.6595-10.2011>.

- Wadiche, J.I. and Jahr, C.E. (2001) 'Multivesicular Release at Climbing Fiber-Purkinje Cell Synapses', *Neuron*, 32(2), pp. 301–313. Available at: [https://doi.org/10.1016/S0896-6273\(01\)00488-3](https://doi.org/10.1016/S0896-6273(01)00488-3).
- Wang, F. *et al.* (2012) 'Bergmann glia modulate cerebellar Purkinje cell bistability via Ca²⁺-dependent K⁺ uptake', *Proceedings of the National Academy of Sciences*, 109(20), pp. 7911–7916. Available at: <https://doi.org/10.1073/pnas.1120380109>.
- Watson, J.F., Ho, H. and Greger, I.H. (2017) 'Synaptic transmission and plasticity require AMPA receptor anchoring via its N-terminal domain', *eLife*. Edited by R. Jahn, 6, p. e23024. Available at: <https://doi.org/10.7554/eLife.23024>.
- Wetmore, C. *et al.* (1990) 'Localization of brain-derived neurotrophic factor mRNA to neurons in the brain by in situ hybridization', *Experimental Neurology*, 109(2), pp. 141–152. Available at: [https://doi.org/10.1016/0014-4886\(90\)90068-4](https://doi.org/10.1016/0014-4886(90)90068-4).
- Whitlock, J.R. *et al.* (2006) 'Learning induces long-term potentiation in the hippocampus', *Science (New York, N.Y.)*, 313(5790), pp. 1093–1097. Available at: <https://doi.org/10.1126/science.1128134>.
- Wigley, R. *et al.* (2007) 'Morphological and physiological interactions of NG2-glia with astrocytes and neurons', *Journal of Anatomy*, 210(6), pp. 661–670. Available at: <https://doi.org/10.1111/j.1469-7580.2007.00729.x>.
- Wigley, R. and Butt, A.M. (2009) 'Integration of NG2-glia (synantocytes) into the neuroglial network', *Neuron Glia Biology*, 5(1–2), pp. 21–28. Available at: <https://doi.org/10.1017/S1740925X09990329>.
- Woo, N.H. *et al.* (2005) 'Activation of p75NTR by proBDNF facilitates hippocampal long-term depression', *Nature Neuroscience*, 8(8), pp. 1069–1077. Available at: <https://doi.org/10.1038/nn1510>.
- Xiao, L. *et al.* (2016) 'Rapid production of new oligodendrocytes is required in the earliest stages of motor-skill learning', *Nature Neuroscience*, 19(9), pp. 1210–1217. Available at: <https://doi.org/10.1038/nn.4351>.
- Xu-Friedman, M.A. and Regehr, W.G. (2003) 'Ultrastructural contributions to desensitization at cerebellar mossy fiber to granule cell synapses', *The Journal of Neuroscience: The Official*

- Journal of the Society for Neuroscience*, 23(6), pp. 2182–2192. Available at: <https://doi.org/10.1523/JNEUROSCI.23-06-02182.2003>.
- Xu-Friedman, M.A. and Regehr, W.G. (2004) ‘Structural contributions to short-term synaptic plasticity’, *Physiological Reviews*, 84(1), pp. 69–85. Available at: <https://doi.org/10.1152/physrev.00016.2003>.
- Yamada, K. and Watanabe, M. (2002) ‘Cytodifferentiation of bergmann glia and its relationship with purkinje cells’, *Anatomical Science International*, 77(2), pp. 94–108. Available at: <https://doi.org/10.1046/j.0022-7722.2002.00021.x>.
- Yamada, K.A. and Tang, C.M. (1993) ‘Benzothiadiazides inhibit rapid glutamate receptor desensitization and enhance glutamatergic synaptic currents’, *Journal of Neuroscience*, 13(9), pp. 3904–3915. Available at: <https://doi.org/10.1523/JNEUROSCI.13-09-03904.1993>.
- Yang, H. and Xu-Friedman, M.A. (2008) ‘Relative roles of different mechanisms of depression at the mouse endbulb of Held’, *Journal of neurophysiology*, 99(5), pp. 2510–2521. Available at: <https://doi.org/10.1152/jn.01293.2007>.
- Yang, J. *et al.* (2014) ‘proBDNF Negatively Regulates Neuronal Remodeling, Synaptic Transmission, and Synaptic Plasticity in Hippocampus’, *Cell Reports*, 7(3), pp. 796–806. Available at: <https://doi.org/10.1016/j.celrep.2014.03.040>.
- Yeung, M.S.Y. *et al.* (2014) ‘Dynamics of Oligodendrocyte Generation and Myelination in the Human Brain’, *Cell*, 159(4), pp. 766–774. Available at: <https://doi.org/10.1016/j.cell.2014.10.011>.
- Yuan, X. *et al.* (1998) ‘A role for glutamate and its receptors in the regulation of oligodendrocyte development in cerebellar tissue slices’, *Development (Cambridge, England)*, 125(15), pp. 2901–2914. Available at: <https://doi.org/10.1242/dev.125.15.2901>.
- Zhang, F. *et al.* (2012) ‘Resveratrol promotes neurotrophic factor release from astroglia’, *Experimental Biology and Medicine*, 237(8), pp. 943–948. Available at: <https://doi.org/10.1258/ebm.2012.012044>.
- Zhang, X. *et al.* (2021) ‘NG2 glia-derived GABA release tunes inhibitory synapses and contributes to stress-induced anxiety’, *Nature Communications*, 12(1), p. 5740. Available at: <https://doi.org/10.1038/s41467-021-25956-y>.

- Zhang, Z. *et al.* (2022) ‘NG2-glia crosstalk with microglia in health and disease’, *CNS Neuroscience & Therapeutics*, 28(11), pp. 1663–1674. Available at: <https://doi.org/10.1111/cns.13948>.
- Zhao, N. *et al.* (2021) ‘L-Type Ca²⁺ Channels of NG2 Glia Determine Proliferation and NMDA Receptor-Dependent Plasticity’, *Frontiers in Cell and Developmental Biology*, 9, p. 759477. Available at: <https://doi.org/10.3389/fcell.2021.759477>.
- Zhou, H. *et al.* (2014) ‘Cerebellar modules operate at different frequencies’, *eLife*, 3, p. e02536. Available at: <https://doi.org/10.7554/eLife.02536>.
- Zhou, L.-J. *et al.* (2019) ‘Microglia Are Indispensable for Synaptic Plasticity in the Spinal Dorsal Horn and Chronic Pain’, *Cell Reports*, 27(13), pp. 3844–3859.e6. Available at: <https://doi.org/10.1016/j.celrep.2019.05.087>.
- Zhou, P. *et al.* (2007) ‘Polarized Signaling Endosomes Coordinate BDNF-Induced Chemotaxis of Cerebellar Precursors’, *Neuron*, 55(1), pp. 53–68. Available at: <https://doi.org/10.1016/j.neuron.2007.05.030>.
- Zhou, Y. and Danbolt, N. (2013) ‘GABA and Glutamate Transporters in Brain’, *Frontiers in Endocrinology*, 4. Available at: <https://www.frontiersin.org/articles/10.3389/fendo.2013.00165>.
- Zhu, L. *et al.* (2007) ‘The effects of fear conditioning on cerebellar LTP and LTD’, *European Journal of Neuroscience*, 26(1), pp. 219–227. Available at: <https://doi.org/10.1111/j.1460-9568.2007.05632.x>.
- Ziskin, J.L. *et al.* (2007) ‘Vesicular release of glutamate from unmyelinated axons in white matter’, *Nature Neuroscience*, 10(3), pp. 321–330. Available at: <https://doi.org/10.1038/nn1854>.
- Zonouzi, M. *et al.* (2011) ‘Bidirectional plasticity of calcium-permeable AMPA receptors in oligodendrocyte lineage cells’, *Nature Neuroscience*, 14(11), pp. 1430–1438. Available at: <https://doi.org/10.1038/nn.2942>.
- Zucker, R.S. and Regehr, W.G. (2002) ‘Short-term synaptic plasticity’, *Annual Review of Physiology*, 64, pp. 355–405. Available at: <https://doi.org/10.1146/annurev.physiol.64.092501.114547>.

10 Appendix

10.1 Abbreviations

7,8-DHF	7,8- dihydroxyflavone
aCSF	Artificial cerebro-spinal fluid
AHP	Afterhyperpolarization amplitude
AMPA	α -amino-3-hydroxy-5-methyl-4-isoxazolepropionic acid receptor
AP	Action Potential
ATP	Adenosine 5'-triphosphate
AUC	Area under the curve
BDNF	Brain-Derived Neurotrophic Factor
BaCl ₂	Barium Chloride
BG	Bergmann glia
BZD	Benzodiazepine
CA	Cornus Ammoni
CAMKII	Ca ²⁺ /calmodulin-dependent protein kinase
CF	Climbing fiber
CI	Ca ²⁺ -impermeable
C _m	Membrane capacitance
CNIH	Cornichon Homologue (AMPA auxiliary protein)
CNS	Central Nervous System
CP	Ca ²⁺ -permeable
CREB	cAMP response element-binding protein
CS	Complex spike
CTD	Carboxy-terminal domain
CTZ	Cyclothiazide
CV	Coefficient of variation
DCN	Deep cerebellar nuclei
DG	Dentate gyrus
DTT	Dithiothreitol
EAAT	Excitatory amino acid transporter
EDTA	Ethylenediaminetetraacetic acid
EGTA	Ethylene glycol tetraacetic acid
ePSC	Evoked post-synaptic current
ER ^{T2}	Estrogen receptor variant 2
EYFP	Enhanced yellow fluorescent protein
FACS	Fluorescence activated cell sorting
fEPSP	Field excitatory post-synaptic potential
FGF	Fibroblast growth factor
fl/fl	Floxed (loxP sites) on both alleles
FV	Fiber volley

GABAR	γ -Aminobutyric acid receptor
Gamma(γ)-DGG	Gamma-D-Glutamylglycine
GAT	GABA transporter
GFAP	Glial fibrillary acidic protein
GL	Granular layer
GluA	AMPA receptor subunit
HC	Hippocampus
HEPES	4-(2-hydroxyethyl)-1-piperazineethanesulfonic acid
ISI	Inter-spike interval
I-V	Current-voltage
KCC2	KCl co-transporter
Kir	Inwardly rectifying K^+ channel
ko	Knockout
LBD	Ligand binding domain
LJP	Liquid junction potential
LTD	Long-term depression
LTP	Long-term potentiation
MAPK	Mitogen-activated protein kinase
MBP	Myelin basic protein
MF	Mossy fiber
ML	Molecular layer
mTOR	Mechanistic target of rapamycin
mGluR1b	Metabotropic Glutamate Receptor 1
NG2	Neural/glial antigen 2
NGF	Nerve-growth factor
NMDAR	N-methyl-D-aspartate receptor
NOLR	Novel object location recognition
NTD	N-terminal domain
OPC	Oligodendrocyte precursor cells
p75 ^{NTR}	p75 neurotrophin receptor
PC	Purkinje cell
PF	Parallel fibers
PKC	Protein-kinase C
PLC	Phospholipase C
PLP	Proteolipid protein
PPD	Paired-pulse depression
PPF	Paired-pulse facilitation
PPR	Paired-pulse ratio
PRT	Partner recognition test
PSC	Post-synaptic current
PTP	Post-tetanic potentiation
R _m	Membrane resistance

R_s	Series resistance
RI	Rectification index
RT-PCR	Reverse transcription polymerase chain reaction
SC	Schaffer collateral
SK	Small conductance calcium-activated potassium channels
SLM	Stratum lacunosum-moleculare
SM	Stratum moleculare
SO	Stratum oriens
SR	Stratum radiatum
STP	Short-term plasticity
TARP	Transmembrane AMPAR regulatory protein
TBS	Theta-burst stimulation
TMD	Transmembrane domain
TrkB	Tropomyosin related kinase B
TRPC	Transient receptor potential channel
TTX	Tetrodotoxin
V_h	Holding potential
V_m	Membrane potential
WT	Wild-type
YFP	Yellow fluorescent protein
Z+, Z-	Zebrin positive, Zebrin negative

10.2 List of figures

Fig. 1.1. Cerebellar localization and anatomy.....	10
Fig. 1.2. Simplified overview of the cerebellar cortical organization and its circuitry.....	11
Fig. 1.3. Sagittal cerebellar stripes.	12
Fig. 1.4. Hippocampal anatomy and circuitry	14
Fig. 1.5. NG2 glia forms functional synapses with neurons	18
Fig. 1.6. Schematic structure of AMPA receptor subunits.....	19
Fig. 1.7. GABAAR structure.....	21
Fig. 1.8. Short-term plasticity.....	25
Fig. 1.9. Roles of mBDNF in myelination.	28
Fig. 4.1. Calculation of passive membrane properties.	42
Fig. 4.2. Schematic representation of intracellular polyamine block.....	44
Fig. 4.3. fEPSP recordings in cerebellar and hippocampal slices.	48
Fig. 4.4. Parameters for action potential analysis in cerebellar PCs.	49
Fig. 4.5. Schematic representation of NOLR test.....	51
Fig. 4.6. Representation of PRT paradigm.....	52
Fig. 4.7. Y-maze test.	52
Fig. 4.8. Scheme of the beam-walking test setup.....	53
Fig. 5.1. Analysis of CP-AMPA expression in hippocampal NG2 glia	59
Fig. 5.2. Synaptic CP-AMPA receptor expression in hippocampal and cerebellar NG2 glia..	61
Fig. 5.3. Intracellular polyamine block of CP-AMPA receptors.	62
Fig. 5.4. Multivesicular release influences synaptic efficiency of NG2 glia.	64
Fig. 5.5. Short-term plasticity mechanisms in cerebellar CF-NG2 synapses.....	66
Fig. 5.6. Loss of AMPAR-mediated inward currents in the cerebellum of GluAko mice.....	68
Fig. 5.7. Experimental protocol for recording fEPSPs in cerebellar slices.....	69
Fig. 5.8. LTP is impaired in the cerebellum of GluAko mice.....	70
Fig. 5.9. Application of a TrkB agonist in GluAko mice rescues LTP in hippocampus and cerebellum.	72
Fig. 5.10. Properties of PCs in control and GluAko slices.....	74
Fig. 5.11. Open-field test shows no differences in locomotor activity.	76
Fig. 5.12. No defects in spatial memory are present in GluAko mice according to the NOLR test.	77
Fig. 5.13. Social memory is not impaired in GluAko mice as assessed by the PRT.	78

Fig. 5.14. Locomotion but not working memory is impaired in GluAko mice during Y-maze test.	79
Fig. 5.15. GluAko mice move slower during the beam-walking test.....	80
Fig. 5.16. Block of CP-AMPA-mediated currents in hippocampal and cerebellar GluA3WT slices.	81
Fig. 5.17. fEPSP recordings from hippocampal and cerebellar GluA3WT slices.	82
Fig. 5.18. mPSC recordings from hippocampal and cerebellar Kir 4.1 ko slices.	84
Fig. 5.19. Rescue of PTP and LTP by 7,8-DHF in hippocampal Kir 4.1 ko slices.....	85
Fig. 5.20. LTP is reduced in cerebellar slices of Kir 4.1 ko mice.	86
Fig. 5.21. GABA uptake blockers prolong ePSC decay only in adult NG2 glia.	88

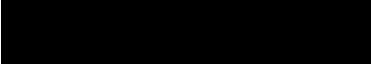
10.3 List of tables

Table 1. Primers used for preamplification for qPCR.....	56
Table 2. PPR of fEPSPs of control and GluAko mice.	71
Table 3. Passive membrane properties of PCs from control and GluAko mice.....	73
Table 4. AP properties and kinetics in control and GluAko slices.	75

Declaration

I hereby declare that this Doctoral Thesis is original and was written independently, using no other sources and aids than stated. This document - in the current or similar form - has not and will not be submitted to any other institution, apart from the University of Bonn.

Bonn, June 2023



Dario Tascio